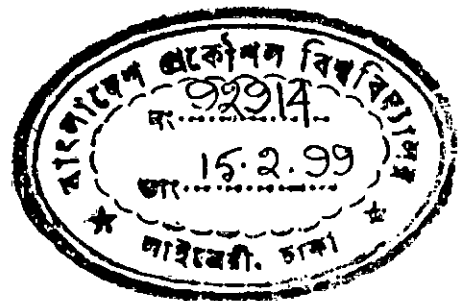
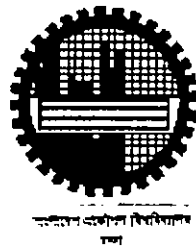


MEASUREMENT OF DOSE DISTRIBUTIONS FOR HIGH ENERGY PHOTON BEAMS USING THERMOLUMINESCENCE DOSIMETER

By
FATEMA NASREEN

A dissertation submitted in partial fulfillment of the requirement for the degree of Ph.D. in the Department of Physics, Bangladesh University of Engineering & Technology, Dhaka



Bangladesh University Of Engineering & Technology
Dhaka, Bangladesh
November 1998



**BANGLADESH UNIVERSITY OF ENGINEERING AND TECHNOLOGY
DHAKA**

DEPARTMENT OF PHYSICS

Certification of Thesis work

A Thesis on

**MEASUREMENT OF DOSE DISTRIBUTIONS FOR HIGH ENERGY PHOTON
BEAMS USING THERMOLUMINESCENCE DOSIMETER**

By

FATEMA NASREEN

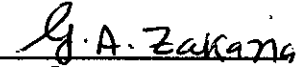
has been accepted as satisfactory in partial fulfilment for the degree of Doctor of Philosophy in Physics and certifying that the student demonstrated a satisfactory knowledge of the field covered by this thesis in an oral examination held on November 19, 1998.

Board of Examiners


1 Prof. Gias uddin Ahmad
Dept. of Physics, BUET


Supervisor & Chairman

2 Dr. G. A. Zakaria
Head, Dept. of Radiation Therapy
Gummersbach Hospital
5270, Gummersbach, Germany.


Co-supervisor

3 Prof. Mominul Huq
Head, Dept. of Physics, BUET


Member

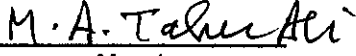
4 Prof. M. A. Asgar
Dept. of Physics, BUET


Member

5 Prof. T. Hossain
Dept. of Physics, BUET


Member

6 Prof. M. A. Taher Ali
Dept. of Mech. Engg., BUET


Member

7 Prof. Fazle Elahi
Director, National Institute of Cancer
Research & Hospital, Dhaka

Member

8 Dr. S. R. Husain
Delta Clinic (Oncology Unit)
Mirpur, Dhaka


Member

9 Dr. Karl-Heinz Hoever
Chief, Radiation Diagnosis & Therapy Division,
German Cancer Research Centre (DKFZ)
1m Neuenheimer Feld 280, 69120 Heidelberg, Germany


Member (External)

Acknowledgment

I would like to express my profound gratitude to my supervisors Dr. Gias uddin Ahmad, Professor, Department of Physics, Bangladeshi University of Engineering & Technology (BUET) and Dr. G. A. Zakaria, Head, Department of Radiation Therapeutic Physics, Gummersbach Hospital, Germany for their constant guidance and supervision throughout the progress of this work.

I am grateful to DAAD (Deutsche Akademische Austauschdienst) organization and its honourable president, Prof. Dr. Dr. h. c. mult. Theodor Berchem and also to Dr. Christia Klaus, the consultant, for awarding the scholarship and as well as the continuous encouragement for the progress of studies in Germany. It was a great pleasure for me to make opportunity to get to know Germany, its people and its culture.

A major part of the experiment has been done in the dept. of Radiation Therapeutic Physics, Gummersbach, Germany. I would like to express my gratitude to the authority of the Gummersbach Hospital for extending laboratory facilities for carrying out the work. I have received all out co-operation and help from Mr. Schütte, Medical Physicist and from Mr. Berger, Mr. Radant and from all others staff in that department. Without their co-operation it would have been impossible to complete this work.

I would like to express my sincere gratitude to Prof. Dr. U. Quast and Mr. Gläser in Essen University clinic and to Dr. H. Feist, Ms. Mischeil in the dept. of Radiation Therapy Physics, Grossharder Uni-clinic Munich for their valuable ideas on the therapeutic system and to provide lab facilities. A part of this work has been carried out with their kind co-operation. I would like to thank Prof. Quast for giving a lung analogue phantom with which some significant dose measurement were carried out using TLDs.

I would like to express my sincere gratitude to Prof. Mominul Haq, Head, Department of Physics, BUET, Prof. M. A. Asgar and Prof. T. Hossain of the same department, for their encouragement and keen interest. I would like to thank Dr. Feroz Alam Khan, for helping me to translate some tables from German. My thanks are also to Dr. Nazma Zaman, Ms. Dil Afroz Ahmed, Ms. Fatima Khanam, Dr. Jiban Podder and all others teaching staffs and other members of the same department for their encouragement and interest in the work.

I would also like to extend my sincere gratitude to Prof. Dr. Hamida Banu, Director General, Secondary and Higher Education Directorate; Prof. M. F. N. Siddiqua Begum, Head of the Physics Department, Eden College and Prof. Mahera Ahmed of the same department for their inspiration. I would like to express my gratitude to Dr. Golam Subhani Chowdhury, Assist. Prof. of that department for his valuable suggestions in writing the thesis.

I would like to express my gratitude to Jamir Uddin Ahmed, P.S. to Secretary, Ministry of Youth and Sports for his constant inspiration and help in writing the thesis when doubt and hesitation assail me.

I would like to thank the members of the Doctoral Committee for their encouragement and valuable suggestions.

I am grateful to BUET for extending financial assistance and technical and laboratory facilities during the course of this study.

At last, I express my gratitude to my colleagues and friends for their encouragement and inspiration during the study at Köln University, Germany.

Abstract

In this work, the dose distribution of high-energy photon beams was measured using thermoluminescence (TL) dosimeters. The purpose of this work was to introduce the TLDs in clinical dose measurements, which are normally done with ion chamber dosimeter. For this, the rod of $1 \times 1 \times 6 \text{ mm}^3$ size of TLD was used. Most of the measurements were carried out for the photon beams of energies 4.0 & 10MV. The reliability of the detector was tested by comparison with an ion-chamber and a Markus chamber dosimeter.

Chapter 1 describes the scope and aim of the studies. Here, the quality of the high-energy photon beams, which comprises the prime conditions of radiotherapy treatment, is also discussed.

In chapter 2, 3 and 4, the review of some related works, theoretical aspects of thermoluminescence including glow curve theory and some necessary equipment have been discussed.

In chapter 5 and 6, the reproducibility of the TLDs via the thermal treatment in four-step application cycle of TLD, the sensitivity factor and calibration of the TLDs have been discussed. Detail studies with the practical problems including those associated with the annealing, storage, handling, irradiation, readout and calibration have also been discussed.

In chapter 7 and 8, the technique of dose accuracy has been established through some homogeneous and inhomogeneous measurements. Here, the independent characteristics of field sizes, depths of phantom for TL-dosimeter like ion-chamber dosimetry were obtained through those measurements.

*Chapter 9 describes the uses of TLDs in *invivo* dosimetry by following a new methodology. The entrance and exit dose was measured using TLDs. The method provides more accurate target dose (within 0.17% variation from the direct target dose value).*

Chapter 10 describes the development of a new PC program for treatment of cancer using multiple asymmetric fields and its experimental verification.

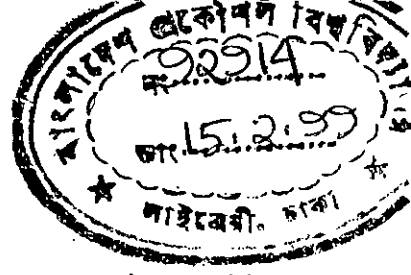
Chapter 11 describes the use of TLDs for measuring dose during whole body irradiation with high-energy photon beams.

Finally, in Chapter 12, the findings of the experiments are discussed.

Contents

	<i>Page</i>
1.0 <i>Scope and aim of the studies</i>	1
2.0 <i>Review of some related works</i>	5
3.0 <i>Theoretical aspects of thermoluminescence</i>	15
3.1 <i>Mechanism of thermoluminescence</i>	15
3.1.1 <i>The role of lattice defects in the thermoluminescence</i>	15
3.2 <i>A general model for thermoluminescence</i>	16
3.3 <i>The TL-process in Lithium-fluoride doped with magnesium and titanium.</i>	18
3.3.1 <i>The thermal effect and the resulting glow-curves</i>	18
3.3.1a <i>The role of magnesium and Titanium ions.</i>	19
3.3.1b <i>The role of Titanium and Hydroxyl ions.</i>	22
4.0 <i>Materials used for experiment and their irradiation facilities</i>	23
4.1 <i>TLD material in TL-dosimetry.</i>	23
4.2 <i>Reference dosimetry.</i>	26
4.3 <i>Irradiation facilities.</i>	27
4.4 <i>Phantom.</i>	27
5.0 <i>Thermal treatment and the reproducibility of the TL-LiF crystal dosimeters</i>	28
5.1 <i>Introduction</i>	28
5.2 <i>Four-step application-cycle for TL-dosimeter</i>	28
5.3 <i>Sensitivity factor and grouping of TL-dosimeters</i>	40
6.0 <i>Calibration of thermoluminescence dosimeter</i>	44
6.1 <i>Introduction</i>	44
6.2 <i>Light dependence calibration factor of the thermoluminescence</i>	44
6.3 <i>Dose dependence calibration factor (supralinearity factor) of the TL-dosimeters</i>	53
6.4 <i>Energy dependent calibration factor of the TL-dosimeters</i>	56

7.0	<i>Comparison of TL-dosimeter measurements with other standard dosimeters for standard fields of homogeneous phantom</i>	59
7.1	<i>Dose accuracy of TL-dosimetry in the phantom</i>	59
7.2	<i>Depth dose, profile-dose, penumbra dose and build up region dose distributions using TLDs and comparison with others standard dosimeters for some standard symmetric and asymmetric fields in the homogeneous phantom</i>	65
8.0	<i>Comparison of TL-dosimetry with other standard dosimetry in some inhomogeneous situations.</i>	78
8.1.a.	<i>Dose distribution in phantom containing air inhomogeneity.</i>	78
8.1.b	<i>Dose measurement in Plexiglas-Cork-Plexiglas phantom to investigate the electronic equilibrium.</i>	81
8.2	<i>Dose distribution on a phantom for tangential field used in breast irradiation.</i>	87
8.3	<i>Depth dose and x-profile distribution in Lung-phantom of finite geometry.</i>	89
8.4	<i>Measurement of dose-distribution in the vicinity of Aluminum interface</i>	96
9.0	<i>Clinical application of TLDs and associated methodology</i>	99
10.0	<i>Verification of calculated dose distribution performed by a new installed program for asymmetry photon beams using TLD</i>	103
11.0	<i>Measurement of doses using TLD in total body irradiation.</i>	115
12.0	<i>Results and Discussions</i>	123
	Appendix – A	129
	<i>The Linear Accelerator</i>	
	Appendix -B	132
	<i>Definitions and explanations of the terms.</i>	
	Appendix –C	138
	<i>Paper based on the present work published in Medicinische Physik, Vol. 28, 1997, p-21</i>	
	References	140



1.0 SCOPE AND AIM OF THE STUDIES

The advantage of megavoltage linear accelerator (linac) in comparison with cobalt machine or orthovoltage X-rays deep therapy machine for external beam therapy is now fully recognized all over the world²⁷. High-energy photon and electron beams produced by linac covers the whole spectrum of tumors of a human body. About 80 percent of body tumors are located at a depth for which the treatment is possible by using only the photon beams. However, for the treatment of surface or shallow depth tumors where sparing of underlying tissue is necessary, the electron beams are used either alone or combined with photon beams¹⁵. The physical advantages of the high-energy photon beams relative to electron beams or orthovoltage X-rays can be described as⁴¹.

1. low skin dose and maximum dose at a certain distance below the surface
2. slow fall-off of depth dose because of high penetration of photon
3. less lateral photon scatter with increasing photon energy because of the decrease in the main photon scattering angle.

Moreover, before irradiating the patient, the computerized physical radiotherapy treatment plan is needed for assuring the following prime conditions^{15, 50}.

- to provide a homogeneous dose of maximum 5 percent variation within the target volume
- to minimize the dose to the surrounding uninvolved tissues
- to keep the tolerance dose of limits for the critical organs

For this assessment, it is very essential to know the dose distributions on a human body. Generally the dose distribution in medium is described²⁷ by the equation:

$$D(X, Y, Z) = D(Z) \cdot QP(X, Y) \quad 1.1$$

where $D(Z)$ is the dose at a depth Z , in the central axis of the beam direction (depth dose) and $QP(X,Y)$ is the dose profile in both crossplane and inplane through that point.

There exists no practical analytical model to account for the accurate dose distributions of human body. Therefore, it depends on some semi-empirical calculations or on measurement from tissue equivalent phantoms. In the commercial treatment planning, the basic dose data (depth dose, profile dose, output values) are measured in water phantom^{27, 50}. For the calculation of dose distributions for human body the measured dose data are to be modified using some correction factor for body curvature, beam obliquity and tissue inhomogeneities¹⁹. So the measurement technique plays an important role for the assessment of body dose distributions.

Various dosimetric methods are available for the measurement of dose distributions. Ionization and film dosimetry are mostly used for homogeneous phantoms. Although these are used in some simple inhomogeneous cases, in sharp dose gradient regions and in complex inhomogeneous situations, the dosimeter having small dimensions like thermoluminescence (TL) dosimeter and diode are specially preferred^{41, 44}. The TL dosimeter has a number of extraordinary properties of tissue equivalent material; it does not require any cable or electrical equipment. Moreover, because of its ability for long term storage of the absorbed dose, the TL dosimeter is used for measurement of dose on patients directly^{43, 37} and to compare the absolute dosimetry of the various centers. It may be mentioned here that the International Atomic Energy Agency (IAEA) and World Health Organization (WHO) have taken a joint program to investigate the output of the machines used at the radiotherapy centers in their respective countries using TL dosimeters⁶⁶. The film dosimetry is good for its spatial resolution and its ability to yield an entire dose distribution with a single exposure. For this, it needs a very definite amount of low dose, which also depends on the depth of the body phantom and can not be reused. On the

contrary the TL dosimeter has the wide range (μGy to kGy) of dose determination capability⁷⁵ and can be reused many times. And due to its small size, it can distinctly resolve the dose at point. It is also hoped that chemical dosimetry will be gradually replaced by TL dosimetry to compare the applied dose values within different related departments²⁰. Thus the applications of the TL-dosimeter for measurement of single point doses are available but the measurement data for dose distributions with TL-dosimeter have not been reported.

The aim of the present study is to measure the dose distributions in homogeneous and inhomogeneous phantom. For homogeneous phantom, the dose distribution at the build up region, penumbra region and asymmetric fields will be emphasized, whereas for inhomogeneous phantoms, the dose distribution at the interface region of different densities and the thorax region has been considered. For this, 4MV and 10MV photon beams from linear accelerators (Mevatron M6300 and Mevatron M7445 of SIEMENS) in the Radiation Physics Department, Gummersbach Hospital, Germany have been used while performing the works mentioned above. The TL dosimeters were first compared with ionization measurement of some standard fields for the given energies in Plexiglas phantom as ionization dosimetry has already been accepted as a clinical tool of dose determination in homogeneous phantom. The following studies were then carried out.

- a. calibration of TL- dosimetry for photon beams of 4.0MV and 10MV energies
- b. comparison of TL- dosimeter measurements with ionization dosimeter for standard fields of homogeneous phantom
- c. comparison of TL- dosimetry with ionization dosimetry in some inhomogeneous situations
- d. comparison of measured dose distributions in human body phantom with predicted values evaluated by computer algorithm⁷⁷
- e. clinical application of TL-dosimeters
- f. TL-dosimeters in total body irradiation.

The results obtained were analyzed with the existing theoretical-physical models. The experience acquired by TL dosimetry can be used for dose measurements on patients and for controlling the irradiation planning system of **Radiotherapy Departments in Bangladesh**. Further TL dosimeter can be treated as a good device for comparison of the therapy doses within different institutions in Bangladesh and as well as the other countries.

2.0 REVIEW OF SOME RELATED WORKS

The TLD dosimeters were selected for dose distribution measurements from the point of view of its precision, resolution and easy handling. Minimization of the cost against benefit must also be included and also from the point of view of cost effectiveness.

In this respect various studies have been reported, some of which will be reviewed in the subsequent pages. While reviewing, the following three points were specially noted

- the TLD application technique
- the different dependent parameters for TL-dose measurement
- the impact of the findings.

Wong, T. P. Y, Metcalfe, P. E and Chan, C. L.⁷⁴ had investigated "The effect of low density media on X-ray dose distribution". They used a lung phantom consists of 8.0cm lung analogue (density = 0.3) sandwiched between two 4.0cm slabs of solid water (density = 1.0). For depth dose measurement of 6 MV and 18 MV X-ray beams, a PTW thimble chamber and a Markus parallel-plate chamber was used. The beam profiles were measured at mid lung using TLD and films for a field size of $10 \times 10\text{cm}^2$. The dose distribution in the secondary interface beyond the air cavity was also investigated.

A negligible discrepancy was observed between the results obtained by measurement and the ETAR prediction for depth dose distribution.

For cross profile using TLD, a holder with a series of holes measuring $1 \times 1 \times 6\text{cm}$, so that each hole accommodated one rod was used. An individual calibration factor was determined for each rod, resulting in a measurement precision of approximately $\pm 5\%$ and to fit the TLD data in order to smooth the results, the penumbra forming functions given by Johns and Cunnigham²⁷ was used. The result of penumbral width measured by film and TLD was compared

with the measurement of the beam profile predicted by the ETAR algorithm. The film results over predict the penumbra flaring. The results obtained by TLD were most accurate. The ETAR algorithm under estimates the penumbra width.

Metcalf Peter et al⁴⁷ studied the dosimetry of 6-MV x-ray beam penumbra using silicon diode, ionization chamber, TLD and film dosimetry. The TLD reading was evaluated using four rods of a batch with known radiation response as standards exposed to 100cGy under standard conditions using this technique, a reproducibility of $\pm 3\%$ of the dose was obtained. Here a side by side clustered of rods was used for dose profile measurement and 5% higher readings were obtained than the readings obtained with TLDs separated by solid water. After renormalization no significant difference could be observed between the profile width and shape predicted within the statistical uncertainty of the results.

They noted that the TLDs show sharper curves in the dose profile than that of diode and film results. This was expected, as the TLD has a better resolution than the diode. The film results showed a similar response to the diode.

Korn, Tomas et al³³ studied the penumbra of a 6.0MV x-ray beam by using TL-dosimetry. LiF thermoluminescent ribbons and rods were used. The TL dosimeters were read in a manual TLD reader (Vicron TLD reader 2800M) in a two step readout cycle (preheat: 160°C per 10s, chips readout: 300°C for 10s, rods readout: 320°C for 12s) after pre-read annealing at 100°C for 10min.s (PTW TLDO annealing oven). All crystals were annealed (1 hr. at 400°C followed by 2 hr. at 100°C) in the oven after each readout. A precision of $\pm 3\%$ of the reading (chips) and $\pm 5\%$ (rods) was achieved. A forming function based on an inverse square root was used to fit the experimental penumbra measurements.

The chips and rods were tested for supralinearity. This was found to be negligible (smaller 3%) in the experiments since only doses of 1.0Gy or less were administered to avoid problems with the supralinearity of LiF.

For profile doses, the TLDs were embedded in solid water holders with holes, which just accommodate one chip or one rod each. All measurements were done in a solid water step phantom. The same measurements were also carried out using diode. The three different effective detector sizes produce a different penumbral width. The largest detector produces the widest measured penumbra.

Feist. H²⁴ has studied the impact of the annealing and reading procedure on the supralinear behavior of LiF thermoluminescence dosimeters. He observed that the measurements with LiF dosimeters in the absorbed dose range up to 6.0Gy strongly depend on the annealing and reading procedure and the extent of the supralinearity. Two annealing procedures have been investigated. A theoretical model, which takes the formation of vacancies, explains the results, by hydroxyl ions into account. A slight effect of the LET is also observed. Since a straight line fit to the measured dose dependent deviations from linearity is possible. A quadratic equation for the calculation of correct absorbed dose values is derived. With this regard three TLD readers were used of them two were manual and one was automatic type. In manual reader, the TLD was heated taking it on heating Al-planchette and in automatic reader, the TLD was heated with hot nitrogen gas. For annealing, the TLDs were taken on an Aluminum tray and put it into the oven. The oven was run 1 hr. at 400°C followed by 20min with temperature of 100°C.

David Steidley K. and Rosen Coleman W¹⁶ studied the dosimetric aspects of 3.3 MV linear accelerator. Here both the design and dosimetric properties of the Siemens Model 5800 linac were observed. They initiate ⁶⁰Co teletherapy for measuring the depth doses. For this a computer controlled water phantom connected with a 0.1cm³ ion- chamber was used for depth doses and beam profiles measurement. For output variation factor a 0.6cm³ PR-06C chamber was used. This equipment was also used for determinations of transmission factor, wedges and trays and HVL measurements. Buildup region dose was measured using parallel plate ion chamber.

A new accelerator featuring a 28-cm long wave-guide to ^{60}Co has been described. It has 58.9% depth dose at 10cm depth for $10 \times 10\text{cm}^2$ field at 100cm S.S.D. and has a d_{max} of about 0.7cm. Since various wave-guides and target combinations were produced for this project. It was possible to study the relationship between d_{max} and a linear relationship was found. The energy of the accelerator from direct electron measurements is 3.3MV. As part of the procedure, central axis depth doses including the buildup regions relation output factors wedge factors, penumbra, beam profile backscatter factors and virtual source position were measured.

Das Indra, J. et al¹⁷ has studied the validity of transition zone dosimetry at high atomic number interfaces by megavoltage photon beams. This paper critically analyses the factors (stopping power ratio and charge collection) for the dose measurements at interfaces. The validity of dose measurements was studied for the photon beams in the range of ^{60}Co gamma rays to 24-MV x-rays at bone and lead interfaces with polystyrene, using TL-dosimeters, extrapolation chamber and several types of commercially available parallel plate ion chambers. It is observed that for energies >10 MV most parallel plate chambers can be used to measure dose accurately. At lower energies, significant differences between measured doses with different detectors were noticed. It is suggested that at high interfaces and lower energies, the dose measurement should be performed with ultrathin window parallel plate ion chambers or extrapolation.

Bengt, K. A. Martensson⁷ has investigated a statistical analysis of the influence of pre-annealing on the precision of measurement. Here the standard deviation of the signals recorded from TL-LiF as a function of the thermal treatment before irradiation (pre-annealing) has been studied. In each experiment, a dose of 70 rad. was delivered on 0.13 and 0.25mm thick LiF Teflon dosimeters. Different factors contributing to the standard deviation are analyzed. A consequence of this is that in pre-annealing, high temperature should be used

for periods as short as possible. If the thermal treatment during the readout (a few seconds at approximately 300°C) is only the high temperature treatment of the dosimeter, a standard deviation of 0.22% in the measured signal can be obtained.

Sevensoon, H. et al⁶⁶ have studied the IAEA/WHO TL-dosimetry service per radiotherapy center. A batch of capsules, all containing LiF powder in Teflon (3mm inner diameter, 20mm inner length and 1.0mm wall thickness) and annealed at 400°C for 1h and at 80°C for 24h is prepared by the IAEA and sent through the WHO in Geneva (to the regional offices of WHO). These offices then deliver the dosimeters to the radiotherapy center. The TLD capsule within a plastic holder was irradiated to 2.0Gy due at 5.0cm water phantom for $10 \times 10\text{cm}^2$ field and sent back to the respective authority.

IAEA evaluated the absorbed dose (in water). Various methods were used for determining the dose. The total uncertainty of the method, using the dose determination from the primary dosimetry laboratories (PSDLs) as a reference had been evaluated. The results obtained were unsatisfactory as 50% of the center had more than 5% deviation of delivering dose.

Dawson, D. J. et al¹⁴ studied the physical parameters associated with the measurement of high-energy x-ray penumbra. Here the effect of dosimeter type and configuration on the measured penumbra distribution for ⁶⁰Co, 6.0 and 31 MV x-rays have been determined in air using equilibrium build up caps for three commercial detection systems including a silicon diode and two ionization chambers. The experimental results establish that the measured penumbral distributions are strongly dependent upon the dosimetric system used. It is emphasized that the diodes approximate photon detectors while ionization chambers are electron detectors.

Gerbi, B. J. and Khan, Faiz, M²⁶ have studied the dose in the buildup region measured by using fixed separation plane parallel ionization chambers. The energies of ⁶⁰Co, 6-, 10-, 18 and 24 - MV photon beam were used. The results

were compared with those obtained using extrapolation chamber and LiF thermoluminescent detectors. The TLD was annealed before use for 1 hr at 400°C followed by 16-24 hr at 80°C. For each measurement point, monolayer of powder was used and only one layer of powder was irradiated at a time. The TLD was always read at least 24h after the exposure to allow for the decay of the short half-life glow peaks. An individual calibration factor was determined for each chip resulting in a measurement precision of about $\pm 3\%$. They found the differences in the percent depth dose at the surface of the phantom of $>19\%$ for one of the chambers. All chambers over responded in the buildup region to some degree based upon their internal dimensions.

They found the TLD method is good for determining the doses throughout the entire buildup region.

Kron Tomas and Ostwald Patricia³⁶ investigated the skin exit dose in megavoltage x-ray beams by means of a plane parallel ionization chamber (Attix chamber). Measurements were performed in the 6 MV and 18 MV x-ray beams of Varian linac 1800. Solid water blocks of $30 \times 30 \text{ cm}^2$ were placed at 100 cm S.S.D on the outside cover of a tennis racquet on the treatment couch. The results obtained with the Attix chamber were compared to TLD measurements under same irradiation conditions.

They conclude that Attix chamber in exit surface dose measurements is well suited to obtain a fast and reliable estimate of the dose received by the skin in the exit portal of megavoltage beams.

Surendra N. Rustgi has studied⁶⁸ the dosimetric properties of a new diamond detector for the measurement of relative dose in photon beam. He studied a profile dose distribution and TMR curves of 6 MV x-ray beam by using 0.14-cm ion chamber diode and diamond detectors at 1.7-cm depth of water phantom. For profile dose, the narrow beam size of $1 \times 20 \text{ cm}$ and $3 \times 20 \text{ cm}^2$ were used. He finds that the spatial resolution of the diamond detector is slightly inferior to that of the diode detector but much superior to that of small volume ionization chambers.

Tsuda. M et al have studied⁷⁰ the LiF and CaF₂. Dy thermoluminescent dosimeters. The characteristics of the LiF glow curve as a function of annealing temperature and time were studied. The annealing method affects the shape of the glow curve. Two heating methods were applied .The TLD 2000A with a planchette whereas the UD-502B applies hot air stream. The period was 10 or 30sec.After annealing, the phosphors were withdrawn from the furnace and cooled down to room temperature. If the annealing procedure and the measurement time after irradiation is constant the fading does not affect the results, except over a long time for uses in personnel dosimetry. For LiF, TLD-600 had a higher sensitivity per ⁶⁰Co gamma rays than TLD-100 and 700. For CaF₂: Dy, glow curves of unusual shape were obtained and its relative response was several times greater than that of normal phosphors.

Thomas S. J. and Thomas R. L.⁷¹ have developed a beam generation algorithm for linear accelerator with independent collimators. Here a method is described of calculating the beam profiles depth doses and output factors for asymmetric fields of radiation. Values are calculated from data measured for symmetric fields. The only additional measurements required are a beam profile in air across the diagonal of the largest field size, and data on radial variation of beam quality. Measurement on beams of 8.0 MV x-rays show that beam hardening in the flattening filter can alter the beam properties by several percent.

Van Dam, J and Marinello, G.⁷² has published a booklet of methods for in-vivo dosimetry in External Radiotherapy. Here some very useful methodology in regards to target dose determination precisely in the in-vivo system using TLD and diode dosimetry has been discussed.

Kannan, a. et al³⁵ in their publication described signal correction technique for dose measurements with TL dosimeters. They identified problems encountered for reliable dose measurements with TLD. These are (a) the sensitivity variations of the photo-multiplier which measures the light emitted by the

phosphor and (b) the variations in the heating rate of the phosphor due to small changes in the contact resistance of heater. After making correction for the signal drift, the TL dose was found to be linear in the range of 1.5 to 2.5 Gy at ^{60}Co energy.

Jens Juul Christensen and Akmal Ahmad Safwat, M. D.²⁸, has determined the dose to the lung, calculated. Here the dose distribution in lung tissue of an Alderson phantom was measured under TBI conditions. From the distribution, the dose to the central plane of the lung is selected and compared with both calculations based on the beam zone method and with entrance and exit dose measurements using diodes. The agreement is fine and in the order of the uncertainty of the TLD measurements.

Carl, A. Carlsson¹¹ has studied the thermoluminescence of LiF: dependence of thermal history. The work examines the influence of various thermal treatments on LiF to derive appropriate methods of using LiF suspended in Teflon (C_2F_4)_n, for obtaining higher precision of the dosimetry. For precision, it is suggested that pre annealing at high temperature should last only long enough to give thermal equilibrium and to empty all filled traps. Especially important is reproducibility of the cooling rate. With an appropriate heating circuit, both pre- annealing and cooling rate can be satisfied with the readout heating.

Ciesielski, B and Reinstein, L. E.¹² has evaluated the change in dose distributions in buildup region resulting from the presence of lead, aluminum, and Lucite absorbers above the surface of a polystyrene phantom. Data were taken using a parallel-plate chamber (PTW/Markus)(diameter = 5.0 mm, plate separation = 2mm) and chamber window of 2.3 mg/cm² thickness. The surface dose, as well as the influence of the air gap between the lead absorber and the phantom surface. It has been found that the surface dose does not depend in absorber thickness for absorbers thicker than the range of secondary electrons in the absorber material (after corrections for the attenuation of the primary beam in the absorber). Similarly, the depth dose curves in the phantom

were carried out only at depths lower than the range of secondary electrons in the phantom. The applicability of the presented data in clinical radiotherapy is discussed.

Nilsson, B and et al.⁵³ has been investigated the interface effects in ⁶⁰Co beam using a thin-walled parallel plate ionization chamber. The chamber has been used to perform detailed experimental investigations on interface phenomena in transition zones using a wide range of elements ($z = 4-82$) as front and back-scattering layers and clinically relevant ⁶⁰Co γ -ray field sizes. The effects of the configuration of the chamber (wall thickness, cavity height) and experimental setup (depth of measurement) on the measured ionization have been investigated. Results show the dose at interface depends on the depth of measurement, due to the increasing component of low-energy secondary photons when the thickness of scattering material increases.

The simple geometry of the ion chamber has been found optimum for benchmarking Monte Carlo calculations, making it possible to investigate experimentally the effect of varying transport parameters used in Monte Carlo simulations. The results presented show that the complex physical mechanisms governing interface dosimetry, particularly regarding the validity of multiple collision models for energy losses and scattering, still make Monte Carlo condensed-history (macroscopic) techniques uncertain. The uncertainty in using different ⁶⁰Co spectra as input to the calculations (about 5%) must however also be pointed out. It is therefore important to emphasize the development of accurate experimental methods, which can be used to overcome the limitations.

Meigoon, Ali. S. et al.⁴⁹ in their publication have experimentally determined the effect of nitrogen gas flow in the TLD reader on the sensitivity, linearity and accuracy of lithium fluoride TLD responses and obtained their low dose limits as a function of TLD size. The investigations were performed using two different TLD sizes, $3.1 \times 3.1 \times 0.89 \text{ mm}^3$ (referred to as large chips) and

1×1×1mm³ (small chips). Measurements were performed using γ -rays from ¹³⁷Cs or x-rays from a 4.0 MV linear accelerator. They found that the nitrogen gas flow reduces the standard deviation of TLD sensitivity when exposed to doses less than 5.0 cGy by up to 200%.

Pradhan, A. S. et al⁵⁶ had investigated the dose measurement at high atomic number interfaces in megavoltage photon beams using TLDs. They used LiF TLD -700 and CaF₂ Dy TLD - 200 powders having average grain size of 150 μ m from Harshaw. A 3.0-mm thick lead plate was taken at 5.0-cm depth of polystyrene phantom. A dose of 0.5 Gy at 5.0cm depth in the phantom for the photon beams of 6.0 MV and 10.0MV was delivered. They obtained 6% to 10% lower dose values (using inhomogeneous to homogeneous ratio) by using CaF₂: Dy than those obtained by LiF.

The reviews reveal that a very high accuracy in dosimetry is needed for normal tissue and for tumor control. To achieve the proposed accuracy level (within $\pm 5\%$ for the delivery of the prescribed dose) is very difficult. Since, one of the most difficult areas of the radiotherapy procedure is the ability to measure the accurate dose, the scientists have preferred the small volume ion-chambers diode, thermoluminescent and film dosimeters. They found the ion-chamber measurements in steep dose gradients and of small beam measurements to be not very satisfactory. This is either the effect of chamber volume or the lack of lateral equilibrium. Techniques for correcting these errors have been reported and the measurement data have been verified using two or more dosimetric methods.

Those papers were selected in which the TL-dosimetry was used for dose measurement. These were helpful to get information about the techniques and the influences of the different effects for establishing the TLD as good dosimeters.

3.0 THEORETICAL ASPECTS OF THERMOLUMINESCENCE⁴³.

Luminescence describes the process of emission of optical radiation from a luminescent material. Luminescent materials (luminophors-light bearers) can absorb energy, store a fraction of it and convert it into optical radiation, which is then emitted. Heating the luminescent material speeds up this optical radiation; hence the process is called the thermoluminescence (TL).

3.1 Mechanism of thermoluminescence

All real crystal contains lattice defects of various kinds and these play an important role in the thermo-luminescent process. The mechanism of TL-process is complex and several models have been suggested but none fully explains the phenomena, particularly the precise roles of the impurity in the trapping and luminescence recombination process.

3.1.1 *The role of lattice defects in the TL-process.*

The presence of defects in a material is important for TL- process. For intrinsic defects, a negative ion vacancy is essentially a region of excess positive charge and as such may be regarded as a potential trap for a free electron. Similarly, a region of excess negative charge will be a potential trap for free positive charge (holes).

The energy band structures for ideal crystal may be represented by energy band diagram as shown in Figure 3.1a. The valence band is a representative of all electrons held in bound states, and the conduction band is a representative of all electrons in unbound states, which are free to migrate through the crystal lattice. In the present discussion, the conduction band will be empty and all

electrons will reside in the valence band. The conduction band and the valence band are widely separated in the energy by the so-called 'forbidden gap'. Without the influence of external forces it is highly improbable for an electron to be able to traverse the forbidden gap from the valence band to conduction band. However, in the case of a crystal containing defects of a simple and or complex nature, other allowed energy levels exist in the forbidden gap region as illustrated in Fig 3.1b. In the description of the general model the energy level labelled E represents an electron trap and the level H represents a hole trap. L is a luminescence centre where electrons and holes may recombine with photon emission.

3.2 A general model for thermoluminescence

The production of thermoluminescence in a material by exposure to ionizing radiation may be divided into two stages:

- i) ionization and electron trapping, and
- ii) electron and hole recombination with photon emission.

Figure 3.2 illustrates the energy band configuration for each stage. Ionizing radiation is absorbed in the material and free electrons are produced. With respect to the energy band diagram this is equivalent to transferring electrons from the valence band to the conduction band (step-1). These electrons are now free to move through the crystal (step 2), but if trapping labels such as E are present the electrons may become trapped (step-3). The production of free electrons is associated with the production of free positive holes, which may also migrate, in energy terms, via the valence band (step-2'). The holes may become trapped (step-3'). The trapped electron centers are lattice defect centers and as such their properties are primarily determined by the lattice and the defect. Many hole-centers are thermally unstable and may decay rapidly at normal room temperature (step-4').

The trapped electrons will remain in their traps provided that they do not acquire sufficient energy to escape. This will be determined by two main factors: the depth of the traps and the temperature of the material. If the temperature of the material is raised, trapped electrons may acquire sufficient thermal energy and be released (step-4). Released electrons may recombine with holes at luminescence centers such as L, and the excess energy is radiated as visible or ultra-violet photons (step-5). While electron capture and delayed recombination with hole at a luminescence center which is the mechanism of thermoluminescence, other electron-hole recombination processes are possible. That is, immediate or delayed recombination with subsequent thermal degradation of energy without photon emission, and fluorescence caused by the immediate recombination of holes and electrons at luminescence centers.

3.3 The TL-process in Lithium Fluoride doped with magnesium and titanium.

The TL-phosphor most widely and intensively studied is lithium fluoride doped with magnesium and titanium–LiF (Mg, Ti). Many difficulties have arisen in understanding the theoretical significance of results of experiments performed on this material, primarily the uncertainties in standardization of phosphor composition. However, it is clear that the TL-process in LiF (Mg, Ti) is complex and is critically dependent on a number of factors including the amount and type of impurities present, their chemical form and method of introduction into the lattice and the thermal, optical and mechanical treatment of the phosphor during its manufacture and use.

3.3.1 *The thermal effect and resulting glow curves.*

If LiF: Mg, Ti is given a pre-irradiation anneal at 400°C (standard phosphor anneal of one hour) and cooled quickly to normal ambient temperature, the resulting glow curve after irradiation contains at least six glow peaks between normal ambient temperatures, and 300°C, as illustrated in figure 3.3. By

convention these are named peaks 1(60°C), 2(120°C), 3(170°C), 4(190°C), 5(210°C) and 6 (285°C). The precise read out temperature and the resolution of each peak will depend on the heating rate employed. Peak 4 & 5 are normally used for practical dosimetry. The low temperature peaks exhibit high fading of stored signal even at normal ambient temperature; the half-life of each peak at normal ambient temperature is also shown in figure 3.3A.

Either the peak height or the total area under the glow curve may be taken as a measure of the original ionizing radiation exposure. Each trapping level will give rise to an associated glow peak maximum, which may or may not be resolved during readout. The area and peak height of each glow peak depends on the number of associated electron traps present. This in turn depends on the number of lattice defects and, for real phosphors, on the type and amount of impurity atoms present, as well as on the thermal history and temperature of the materials. It is possible, however, effectively to reduce the number of electron traps with which the low- temperature are associated by thermally annealing the material for 1-2 h at 100°C or 16-24 h at 80°C prior to irradiation. This procedure results in the much more satisfactory glow curve also as shown in figure 3.3B.

3.3.1(a) *The role of magnesium and titanium ions*

The magnesium ions are presumed to form electron traps in combination with certain defect centers in the lattice. The influence of titanium in the trapping process is unclear and its role is thought to be primarily in the formation of luminescence recombination centers. The divalent magnesium ion (Mg^{2+}) is introduced into a lattice consisting of an array of monovalent lithium (Li^+) and fluorine (F^-) ions. The substitution of Li^+ ion by Mg^{2+} ion results in an excess positive charge at the lattice site. Coulomb attraction results in the formation

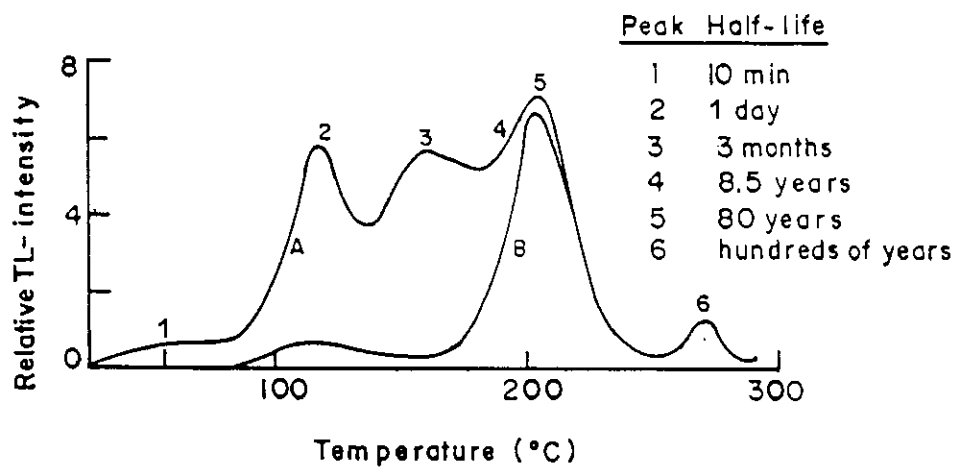


Fig. 3.3 Glow curves for LiF : Mg.Ti (TLD 100) annealed for 1 hr. at 400 °C followed by: A, Cooling (10^3 °C min^{-1}) to normal ambient temperature ; B, 16 hr. anneal at 80 °C , followed by irradiation.

of nearest - neighbor pairs (dipoles) consisting of a substitution Mg^{2+} ion in combination with a Li^+ ion vacancy. Under certain thermal conditions the dipoles are believed to aggregate forming dimmers, trimmers and higher-order complexes. There is evidence that the simple dipole arrangement is associated with the electron trapping centers responsible for the low - temperature glow peaks 2 and 3 (Figure 3.3). Dipole complexes are associated with the main dosimetry glow peaks 4 and 5. The aggregation of simple dipoles to form complexes is crucially dependent on temperature, and heating and cooling rates. Dipoles are electrically neutral in the lattice in the actual electron-trapping center. This model for trapping can be used to explain the changes in the relative heights of the glow peaks due to pre-irradiation annealing of the phosphors. Indeed this is true for any anneal temperature above about $180^{\circ}C$. With increasing anneal temperature simple complexes such as dimmers and trimmers are broken up into dipoles, producing the relatively large peaks 2 & 3. If the phosphor is then annealed at a temperature $< 100^{\circ}C$, as such as for 1 or 2 h at $100^{\circ}C$ or 16-24h at $80^{\circ}C$, aggregation occurs enhancing the main dosimetry peaks 4 & 5 at the expense of the low - temperature peaks. Further evidence for aggregation is provided by examining the effect on the glow curve of the cooling rate from $400^{\circ}C$ to normal room temperature. If the phosphor is cooled rapidly a number of associated trapping centers are frozen into the lattice resulting in a relative enhancement of peak 2. A slower cooling rate allows aggregation, which relatively enhances peaks 4 & 5. A Very slow cooling rate results the formations of higher order complexes and Mg precipitation and a reduction of peaks 4 & 5. It has been suggested that peaks 1 and 6 be not directly connected with the presence of either magnesium or titanium but possibly with intrinsic lattice. However, Attix (1975) has suggested that peak 6 may be associated with magnesium dipole trapping centers which have trapped more than one electron.

3.3.1(b) *The role of titanium and hydroxyl ions.*

The presence of titanium in combination with hydroxyl (OH) ions is a prerequisite for efficient thermoluminescence emission in LiF. All crystalline materials grown under air from their melt contain OH ions in concentrations of several tens of parts per million. The thermoluminescence sensitivity of LiF:Mg:Ti has been shown to increase with increasing concentration with titanium ion present to a maximum content of 7 ppm. Where high concentrations of titanium exist the thermoluminescence sensitivity appears to be controlled by low OH ion concentration and vice versa. The results of ionic conductivity experiments indicate that titanium may be present in the divalent state Ti^{2+} , possibly forming $Ti^{2+} - Li^+$ vacancy dipoles in a similar manner of Mg^{2+} . As the concentration of titanium appears to change the relative shapes of the glow peaks it may also be involved in an unknown way in the formation of electron trapping centers.

4.0 MATERIALS USED FOR EXPERIMENT AND THEIR IRRADIATION FACILITIES

4.1 TLD material and TL-dosimetry

For the studies mentioned in chapter 1, the TL-dosimeters of 1-mm diameter × 6-mm length as employed in radiotherapy were used. The dosimeter (TLD-100) was made of LiF crystal containing the natural isotope of lithium (7.41%⁶Li + 92.6% ⁷Li) doped with magnesium and titanium^{6, 44}. A total number of hundred rods were obtained from Harshaw Chemical Company. The rods shown in figure 4.1 were chosen for their size and for easy identification compared to chips and powder TLDs.

For TL-dosimeter system, the followings are to be used:

- Oven (PTW-TLDO) with two heating programs. The program-1 runs at temperature 400°C for 1-hr followed by 100°C for 3hrs. And the program-2 runs at temperature 100°C for 20 minutes.
- Reader (Harshaw QS, 3500 model) associated with a commodore PC 50-II named as TLD shell model program.

Reader (TLDO, PTW)

Heating and light collection are made in a readout system called the reader (Figure 4.1, 4.2). In the reader the irradiated dosimeter is placed on a heating support called planchette, situated within the readout chamber. The readout temperature is used to collect the information from the dosimeter. The temperature to the support is supplied by a thermocouple, which is in close thermal contact with it. The light emitted by the hot LiF -TL passes through one or more optical filters and then goes to a photomultiplier tube (PM-tube). The light output collected from the PM-tube is proportional to the light emitted by the TLD and therefore to the absorbed dose previously received by the TLD

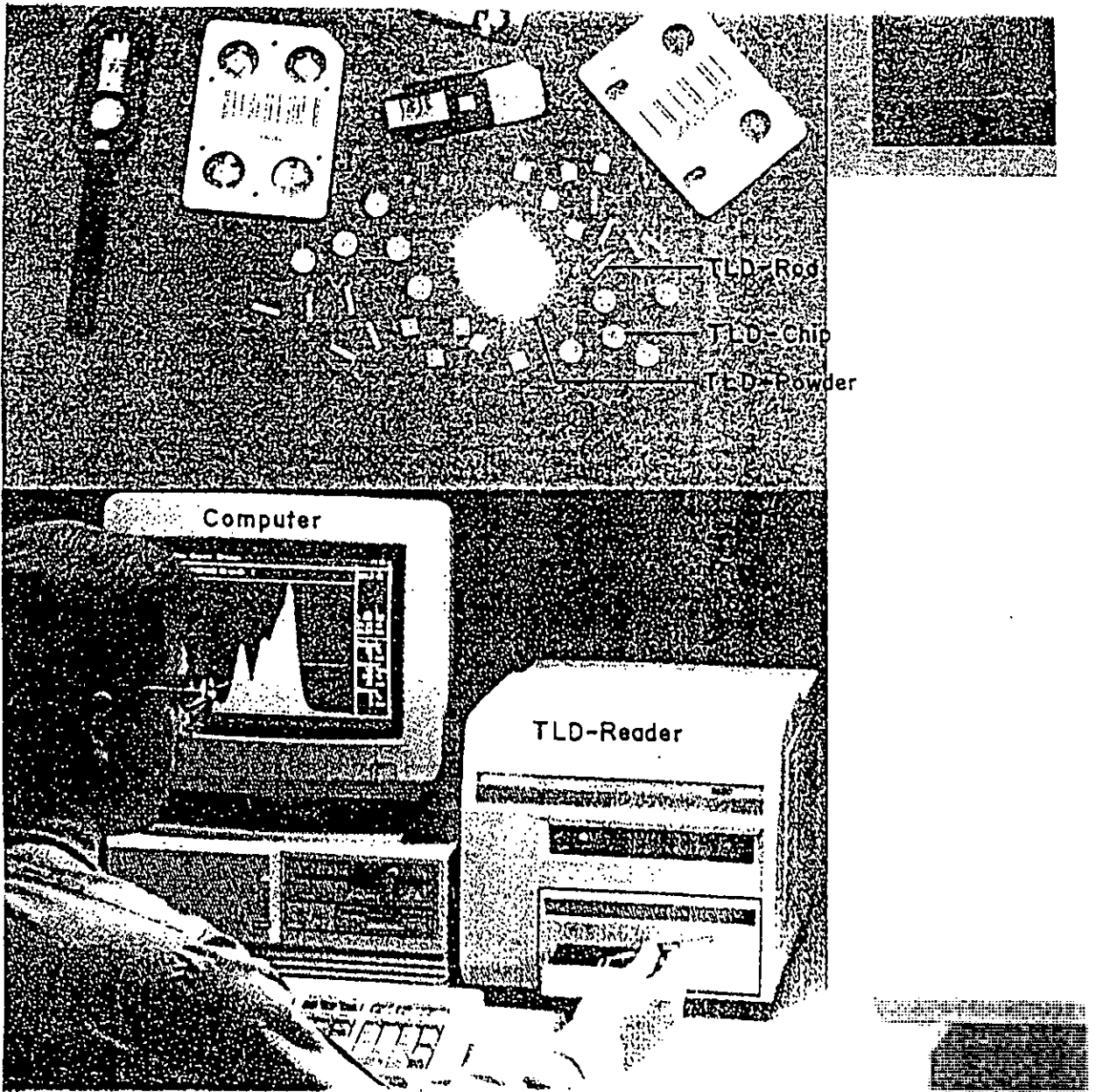


Fig. 4.1 Different forms of TLDs and a TLD-reader associated with a computer.

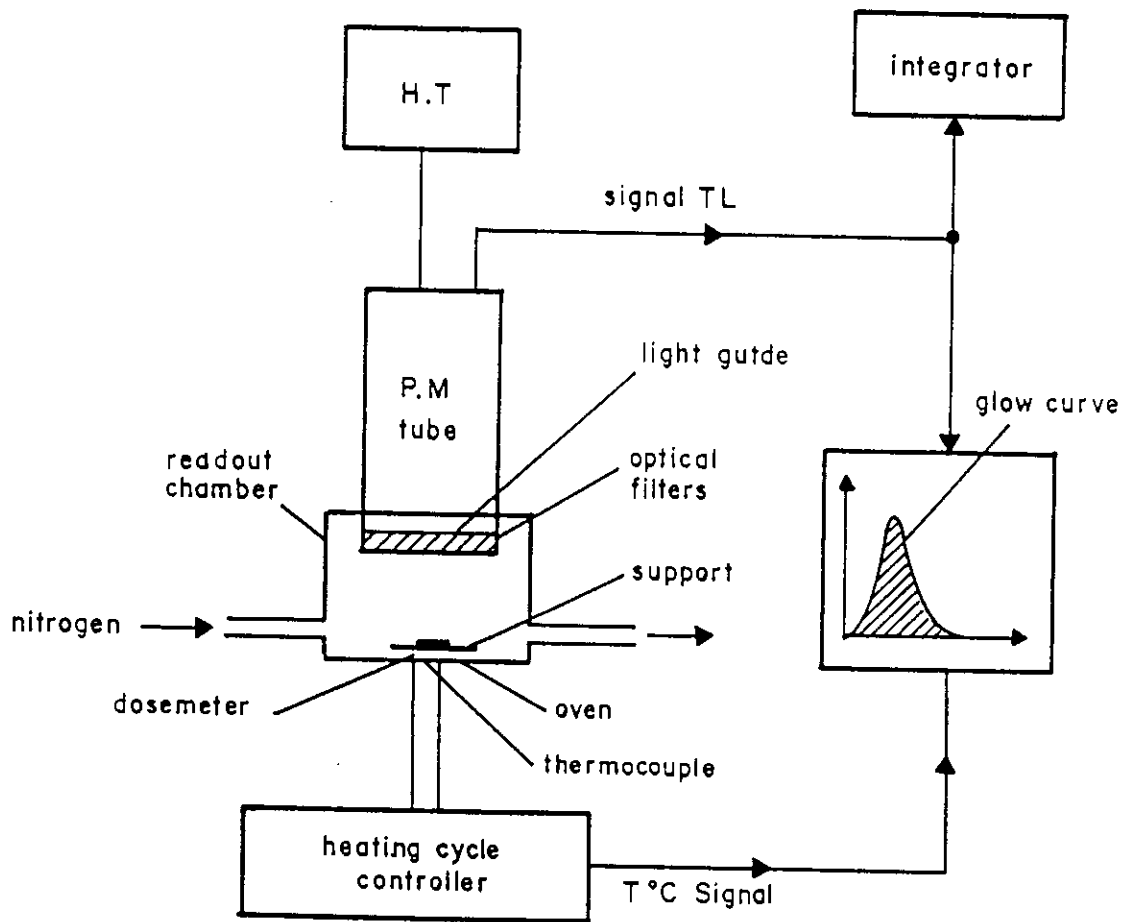


Fig.4.2 Schematic diagram of a classical TLD reader.

itself. The TLD is heated with increasing linear temperature of the readout system. The close contact between TL-dosimeter, planchette and heating system is necessary to obtain a good reproducibility. The whole unit has to be switched on for at least 30 minutes before use so as to obtain the voltage stability and hence to obtain good reproducibility of measurements. The result has to be converted in to absorb dose and can be stored on the computer disk. The glow curves are also displayed during dose measurements.

4.2 Reference dosimetry system

An ion-chamber of cylindrical type (0.3 cm^3 ; Normal M 233332, PTW, Freiburg) and a Markus chamber of circular disc type dosimeter having a very thin surface and small volume (0.02 cm^3 , PTW Freiburg) along with the following accessories were used as a reference dosimetry:

- two electrometers (DL4D, DL4I)
- thermometer
- barometer

Electrometers

The charge (or current) induced in an ionization chamber is extremely small which is measured by a very sensitive charge measuring device known as electrometer. Such instruments are delicate and must be handled with care. Ideally, the electrometer should be provided with a digital display and should be capable of four-digit resolution.

The electrometer and the ionization chamber can be calibrated separately. However, in some cases the electrometer is an integral part of the dosimetry system and the ionization chamber and electrometer must be calibrated as a unit.

4.3 Irradiation facilities

The irradiation facilities of high-energy photon beams were taken from linear accelerator available in the therapeutic physics department in Gummersbach hospital, Gummersbach, Germany. The energy of the photon beam and the type of the accelerators were as follows:

- 4.0 MV; Mevatron M 6300, SIEMENS
- 10.0 MV; Mevatron M 7445, SIEMENS

A detailed description of a linear accelerator is described in appendix A.

4.4 Phantom

The phantom made with Plexiglas ($C_5H_8O_2$; $\rho = 1.136 \text{ g/cm}^3$), a tissue equivalent material, was used for the measurement of the absorbed dose from high-energy photon beam. The phantom consists of different thickness of plates so that by placing on top of each other, any depth could be used for the dose measurement in the total volume of $30 \times 30 \times 30 \text{ cm}^3$. For TL-dosimeter the rod-size grooves arrangement ($1 \times 1 \times 6 \text{ mm}^3$) were made on the central surface of a plate (Figure 5.2). For chamber dosimeter, the same size of chamber and cable size hole along the central thickness of a plate was used.

5.0 THERMAL TREATMENT AND THE REPRODUCIBILITY OF THE TL-LiF CRYSTAL DOSIMETERS.

5.1 Introduction

The basis of the TL-LiF crystal dosimetry is to expose the crystals to radiation and then measure the energy stored by the application of heat. The current of the PM-tube is recorded as a function of time, corresponding to the increase of heating temperature. This record is called the glow-curve⁷⁰. In the figure 3.3 the characteristic and the glow-curve of a LiF crystal dosimeter is investigated. The area under the glow curve, which is proportional to the number of emitted photons, has been used as a measure of absorbed dose.

It has been reported that after irradiation, peak-1 through 5 decays at room temperature with approximately the following half-lives 5min, 10hr., 0.5yr., 7.0yr., and 70yr respectively. Because of long-time stability, peak 4 and 5 are most suitable for dosimetrical^{42, 43,79} use. Stability and reproducibility of the glow curve would assure the use of LiF crystal rod as a dosimeter.

As the TL-LiF crystal rods have all been taken from the same manufacturing run. They may be assumed to have consistent "batch characteristics", which include TL fading, dose response, non-linearity and energy dependence³⁰.

5.2 Four-step application-cycle for TL-dosimeter

For dose measurement and as well as for re-using the TL-dosimeter, a four-step application-cycle described below was followed.

First step: Pre-irradiation annealing of the TL-LiF dosimeters.

The pre-irradiation annealing of the TL-dosimeters was done by taking the TL-LiF crystal rods on the two different heating trays (the hundred LiF rods were

taken into two groups for easy handling) into the oven (PTW-TLDO, Freiburg). The trays were made of stainless steel on which circular disk-type grooves (supplied by Harshaw) were arranged. The TL-LiF crystals were identified by their arrangement on these grooves. Using the heating programme-1, which heats the oven at a temperature of 400°C for 1-hour followed by 100°C for 3-hours. As the thermal pre-irradiation annealing takes a long time, so, it was carried over the whole night. After completing the heating cycle of the oven, the LiF rods were found to be stored at 30°C in the oven. The thermal treatment of TL-LiF crystal dosimeters was done for complete bleaching of the previous dose information and for re-generation of the specific defect in the crystal⁷.

Second step: Irradiation of the TL-LiF crystal dosimeters.

For irradiating the dosimeters, photon beams of 4.0 MV energy from Mevatron M6300, Siemens was used. Grooves for holding the LiF crystal were made on a plexiglas plate (Figure 5.2b) and the LiF-crystal rods were put there. The plexiglas plate with these dosimeters was kept into the 5.0 cm depth⁷⁹ of phantom (30 × 30 × 30 cm³) of the same material. For 1.0 Gy dose at 5.0 cm (5.68 cm water equivalent) depth, the calibrated monitor unit (MU) for 10 × 10 cm² field at 100 cm source to surface distance (S.S.D) were delivered from the linac. The MU was carried out from the measurement using the standard ionization chamber (P.T.W, Freiburg) for the same photon beam condition. On receiving the dose from ionizing beams, the electrons of the crystal are transferred to the different trappings.

Third step: Pre-readout annealing of the irradiated TL-dosimeters.

This part of the cycle is sometimes called post-irradiation annealing. After irradiation, the TL-dosimeters were again taken on the heating tray as before and were annealed with 100°C for 20 min using the program-2 of the same oven (PTW-TLDO). The pre-readout annealing was done to make the lower trap free of electrons before readout. This minimizes the variation of the total

charge (nC) in the glow-curve due to fading (The fading may be due to thermally or optically stimulated release of the electrons or a combination of both before readout⁴³)

Fourth step: Readout of the TL-dosimeters

To read the TL-light of the irradiated LiF-crystal dosimeter, the manual reader, Harshaw QS, 3500 model associated with Commodore PC 50-II was used. In this reader, the heat to the TL-dosimeter was supplied through the planchette of stainless steel contact. The heating and cooling rate of the planchette is automatically controlled by the Time-Temp. -Profile (T.T.P), of the P.C. For every TL-dosimeter readout, the program maintained the following T.T.P file.

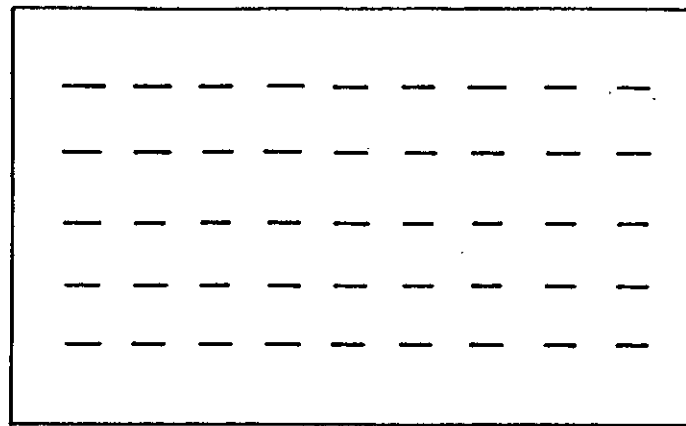
Calibration region 1 to 200 channels.

Pre-heat temp	80°C; 0 sec.
Acquire rate of temperature	10°C/sec.
Maximum temperature	300°C
Measurements time	30 sec.
PMT- High voltage	827 V

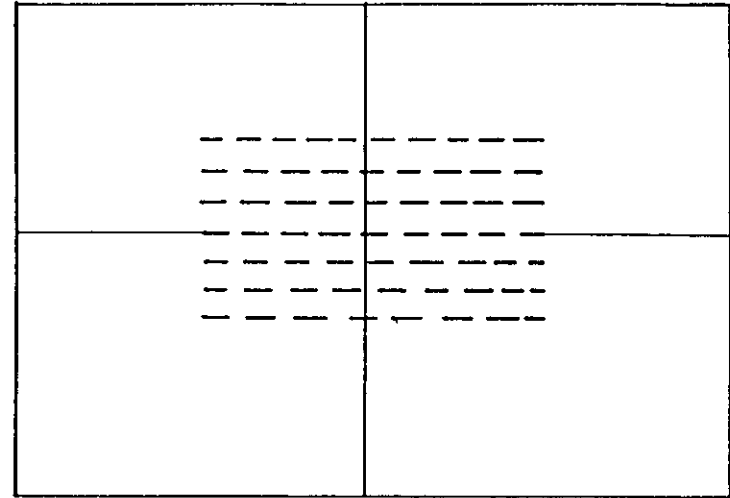
The light output (glow curve) over the calibration region was recorded from the charge collection through the photo-multiplier (PM) tube in nano-coulomb (nC) and was read out from the PC-screen. This charge directly reflects the absorbed dose from the photon beams. To read the charge value obtained from the glow-curve, the first step of the calibration procedure on the program ver.25282.004 was used. The dosimeter file preserves the light output value with a definite given identity number as arranged in the tray. Before starting the readout a minimum 30min was allowed for warm-up of the PM-tube of the reader.

For each LiF dosimeter, the procedure was repeated 20 times and the reproduced total charges (nC) of the glow curve was recorded. This was done to check the reproducibility of the dosimeters. Thus, the reproducibility

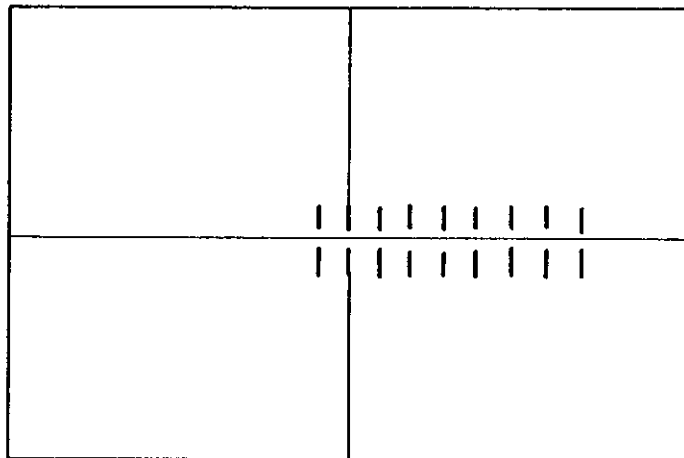
of the dose sensitivity (charge obtained for 1.0Gy absorbed dose for a certain definite quality of the reader) variation of the individual TL-LiF crystal dosimeter for the last 10 reading pursued over the 20 repeated uses were observed. The result obtained for the first 20 identified TL-dosimeters was shown in figure 5.3. Initially all had higher sensitivity, which then fluctuates significantly for the successive measurements. The experiment was repeated 10 times more by taking LiF dosimeters on an Aluminum tray^{24, 49} instead of the stainless steel tray. Cylindrical type of grooves having the same size of TLD rod was made on the tray for placing the dosimeters (Figure 5.2a). Great care was taken to make sure that the tray was always at the same position in the oven. This was ensured by marking the tray corners and always loading it at the same geometrical condition on the platform in the oven. The cooling temperature of the oven was always maintained at 45°C. After reproducing the pre-irradiation annealing of the TL-dosimeters the TLD-tray was withdrawn from the furnace and cooled down to room temperature. A minimum time of 30 minutes¹¹ was allowed for the dosimeters to come to the temperature of its surroundings before irradiation. Then during readout, a strong care was taken for loading it on the planchette always at the central diagonal position (reader drawer required to be closed and opened slowly). During read out of the TL-dosimeter, the cooling temperature of the read out cycle was maintained at 45°C. As a result, most of the sensitivities of the TL-dosimeters were found to be less fluctuating and the variation of the successive sensitivities from the average value obtained for the last 5 reproducible sensitivity were assessed as shown on the same figure 5.3. A total of 83 TL-LiF crystal rods were found to have a variation within 5% and the remaining 17 rods found to have a fluctuation of more than 5%. These were taken out and were not used in the subsequent calibration procedures.



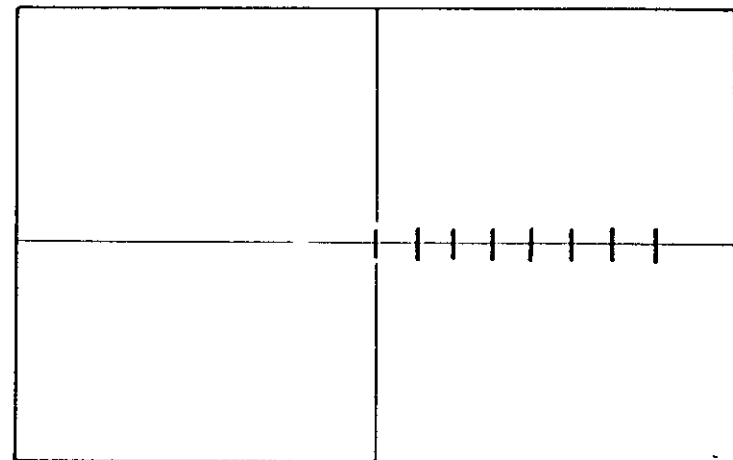
(a)



(b)



(c)



(d)

Fig. 5.2 Arrangement of grooves to put the TLDs (a) on heating tray of Aluminum plate (b) on plexiglas plate during exposure for calibration (c,d) on plexiglas plate during exposure to dose distribution measurement.

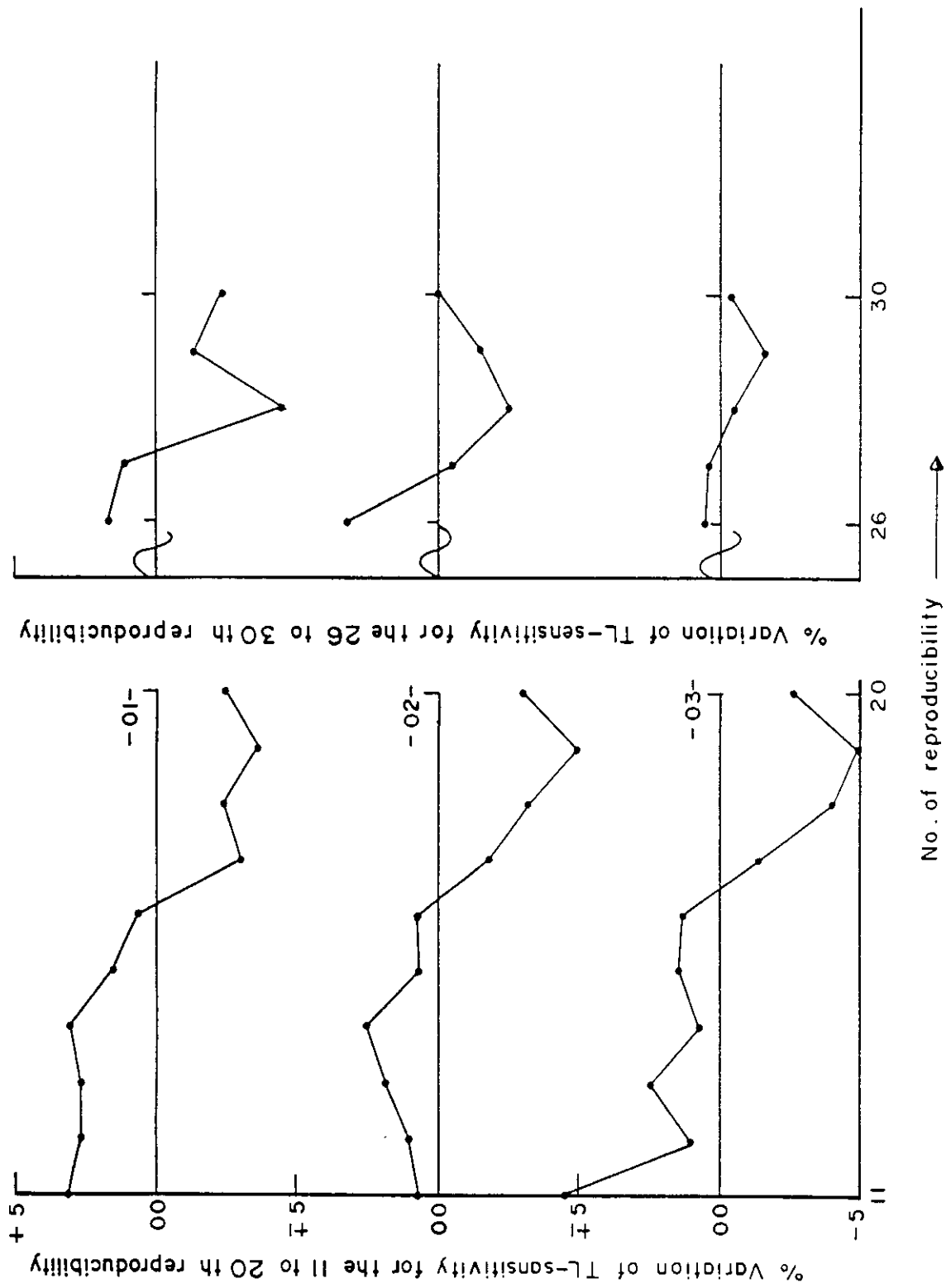
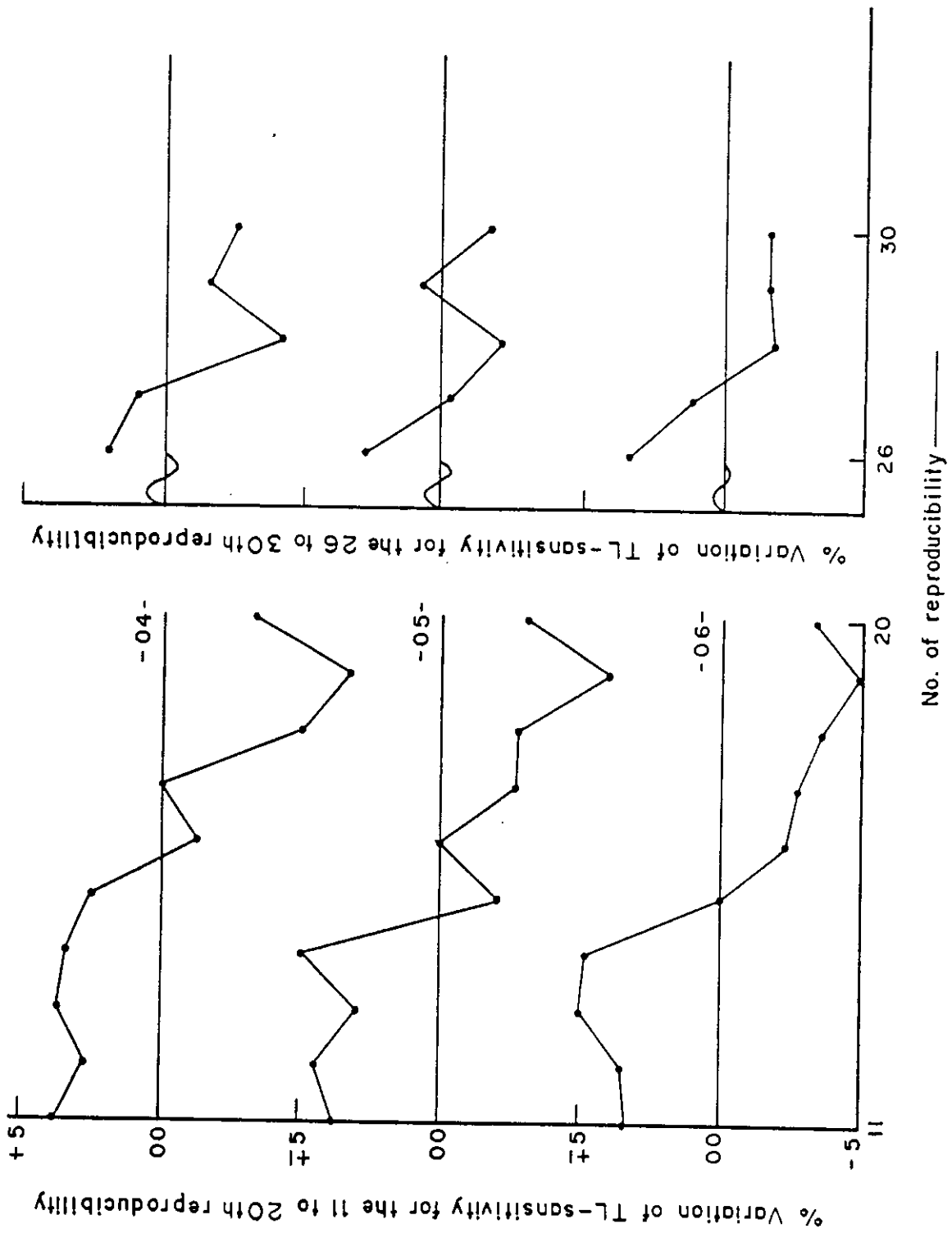
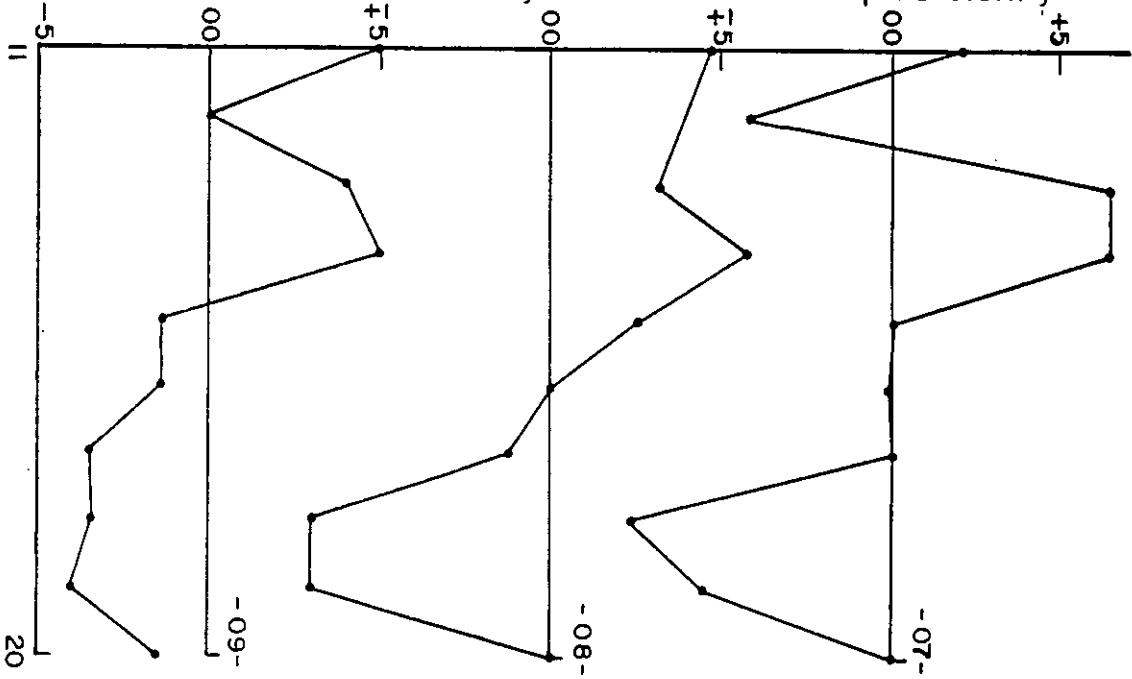


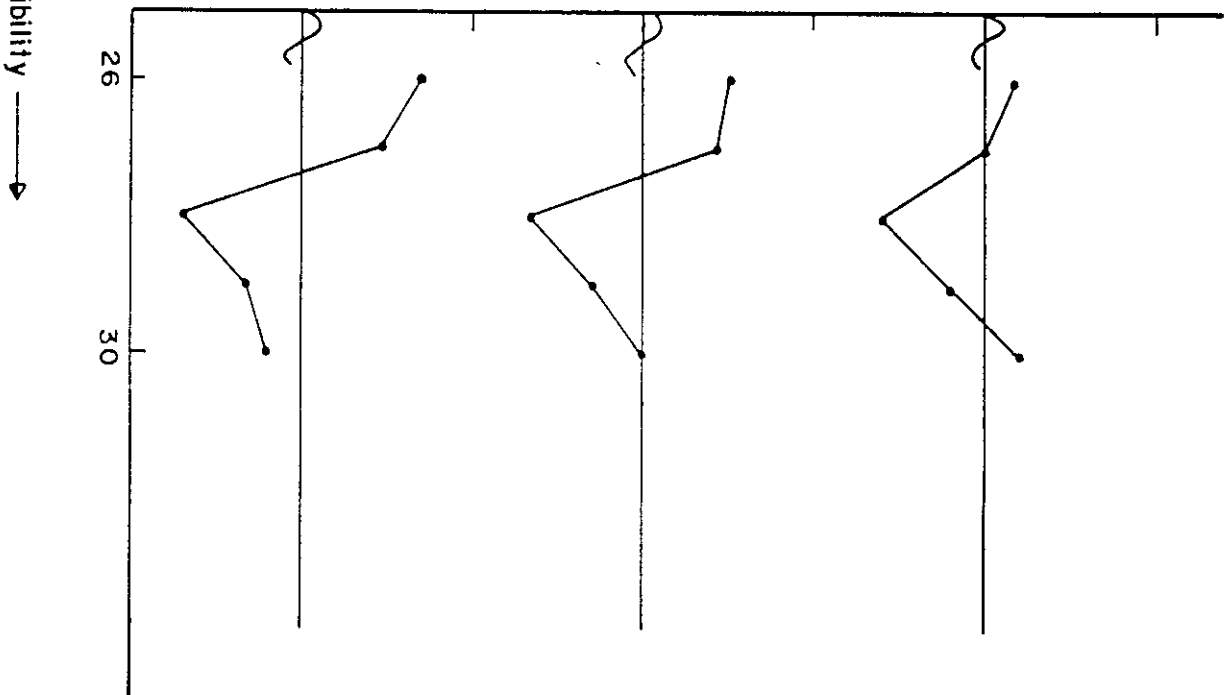
Fig. 5.3 Variation (%) of the successive sensitivities from the average value obtained from the reproducible sensitivities.



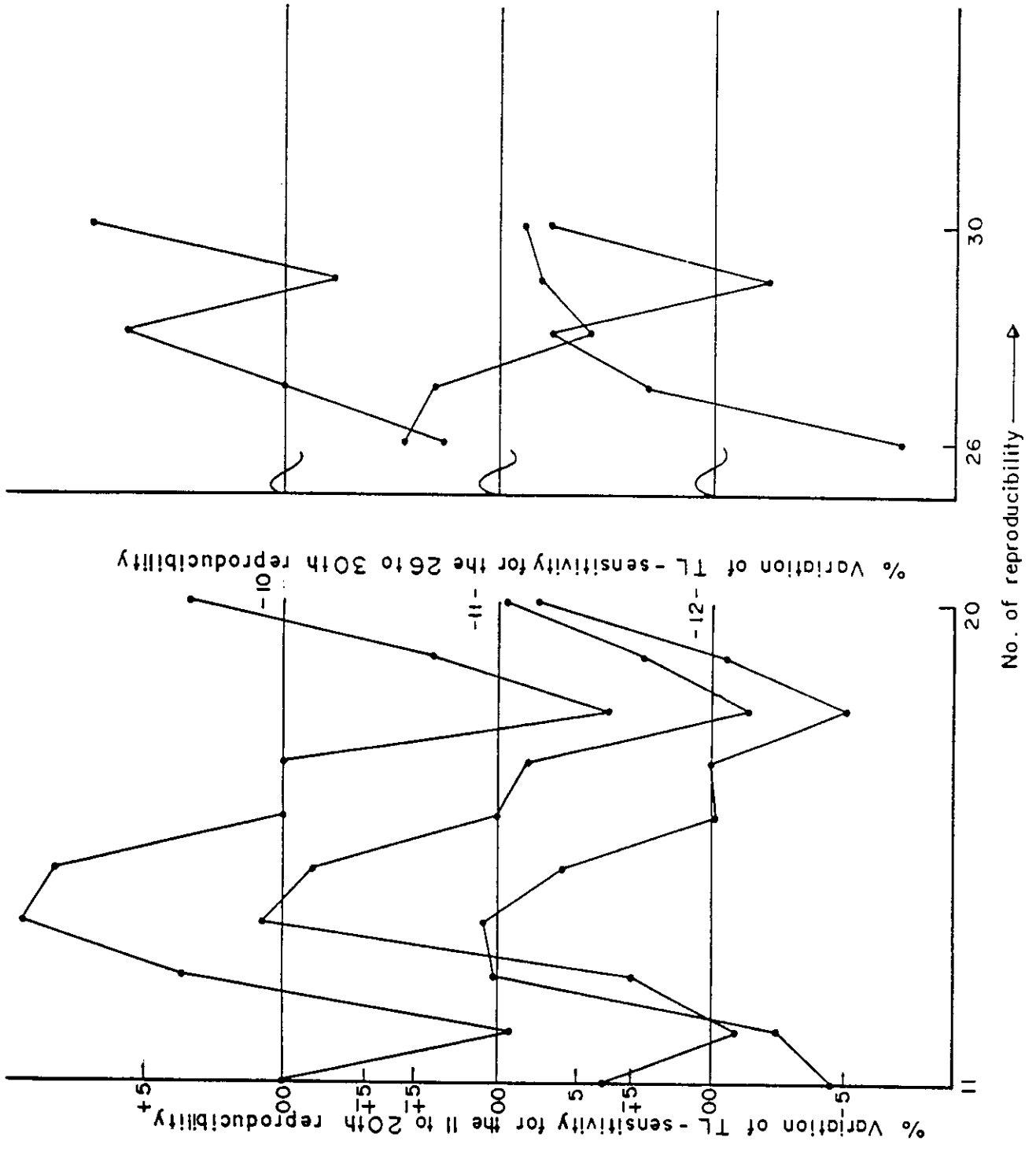
% Variation of TL-sensitivity for the 11 to 20th reproducibility



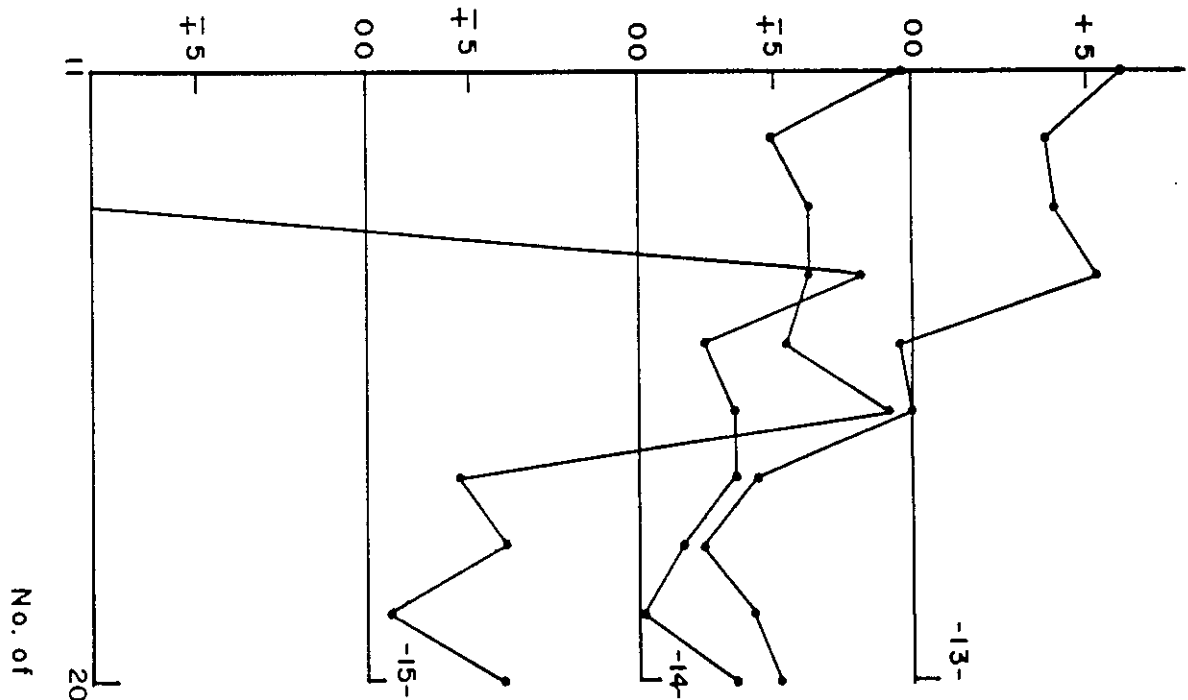
% Variation of TL-sensitivity for the 26 to 30th reproducibility



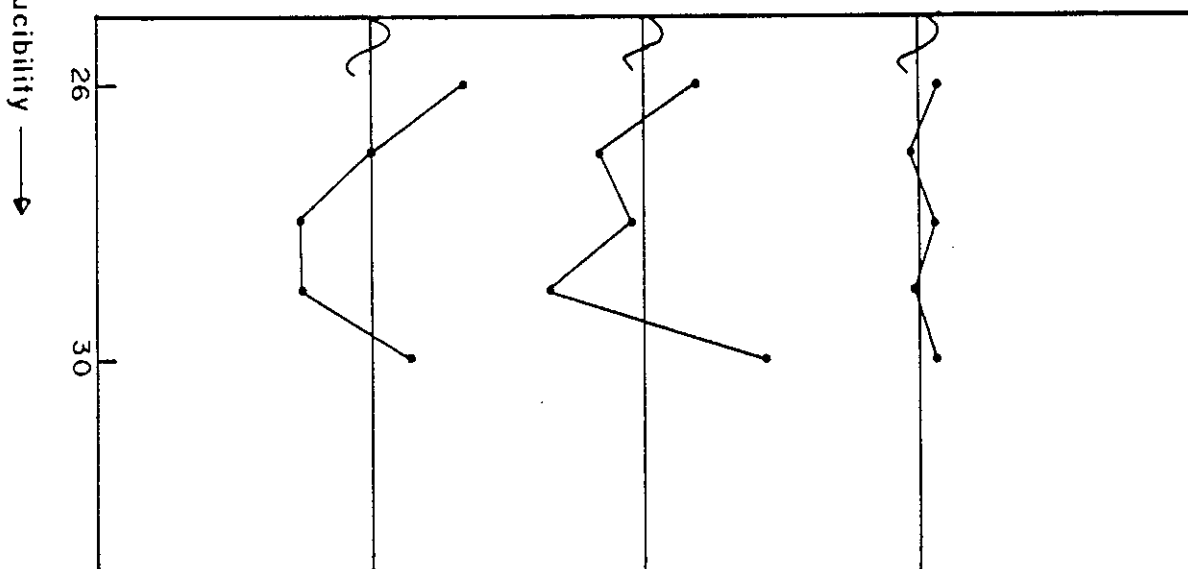
No. of reproducibility —>

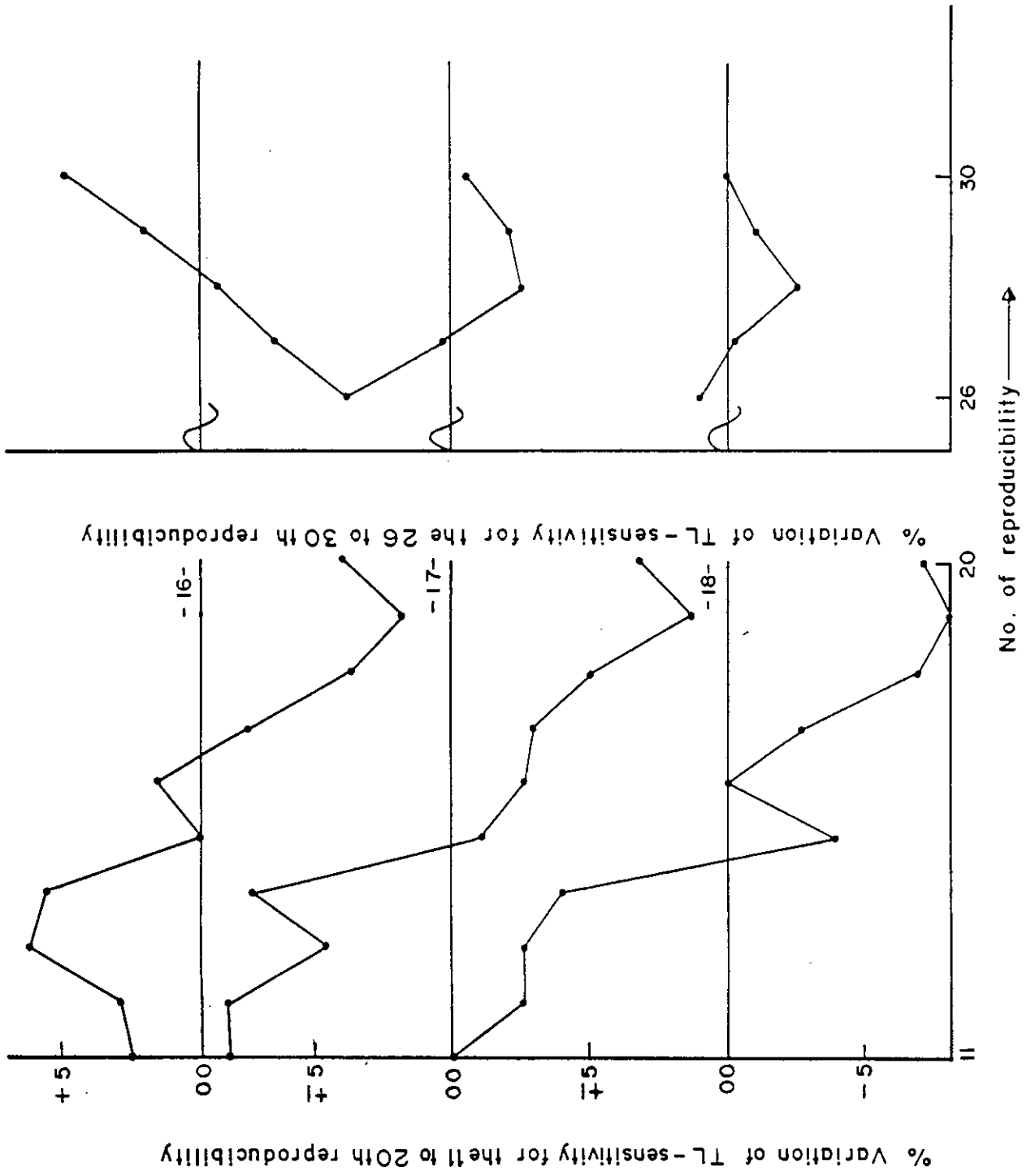


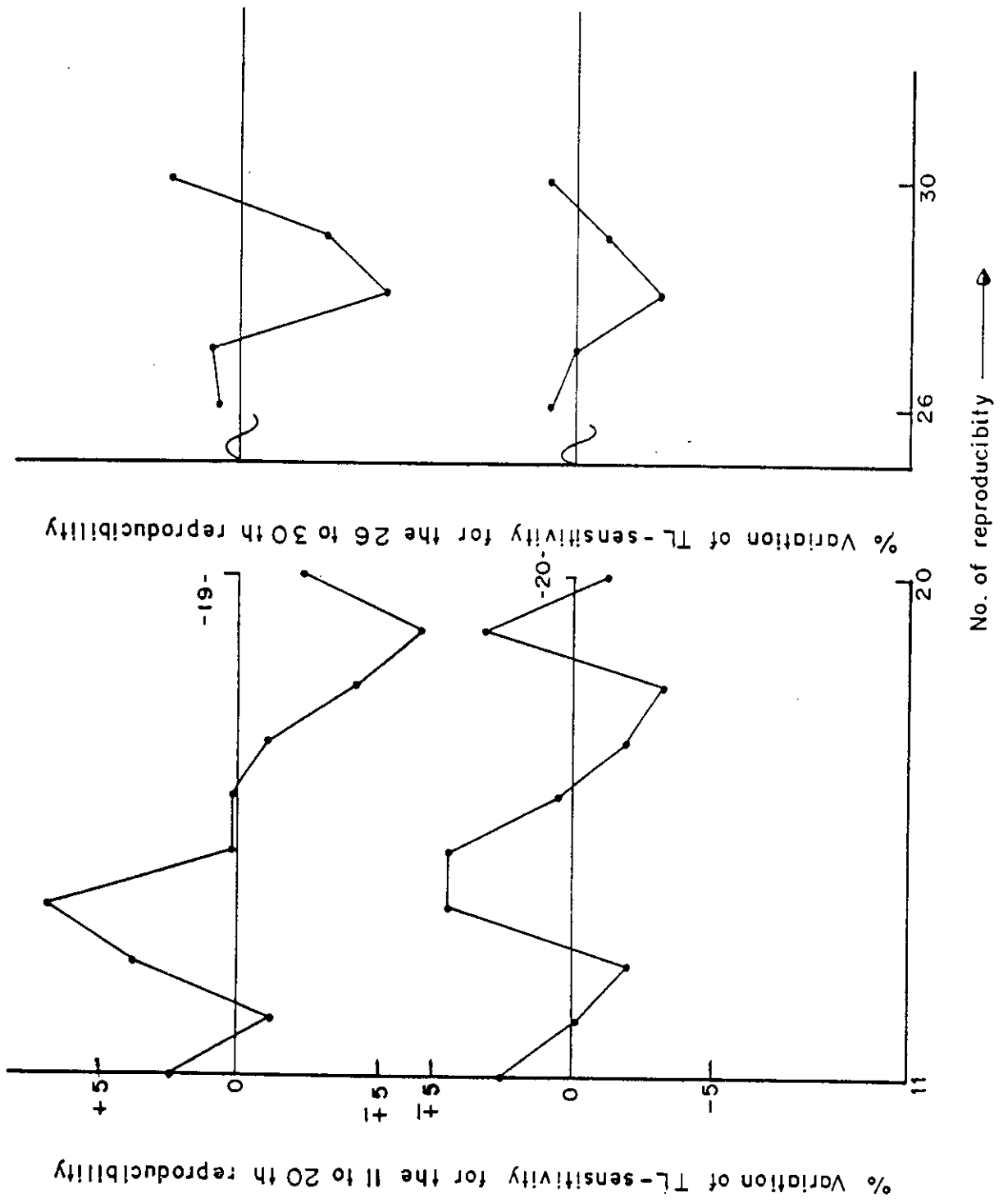
% Variation of TL-sensitivity for the 11 to 20th reproducibility



% Variation of TL-sensitivity for the 26 to 30th reproducibility







5.3 Sensitivity factor and grouping of TL-dosimeters

A sensitivity factor, S_i for a TLD identified by i with a sensitivity response R_i was defined from the average sensitivity response \bar{R}_i for the 83 TLDs using the following equation

$$S_i = \frac{R_i}{\sum_{i=1}^{83} \bar{R}_i} \quad (5.1)$$

Using the equation (5.1) a histogram data for TL-dosimeters within 5% sensitivity factor range were carried out Figure 5.4 and sorted out accordingly as shown in Table-5.1

Sensitivity factor	0.80-0.84	0.84-.882	0.882 - 0.926	0.926-.972	0.972-1.021	1.021-1.072	1.072-1.126	1.128-1.184
No of TLDs	06	08	15	11	07	16	16	04

Table: 5.1 Sensitivity histogram data of 83 TL-dosimeters

It was noted that, although the TL-dosimeters were taken in a batch, a large sensitivity variation of about 39% between the minimum and maximum sensitivity factors were observed. Nevertheless they constitute small groups within $\pm 2.5\%$ fluctuating sensitivity factor from there mid value for the purpose of treating them as dosimeters as observed in the Table 5.1. This variation may be due to either the non-equilibrium doping concentration during production or the lack of equilibrium heat transferred to the TL-dosimeter during the thermal treatment with the material contact (where the surface of the cylindrical rod-type dosimeter and the groove surface of the heating tray were not in perfect contact). The other variations due to

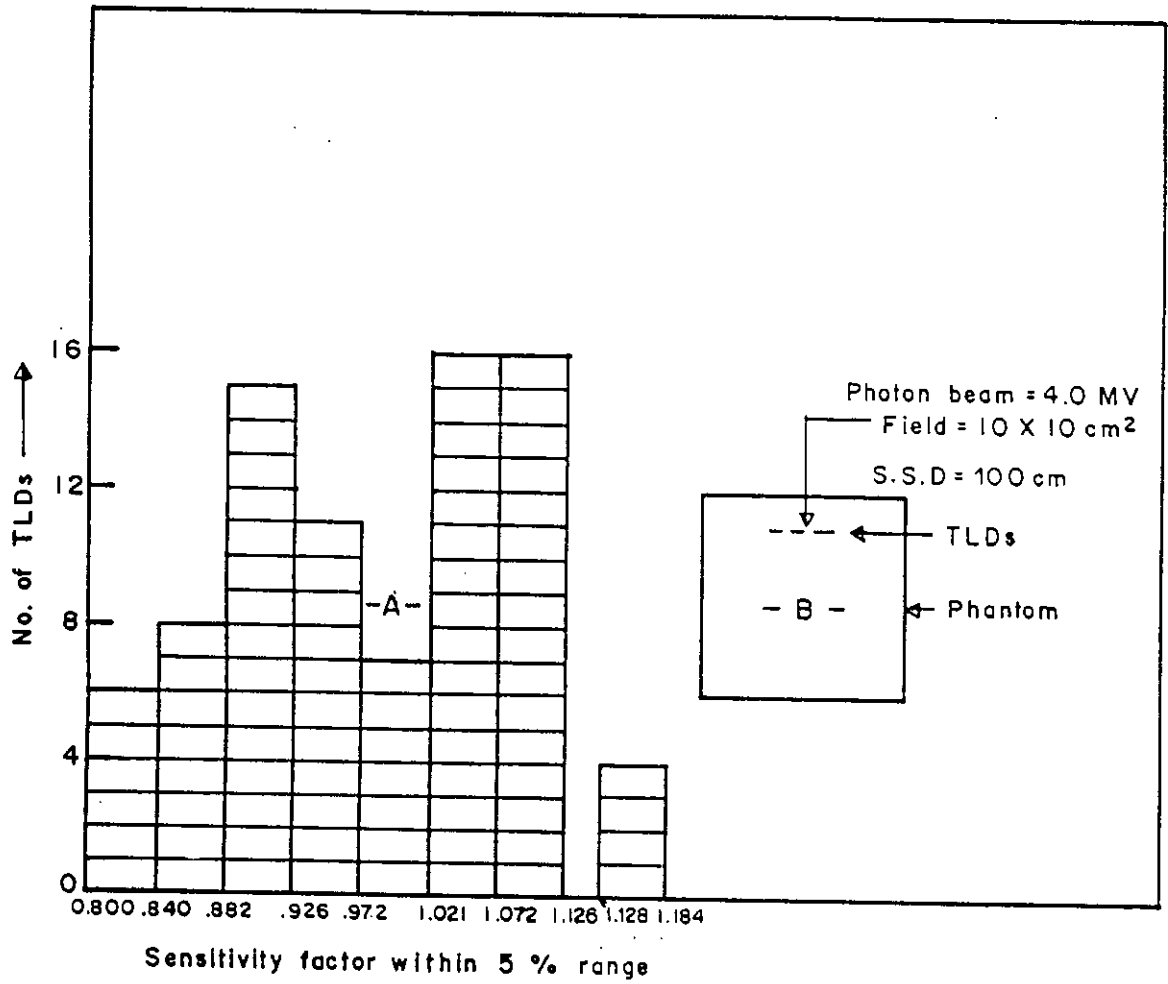


Fig 5.4 A frequency histogram data of 83 TLD(A).TLDs were irradiated with 1.0 Gy dose at 50cm depth of plexiglas phantom (B) for 4.0 MV photon beam. Field size 10 X 10 cm²; S.S.D. 100cm.

electronics of the equipment and for the background of the dosimeter along with the planchette-chamber were automatically controlled by the program by running the **PM-tube noise and test light** at every new start to read the new **response file** to the P.C. A result of $0.057 \pm 2.13 (\sigma)$ for the PM-tube noise and $211.139 \pm 3.64 (\sigma)$ for the test light from the 10 investigations using 30secs for each were observed. The background taken along with the unexposed and without dosimeter did not show any response in dose-value in the reader. The TLDs were handled with vacuum tweezers for avoiding the scratch of the sides or surface of the TLD. Again as the thermal treatment has a strong influence on the glow curve of the detector & as the reproducibility of the glow curve varies with its thermal history^{19, 44} (i.e. temp and cooling rate), so, the thermal condition of the oven was also checked directly by the firm, PTW, Freiburg. The investigation on the time-temp for the two existing programs is shown in figure 5.5. No anomalous condition was seen in that test. Therefore, with every reuse of the TL-LiF dosimeters were maintained uniformly to get the reproducibility of the glow-curve at every reuse. In a report⁷ it has been mentioned that a low fading effect during the first few hours after irradiation can not be eliminated; they can always contribute to make the variation of the measured signal during the first few hours of the irradiation. Therefore, even after pre-readout annealing which gives a glow-curve with low fading, the readout of the dosimeter was always taken after a definite interval, so that the information loss due to fading would be the same in the repeated use of the TL-LiF dosimeter.

Experimentally it was confirmed that better reproducibility of the glow curves could be obtained by heating the exposed TL- dosimeter under nitrogen contact condition than that of planchette contact.

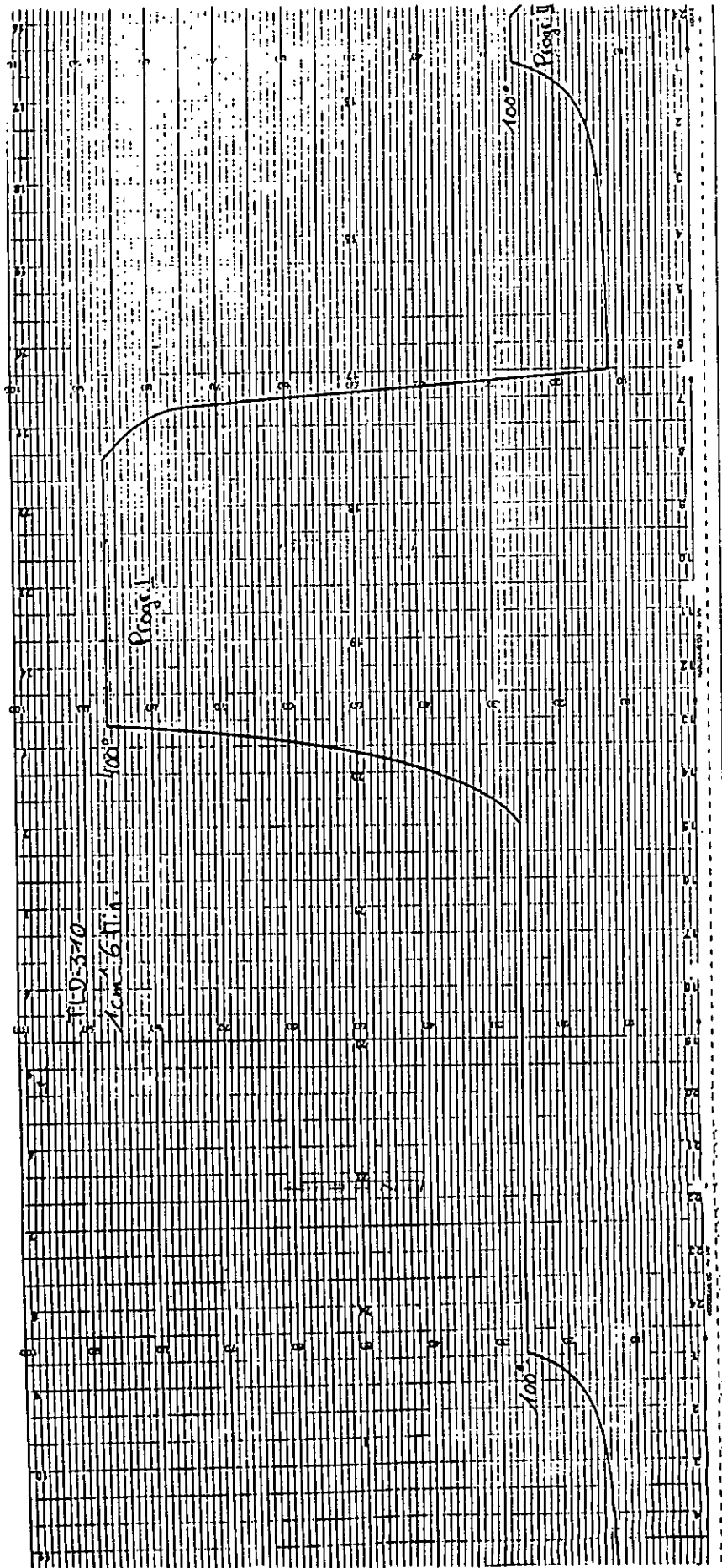


Fig. 5.5 Existing time temperature programme in to the oven (PT W-TLDo, Freiburg).

6.0 CALIBRATION OF THERMOLUMINESCENCE DOSIMETERS

6.1 Introduction

The TL-light output must be calibrated in terms of known standard absorbed dose (Gy) to water. The amount of light emitted by an irradiated TL-dosimeter is directly proportional to the absorbed dose. The proportionality constant called the calibration factor is to be determined from the recognized standard dose. Mathematically the dose (D) obtained from the TL-dosimeter is expressed in the following way.

$$D = F_{light} F_{sup} F_{energy} light \quad 6.1$$

where F is the calibration factor associated with different dependent parameters in the subscript.

6.2 Light dependence calibration factor (F_{light}) of the TL-dosimeters

For calibration of TL-LiF dosimeters, the TLD-shell model program from Harshaw was used. The program describes the calibration factor as the Reader Calibration Factor (RCF). It determines the sensitivity (the light values obtained for 1.0Gy absorbed dose of the TLD) of the detector in Gy/nC. The RCF value was counted from the average light value from the set of TL-dosimeters.

Another calibration factor, the Element Correction Co-efficient (ECC) was determined for each dosimeter, which compensates the variation in the sensitivity. It is a dimensionless parameter. Thus, for the TLD, the factors RCF and ECC are to be determined in advance for 1.0Gy of standard dose of certain definite photon beam. Then the equation (6.1) will be

$$D = \frac{ECC}{RCF} \times F_{sup} \times F_{energy} \times Light \quad 6.2$$

Where

$$F_{light} = \frac{ECC}{RCF} \quad 6.3$$

The factors, RCF and ECC has to be determined in three steps where the TLDs are irradiated twice with the same known dose e.g. 1.0Gy.

The whole procedure can be explained as in the following way:

1st step: All the exposed TLDs in the set are read out with *Generate Cal. Dosimeter* and *None* in *Acquisition* and *Calibration* mode respectively. After completing the read sequence, through *application* mode, the TLDs with the *selected applied ECC limit* within 1% (e.g. 1.01 - 0.99) are to be accepted into the PC. Here, if the light values for the individual dosimeter is represented by the charge integral, Q_i then ECC_i for the individual dosimeter, i , is calculated from the average charge integral of the set, $\langle Q \rangle$ as

$$ECC = \frac{\langle Q \rangle}{Q_i} \quad 6.4$$

2nd step: The TLDs are again irradiated (after regeneration) with the same exposed dose (1.0Gy). Only the accepted identified TLDs during the 1st step with their accepted ECC values are to be read out by running the program *Calibrate reader* and *ECC* in *Acquisition and calibration* mode. The charge integral for each dosimeter was corrected by ECC_i . The average of these charge integrals is the RCF values which has to be accepted in the TTP file. The RCF value thus obtained is

$$RCF = \langle Q' \times ECC_i \rangle \quad 6.5$$

where Q' is the integrated charge counted by the light value for the read out in 2nd step of TL-LiF crystal rod due to absorption of 1.0Gy dose. In the program these TLDs are described as the **reference dosimeter**. Because, here every emitting light value (nC) corrected by the ECC value (which were close to 1.0) accounts for the amount of absorbed dose in Gy.

3rd step: The remaining TLDs (introducing the dosimeter identification [ID] number in the dosimeter file) are to be read out with *Calibrate Dosimeter* and *RCF* in *Acquisition and Calibration Mode*. Here the new ECC known as ECC_i' for every TLDs are counted so that each TLD gave acquires equal performance of sensitivity. Again by *Application* mode and with new selected *Applied ECC limit* (e.g. 1.03 - 0.976) the dosimeters with YES besides the ID number along with calculated dose and ECC_i' value is displayed directly on the PC screen. Here the ECC_i' is generated in the following way,

$$ECC_i' = \frac{RCF \times E}{Q_i''} \quad 6.6$$

where Q_i'' is the reported integrated charge for the individual TLD due to 1.0Gy absorbed dose and E is the calibrated exposure dose (here, it is 1 Gy dose). In the program, the st. dev. (S.D) for the calibration dose value was also displayed which is accounted as in the following way,

$$S.D. = \left[\frac{\sum_{i=1}^n (\langle Q \rangle - Q_i)^2}{n-1} \right]^{1/2} \quad 6.7$$

where, i is the sequential dosimeter number, n is the total number of dosimeter; Q_i is the charge in the glow curve; $\langle Q \rangle$ is the average charge integral. The percent of S.D. is obtained by dividing S.D. with the mean of the accepted readings. It varies with the given ECC limit and are to be observed in the PC screen. Therefore, the limit was selected so that the dose measurement capability of each of the TLD lies within maximum 2% S.D. Finally, only the accepted dosimeter would be used in the field measurement purpose by running the program with *Read dosimeter* and *RCF & ECC* in the *Acquisition of Apply Calibration* mode. The identified TLDs written as *NO* must be deleted from the dosimeter file, the TLDs on the tray are also sorted out accordingly.

During dose measurement using the calibrated dosimeters, each TLD get the

RCF and ECC value with which the TL dose, D_i for the individual TLD would be calculated accordingly,

$$D_i = \frac{ECC_i'}{RCF} \times Q_i''' \quad 6.8$$

where Q_i''' is the integrated charge counted by the light value for the readout of exposed TLD, identified by i in the field measurement. For all the dosimeters in the set, the same RCF value was used and the correction factor of each TLD. ECC_i' (in equation 3) was determined with their individual light value (Q_i'''). Here it should be mentioned that the light value of a TLD was taken within the maximum $\pm 2.5\%$ fluctuation from the mean as discussed earlier. Therefore, if the RCF value is determined from the mean sensitivity of a set of TLDs of same characteristics (having the sensitivities within ± 2.5 fluctuation among themselves), then all the TLDs in the set would be taken as calibrated dosimeters within maximum 2% S.D.

In the TLD shell model program, a multiple of the same program can be installed and different RCF value can be introduced in the TTP-file. Therefore, for several RCF values represented by RCF_n for different sets of TLDs, the equation (6.8) will be,

$$D_{ni} = \frac{ECC_n'}{RCF_n} \times Q_{ni}''' \quad 6.9$$

In the TL-dosimeter, the response dose also depends on the Energy Quality Factor (F_{energy}) as well as on the amount of absorbed dose called the supralinearity factor (F_{sup}). Including the two factors, the equation (6.9) can be written as,

$$D_{ni} = \frac{ECC_{ni}'}{RCF_n} \times Q_{ni}''' \times F_{energy} \times F_{sup} \quad 6.10$$

Again if an average background dose, B_n for the TLDs are counted then a general form of the TL-dose will be

$$D_{ni} = \frac{ECC_{ni}}{RCF_n} \times Q_{ni} \times F_{energy} \times F_{sup} - B_n \quad 6.11$$

All the TLDs in the sets (Table 5.1) were calibrated using 4.0MV-photon beam. The total RCF values for the 6 sets of TLDs were determined individually. For this, six programs were installed and the same time-temperature and the same PM-tube voltage into the TTP files were maintained. Accordingly, the ECC values were also stored in their respective ECC-file. For 1.0Gy dose, the TLDs were irradiated into the 5.0-cm depth of Plexiglas phantom for $10 \times 10\text{-cm}^2$ field and S.S.D of 100 cm. The calibrated MUs for 1 Gy dose were taken from the direct measurement using ion-chamber associated with two electro-dosimeter. The ion-chamber dosimeter was primarily standardized by FeSO_4 dosimetry in PTW, Freiburg.

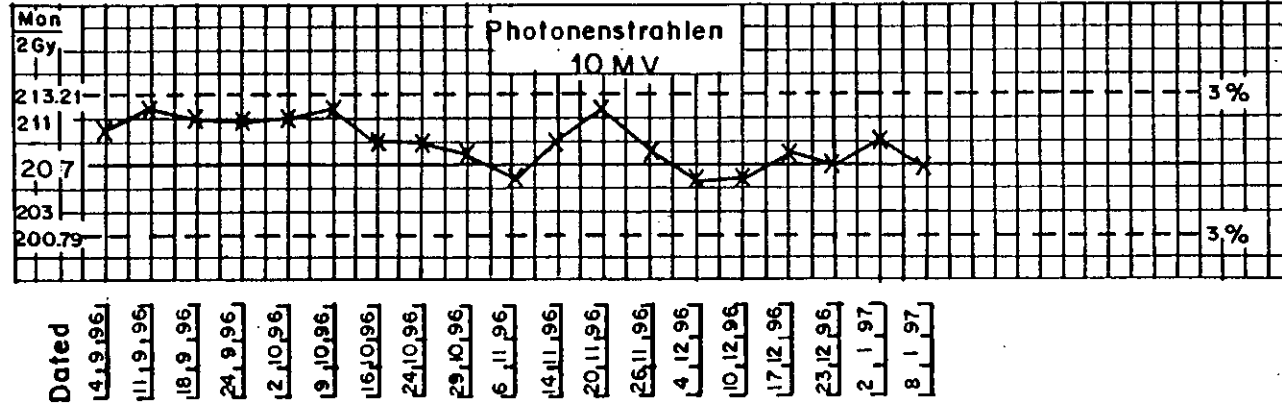
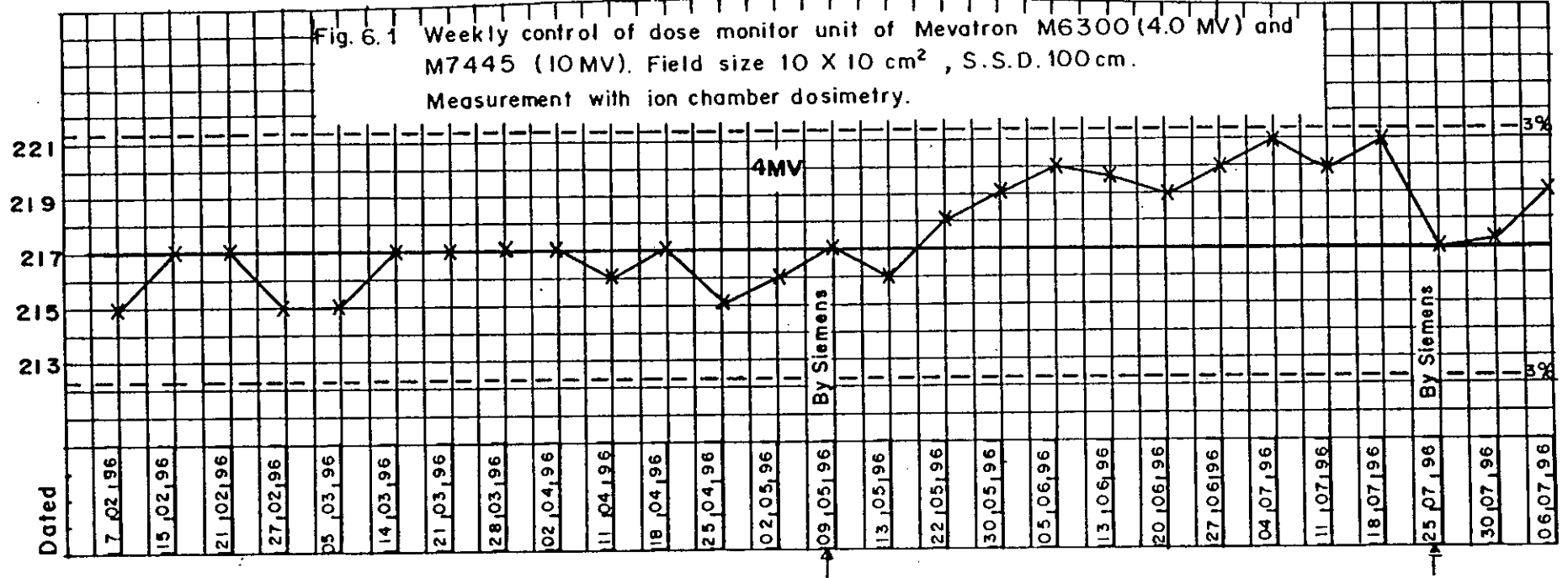
The TLDs having the performance quality to measure the 1.0Gy dose with maximum 2% S.D. were calibrated for 4.0MV energy. In the same way, the TLDs were also calibrated for 10MV energy. The number of calibrated dosimeters with their RCF values for the 4.0 and 10MV energy beams are shown in Table-6.1. During the calibration process, it was noted that the reference TLDs could not be used in the field measurement. It is interesting to note that sometimes most of the TLDs in the set were selected as reference TLDs within the selected limit of 1.01 to 0.99 in the 1st step of the calibration process. It was not necessary to read all the TLDs at the 2nd step to calculate the RCF value. The thermal treatment and the thermal history were standardized and were strictly maintained at every re-use. The reference TLDs were read out. Then all the TLDs of the set including this reference TLDs were regenerated and then exposed to the same energy dose of 1Gy. By taking the readout of all the reference TLDs and again exposing all the TLDs in the set to same energy dose of 1.0Gy, of course after regeneration. The 3rd step of the calibration process was then run. By doing this, it was possible to use all the TLDs in the set within 2% S.D. The procedure was followed for all other sets of TLDs. The number of calibrated TLDs including the reference TLDs

are also shown in Table-6.3. As the precision of the TLDs could only be maintained for a very short period of time³⁵, the TLDs were recalibrate after every one-week by running only the 3rd step of the calibration procedure keeping the RCF value in the TTP-file as before. The TLDs which were not used (having more than 2% S.D.) in the dose measurement purpose were stored in the tray besides their own set position (marking them with pencil). The thermal treatment of the TLDs including these was carried out as usual.

While handling the TLDs, it was observed that the precision of TLDs got change very often. Here, it was noted that the quantities of the supplied photon beams changes within the excepted range of $\pm 3\%$ from its standard value (Figure 6.1). Therefore, after every one-week, the TLDs were re-calibrated to include the MUs changes for 1.0Gy dose to TLDs.

Generally, the dosimeter is to be calibrated with the mono-energetic source of either ^{60}Co or with ^{137}Cs energy. In Gummersbach Therapeutic Physics Department only the 4.0 & 10MV energy beams are available. Therefore, the TLDs were calibrated using the two photon beams separately. Some TLDs were also calibrated with ^{60}Co energy source in Gross-harder Uni-clinic, Essen Uni-clinic and in Aachen Uni-clinic. In Essen and in Aachen Uni-clinic, the same TLD shell models program was followed and the same measurement precision in TLD calibration was observed. In Gross-harder Clinic a different method was followed. The calibration factor was determined from the mean of successive sensitivity. And a correction factor was taken from the percent deviation from the two successive calibrated TL-light values for 1.0Gy dose of ^{60}Co -beam. In determining the calibration factor for 42 TLDs an excellent precision of 0.43% S.D. was obtained.

Fig. 6.1 Weekly control of dose monitor unit of Mevatron M6300 (4.0 MV) and M7445 (10MV). Field size 10 X 10 cm², S.S.D. 100 cm. Measurement with ion chamber dosimetry.



Photon Beam	Supplied MU for 1.0 Gy dose at 5.0 cm depth	Differen t set	RCF (nC/Gy)	Without reference TLD			
				ECC limit upper lower	Read out dose± S.D.%	No. of TLDs read out at 3rd step	No. of accepted Cal. TLDs
10.0 MV Gantry 0° 10×10cm ² 100cm	116	S ₂	1052.25	1.03-0.97	1.00 ±	06	05
		S ₃	1082.34	1.03-0.97	1.99	12	11
		S ₄	1120.85	1.03-0.97	1.01 ±	08	08
					1.63 1.00 ± 1.72		
4.0 MV Gantry 0° 10 × 10cm ² 100cm	128	S ₅	1150.00	1.03 -	0.99 ±	05	05
		S ₆	1193.67	0.97	1.43	13	13
		S ₇	1213.41	1.03-0.97	1.00 ±	12	11
					1.03-0.97 1.56 1.00 ± 1.89		

Table 6.1: Calibrated TLDs for 10.0 and 4.0 MV photon beams.

The readout was taken within 1 to 200ch. of PM tube

Sensitivity factor range	S ₁	S ₂	S ₃	S ₄	S ₅	S ₆
	0.94-0.987	0.987-1.036	1.036-1.088	1.088-1.142	1.142-1.207	1.207-1.344
No. of TLDs	10	15	22	26	05	04

Table 6.2. No. of TLDs within 5% sensitivity factor range. The described data were carried out after 6 months reuse

Photon Beam	Supplied MU For 1.0 Gy dose at 5.0cm depth	Different set	RCF (nC/Gy)	With including reference TLD			
				ECC limit upper-lower	Readout dose ± S.D.%	No. of TLDs readout at 3rd step	No. of accepted Cal. TLDs
10.0 MV Gantry 0° 100cm ² 100cm	116	S ₁	973.84	1.03-0.97	0.99 ± 1.87	10	07
		S ₂	1008.00	1.03-0.96	0.99 ± 1.62	15	12
		S ₃	1034.00	1.03-0.97	1.00 ± 1.57	22	20
		S ₄	1060.66	1.03-0.97	1.00 ± 1.64	26	23
		S ₅	1078.43	1.04-0.96	1.01 ± 1.97	05	04
		S ₆	1243.52	1.02-0.98	1.00 ± 1.33	04	04
4.0 MV Gantry 0° 10 × 10cm ² 100cm	128	S ₁	1000.20	1.03-0.97	1.00 ± 1.84	10	08
		S ₂	1030.00	1.03-0.97	1.00 ± 1.73	15	13
		S ₃	1066.17	1.04-0.96	1.00 ± 1.99	24	23
		S ₄	1088.40	1.03-0.97	1.01 ± 1.78	23	21
		S ₅	1102.33	1.04-0.96	1.00 ± 1.54	06	04
		S ₆	1266.00	1.03-0.97	1.00 ± 1.29	04	04

Table 6.3: No. of calibrated TLDs with RCF value. The read out was taken within 1 to 138ch of PM-tube.

6.3 Dose dependence calibration factor (supralinearity factor) of the TL-dosimeters.

The TL-dosimeter is not usually found to be linear. It always exhibits a certain definite amount of higher dose value than that of actual, for which the response obtained from TL dosimeter, is called as supralinear. Supralinearity leads to higher uncertainty in the measured absorbed dose for which additional calibration factor have to be determined and applied.

Because of thermal treatment using the high temperature there is a probability of existence of ultraviolet and infrared rays, which may contribute to the occurrence of the supralinearity of TL-dose.

Therefore, TL-dose were read-out by using the two-channel width of the PM-tube simultaneously in the following way.

- (i) the TL-response dose measured under the total glow-curve area i.e., by including all the six photo-peaks.
- (ii) the TL-response dose measured under glow-curve area up to fifth photo-peak.

The investigations were carried-out for the dose of 0.25, 0.50, up to 5.0 Gy at the maximum depth dose position (d_{\max}) for both the energy of 4.0 and 10MV in Gummersbach Hospital, Germany. For every dose value the calibrated monitor unit for the respective photon-beam of field $10 \times 10 \text{cm}^2$ at 100cm of S.S.D were supplied. The results obtained are shown in Figure 6.2(a) and 6.2(b). During the investigation it was found that the supralinearity for the first situation started from the dose of 0.50Gy for 4.0 MV energy. For the second situation, the supralinearity were not observed for the dose values up to 4.0 Gy for both the photon beam energy. The relation was simply linear (Figure 6.2).

Another investigation was carried-out for the photon-beam of 0.66MV (^{137}Cs) energy using the same TLDs in Munich Grossharder Univ.- Clinic, Germany.

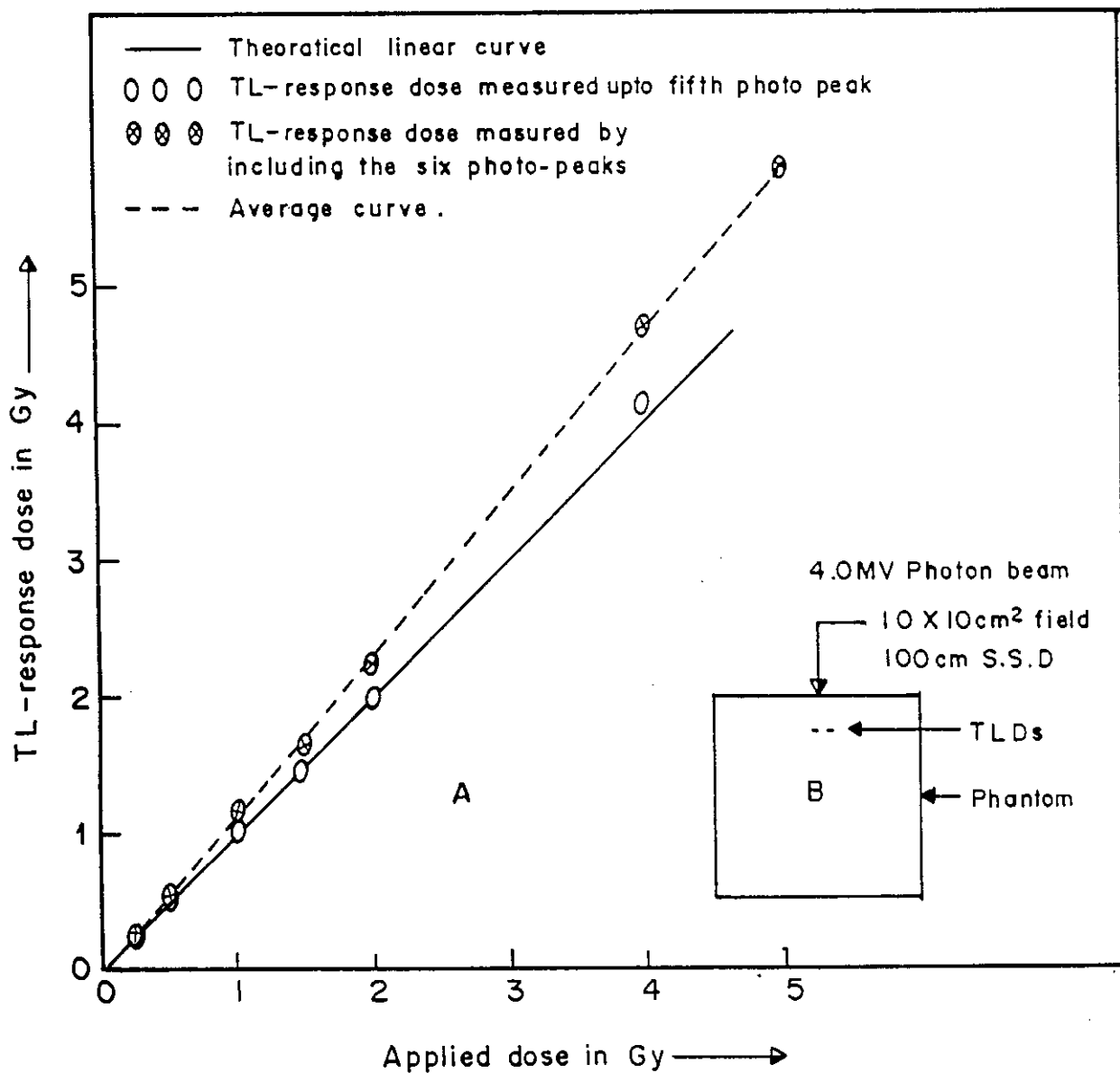


Fig.6.2a Supralinearity curve for TL-dose (A) measured in the phantom (B) for the photon beams of 4.0MV energy; 10 X 10cm² fields sizes and 100cm S.S.D.

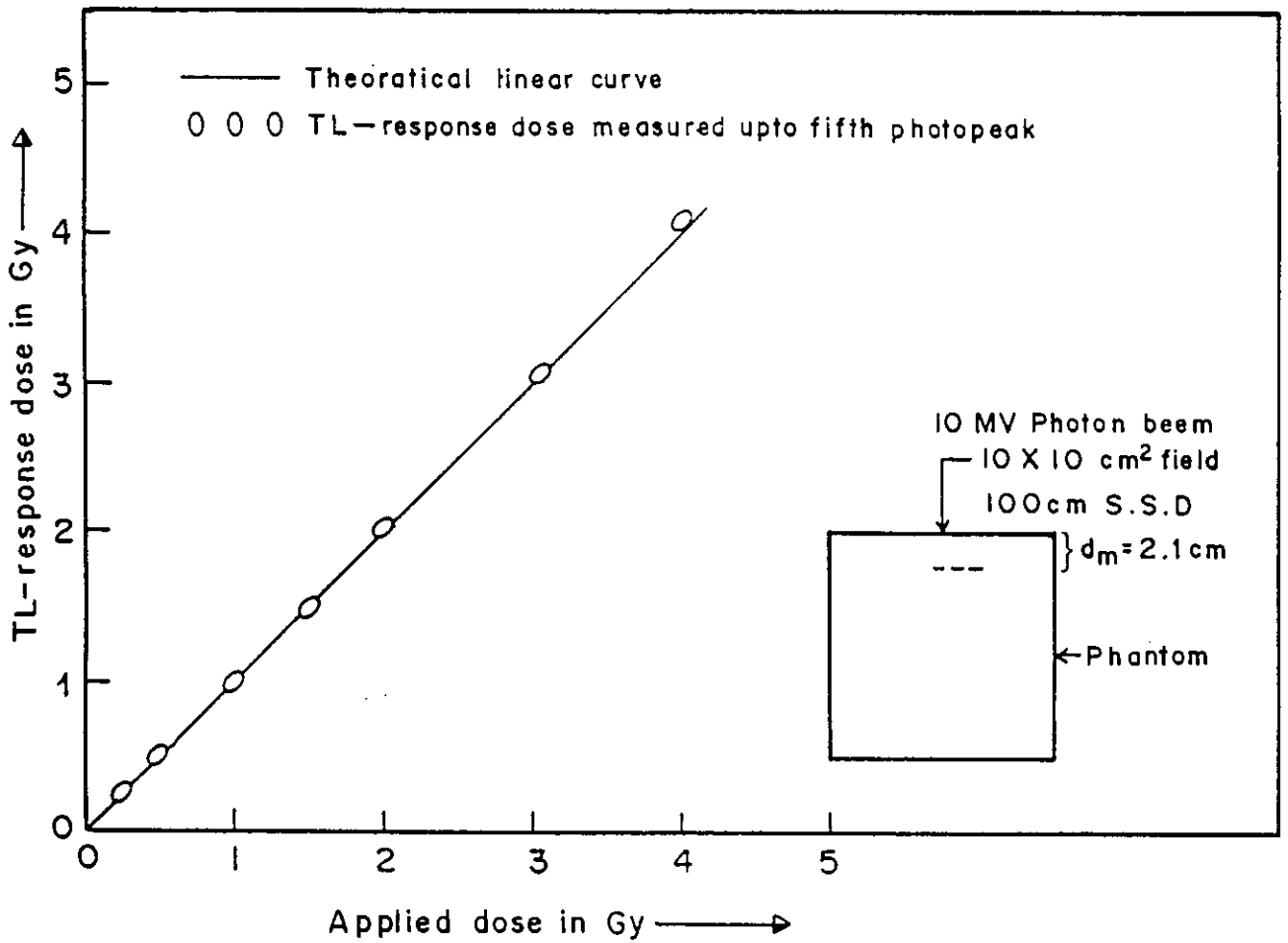


Fig. 6.2b Supralinearity curve for TL-dose for the photon beam of 10 MV energy.

Here, for the first situation, the supralinearity was 3.71% / Gy while for the second situation, a constant increase of the response of 2.23%/ Gy were observed which was less than the first situation. It may happen due to the mono energetic beam of ^{137}Cs source and the different read-out system in two hospitals.

However, all the experiments are to be carried out using 4.0 and 10MV photon beam. And if the TL-dosimeters are always irradiated with a dose less than 1.0 Gy and the TL-dose is read out as described in the second situation, then in this case, the supralinearity factor for the TL-dosimeter could be taken as 1. Hence the equation (6.2) will be

$$D = \frac{ECC}{RCF} \times F_{energy} \times Light \quad 6.12$$

Where $F_{sup} = 1$

6.4 Energy dependent calibration factor of the TL-dosimeters

As the dose-distribution measurement would be carried out using TL-dosimeter for 4.0 and 10.0MV energy, therefore, the energy sensitivity calibration factor, F_{Energy} of 10MV has to be determined considering the factor for 4.0MV energy as 1. If D_1 is the dose measured with TLD for 4.0MV and D_2 is the same amount of dose for 10MV for the same geometrical condition of photon field, then F_{energy} will be

$$F_{Energy} = \frac{D_2 \text{ for } 10MV}{D_1 \text{ for } 4.0MV} \quad 6.13$$

Using the equation (6.13) a calibration factor of 1.03 for the TL-LiF dosimeter for 10MV with respect to 4.0MV was obtained. For this, a group of 10 TLDs having maximum 1.0% S.D of enhanced charge (nC) value for the five successive measurement using 4.0MV energy were taken. The TL-dose was readout with the manual reader of 3500-model.

The investigation is usually done relative to the ^{60}Co standard source. As it was not available in the therapeutic physics department in Gummersbach Hospital, the investigation was carried out in the dept. of therapeutic physics in Aachen Uniclinik, Germany. Here again a set of TLDs was selected which reproduced sensitivity within the maximum S.D of 1.0% for five successive measurements. The TLDs were exposed to a dose of 0.50Gy at 5.0cm depth of Plexiglas phantom. The field was $30\times 30\text{ cm}^2$ at S.S.D of 80 cm. For the other energies of 10 and 18MV, the same dose at the same depth of the same phantom using $30\times 30\text{ cm}^2$ field on S.S.D of 100cm, required a calibrated monitor units of 54, converted from the standard measurement in a water phantom at an equivalent depth of 5.6cm. The TLDs used at Aachen was in fact exposed under the same condition of photon field for the 4.0MV energy in Gummersbach and subsequently taken to Aachen for read out. The required MU of 59 was measured directly, using the standard ion-chamber. All the exposed TLDs were readout with the automatic Harshaw TLD Reader 5500-model available in Aachen. Here the TLDs were readout by heating through the hot Nitrogen gas. TL-response was carried out with the TLD shell model program from Harshaw. The same heating rate ($10^\circ\text{C}/\text{sec}$ for the pre-ht of 80°C to maximum of 300°C) was followed. The total charge of the glow-curve was taken within 1 to 138ch width of PM-tube as in Gummersbach. At every re-use the pre-annealing of TLDs were done on the oven (TLD0, PTW) with 400°C for 1 hour followed by 100°C for 3 hrs. The result of the experiment is given in Table- 6.4.

For a given TL dosimeter associated with a given reader, energy correction factors remain constant and are introduced in the associated computer in order to correct the results automatically.

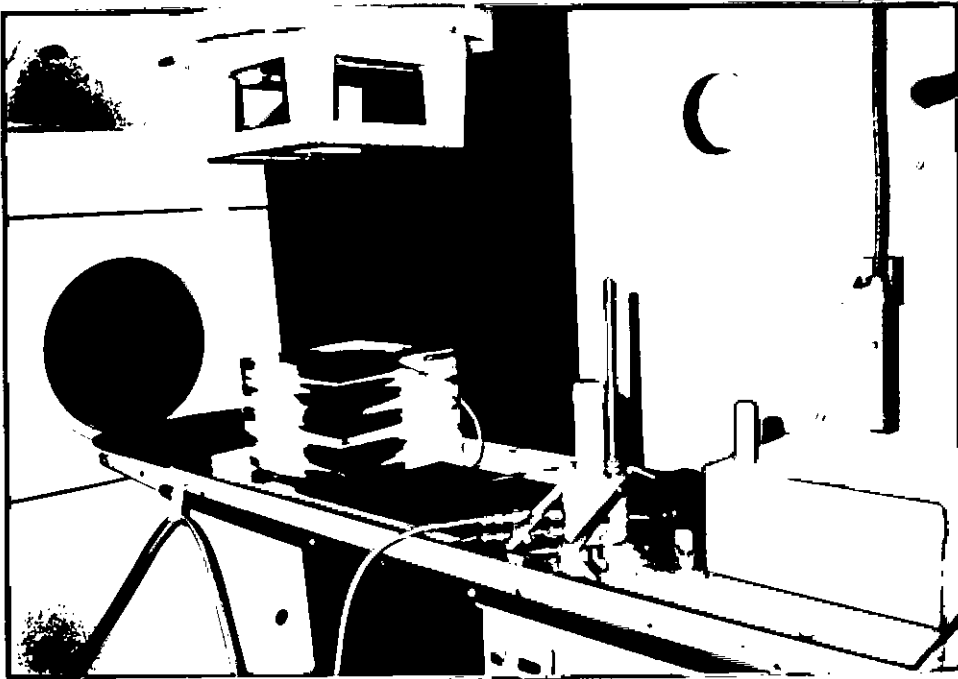
Accelerator	Photon-energy (MV)	Phantom depth (cm)	Energy sensitivity factor of TLD
Gammatrone 80	1.25	5.0	1.000
Mevatron M6300 (Siemens)	4.0	5.0	1.011
Mevatron KD (Siemens)	6.0	5.0	1.037
SL75/10(Philips)	8.0	7.0	1.043*
Mevatron 7445 (Siemens)	10	5.0	1.038
Mevatron KD (Siemens)	15	7.0	1.063*
	18	5.0	1.043

Table 6.4. The energy dependent sensitivity factor of TLD-100 in photon beam by experiment. The TLDs was irradiated into Plexiglas Phantom. (* Values taken from the experiment carryout by Feist for TLD-rods).

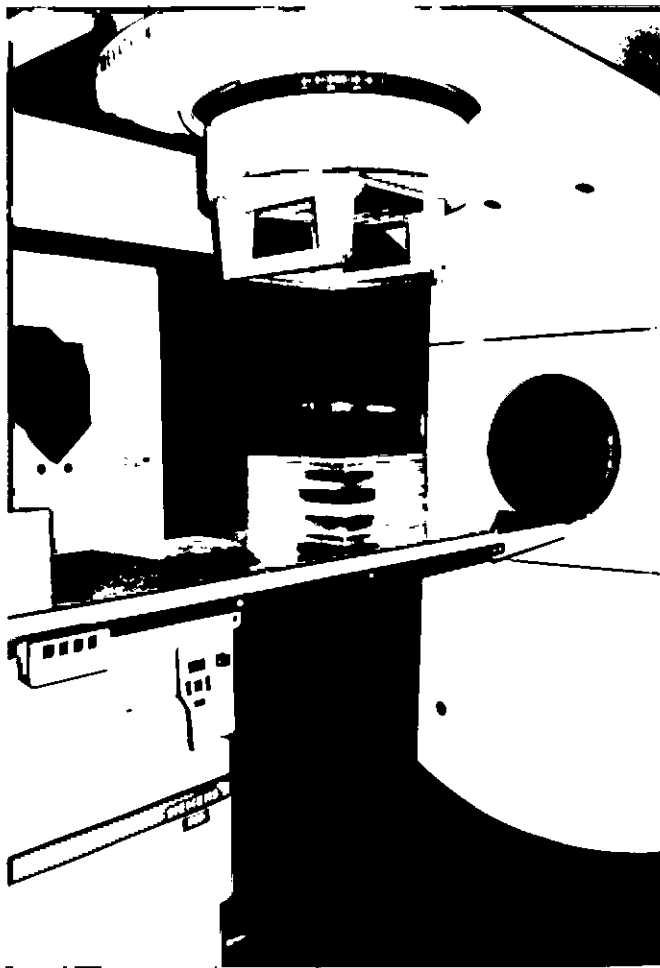
7.0 COMPARISON OF TL-DOSIMETER MEASUREMENTS WITH OTHER STANDARD DOSIMETERS FOR STANDARD FIELDS OF HOMOGENEOUS PHANTOM

7.1 Dose accuracy of TL-dosimetry in the Phantom

To investigate the measurement accuracy of TL-dosimeter, a dose distribution measurement was carried out using a plexiglas phantom for the photon beam of 4.0 and 10 MV. A depth dose distribution and the two cross-profile distribution, one at d_{\max} and another at 10 cm. water equivalent depth, (8.8 cm for Plexiglas) for both the photon beam using $10 \times 10\text{-cm}^2$ field and 100 cm. S.S.D. were taken into account. For comparison, the same distribution was also carried out using a calibrated standard ion-chamber (0.3cm^3 PTW, Freiburg). The experimental set-up of the measurement system is shown in figure 7.1. For TLD, a series of $1 \times 1 \times 6\text{mm}^3$ groove arrangement at 1.0 cm distance apart along the central line of Plexiglas plate (Figure 5.2d) was taken, so that a series of TLDS was acting along a line across the plane. A dose of 100MU was used for every measurement. The distributions were normalized at the maximum central dose value. A significant amount of variation in dose distributions was observed (Figure 7.2, 7.3) between the two dosimetries (ion chamber and TLD). It was found that the calibrated TLDs had measurement precision within 5% S.D. for calibrated dose measurement (1.0 Gy dose). Then by re-calibrating the TLDs, the dosimeters were taken within 1.67% S.D for the calibrated of 1.0 Gy dose measurement. Only 12 out of 42 TLDs used were found with 966 nC/Gy of RCF value for 4.0 MV photon beams. Using these TLDs, the depth dose distribution into the phantom (Figure 7.4) was found to be better compared to the previous measurement. Thereafter, all the calibrated dosimeters were selected having a S.D. within 2% of calibrated dose measurement capacity. Subsequently, the 3 to 5 TLDs measurement technique was considered for the investigations. For this, 5 groove on the central surface of a plexiglas plate at a distance of 1.0cm from the central one were made for



a



b

Fig. 7.1: Experimental set-up of dose measurement using (a) ion-chamber dosimeter and (b) TL-dosimeter in homogeneous phantom

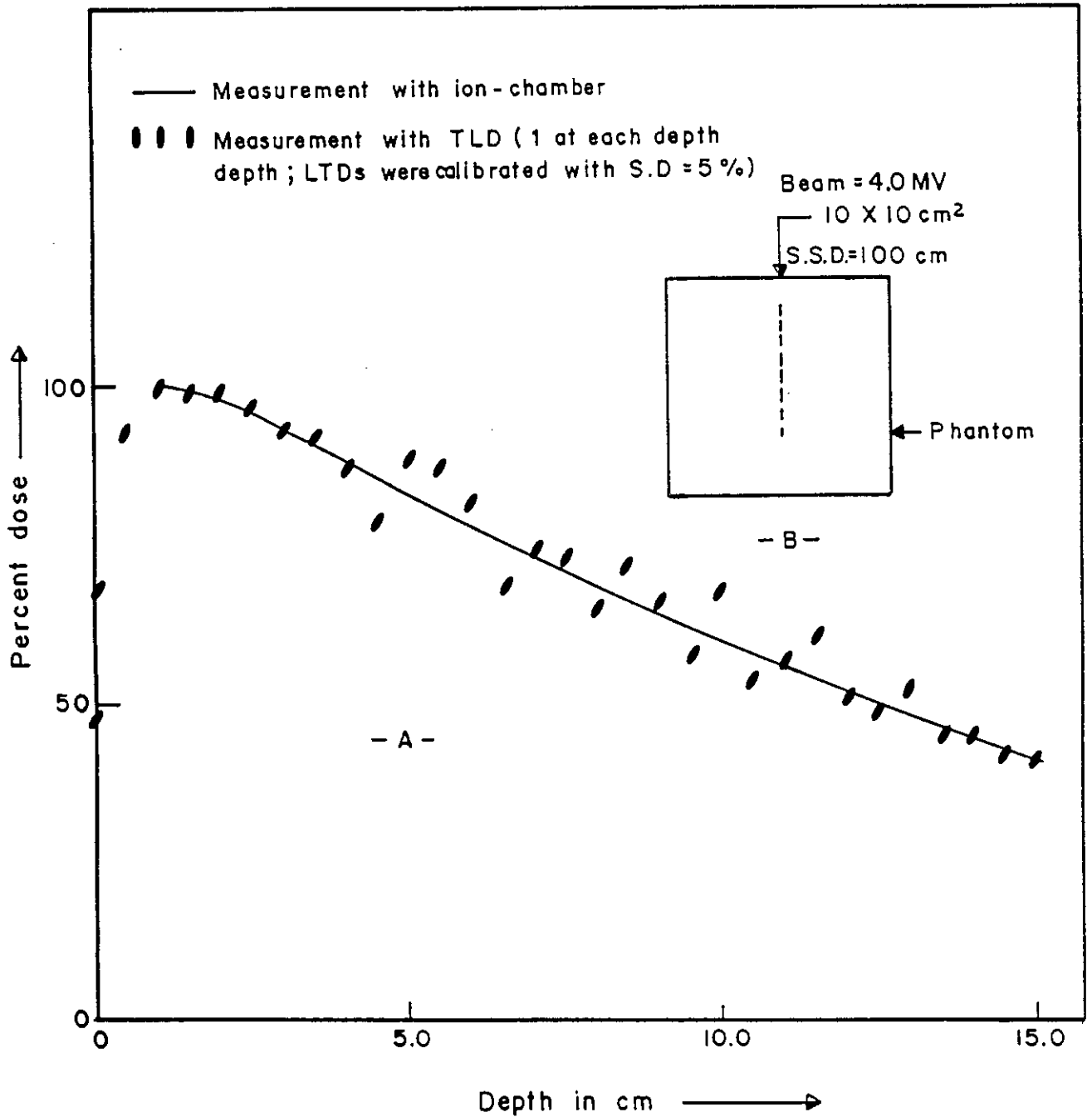


Fig. 7.2 Depth dose curve (A) in plexiglas phantom (B) for 4.0 MV photon beam. Field size 10X 10cm², S.S.D. 100cm.

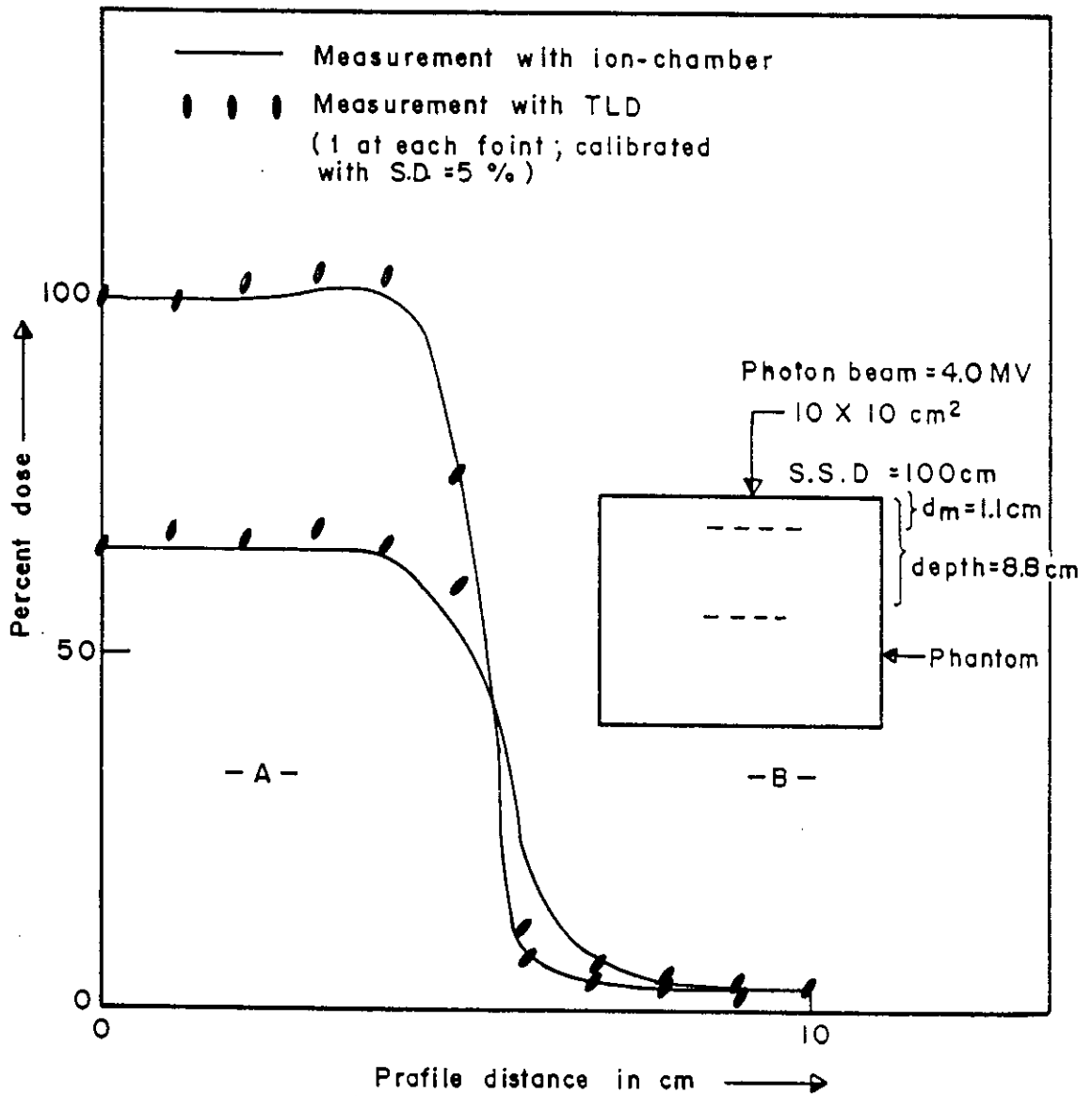


Fig. 7. 3 Dose profiles (A) in depth at 1.1cm and 8.8cm (down word) in plexiglas phantom (B) for 4.0 MV photon beam; field size 10 X 10 cm²; S.S.D. 100cm.

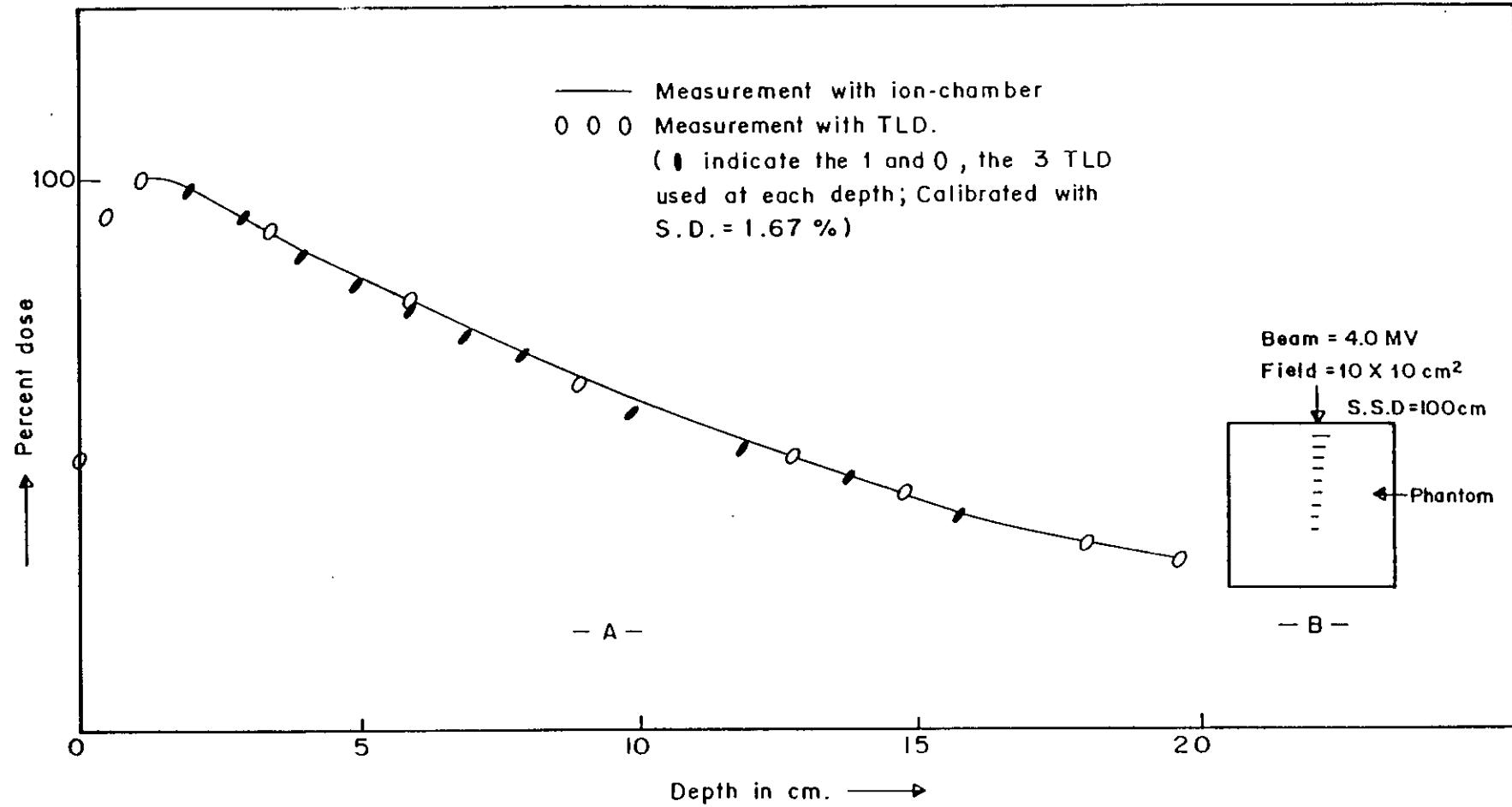


Fig. 7.4 Depth dose curve (A) in plexiglas phantom (B) for 4.0 MV photon beam. Field size 10 X 10 cm²; S.S.D. 100 cm.

using 5 TLDs. The procedure was repeated for different depths. By using the average dose measurement values for each depth of the phantom, the depth-dose distribution curve was found to be quite well matched with that of ion-chamber measurement (Figure 7.4). For profile dose distribution, two TLDs were placed cross-wise at a distance of 1.0mm apart. The pattern was repeated every 1cm along the central line (Figure 5.2c). However, near the supposedly penumbra region the pattern was repeated every 0.5cm. A plexiglas sheet of 1.0mm thickness was placed above it. Then another plexiglas sheet with a single groove (for holding a single TLD) every 1cm apart (0.5 cm near the penumbra region) was placed on it upside down. So in effect three TLDs were used for recording the dose at the same point. Thus the cross profile dose distribution was carried out using 3 TLDs in the distance of 1.0cm (0.5 cm apart on the penumbra region) across the beam into the phantom. The distribution curve was found to be well matched with that of ion-chamber measurement (Figure 7.4). In the same way the dose-distributions for 10MV photon beam were also carried out. As the TLD gives the relative measurement, the average dose value would provide the highest accuracy of dose measurement. Here it was observed that the use of 3 TLDs for each point dose measurement minimizes the error of maximum standard deviation within 1.0 to 1.5 percent for the measurement of dose value. Thus, the two following techniques were established for achieving the accurate dose measurement using TLD

- the calibrated TLD must have measurement precision of maximum 2% S.D of calibrated dose value.
- for better accuracy the 3 TLDs measurement technique will have to be used for each point dose value.

7.2 Depth dose, profile dose, penumbra dose, and build-up region dose distributions using TLDs and comparison with others standard dosimeters for some standard symmetric and asymmetric fields in the homogeneous phantom

The measurement of dose distributions on a homogeneous phantom using TLDs was taken to meet the following specific requirements: --

- Depth and field dependence in routine individual application.
- Investigation of the measurements influence of various available dosimetries on the special region such as buildup and penumbra region.
- Verification and simulation of the practical problems.

For this, sets of measurements were carried out as briefly described in table 7.1. The photon beams with some standard fields were considered and the dose-distributions were taken on the homogeneous plexiglas phantom of $30 \times 30 \times 30 \text{cm}^3$.

(a) Depth dose distributions using TLDs and ion-chamber measurement

A precise investigation on the depth dose-distribution for 5×5 , 10×10 and for $15 \times 15 \text{cm}^2$ field using photon beams of 4.0 and 10.0 MV were carried out using TLDs and as well as a standard ionization chamber (0.3cm^2 ; PTW, *Freiburg*). For ion-chamber measurement, two electrometers (DL4D, DL4I) with operating voltage of 300V to measure the ionization charge were used. The effective measuring area of the chamber was pushed into a cylindrical hole of a plexiglas phantom plate. For TLD measurement the 3TLD arrangement as described in section 7.1 was used. For all depth-dose measurement a dose of 100MU were supplied from the accelerator. The measurements were normalized to 100% at the maximum depth dose value (d_{max} is 1.1 cm for 4.0 MV and 2.1cm for 10MV).

The distribution curves are shown in the figure 7.5.

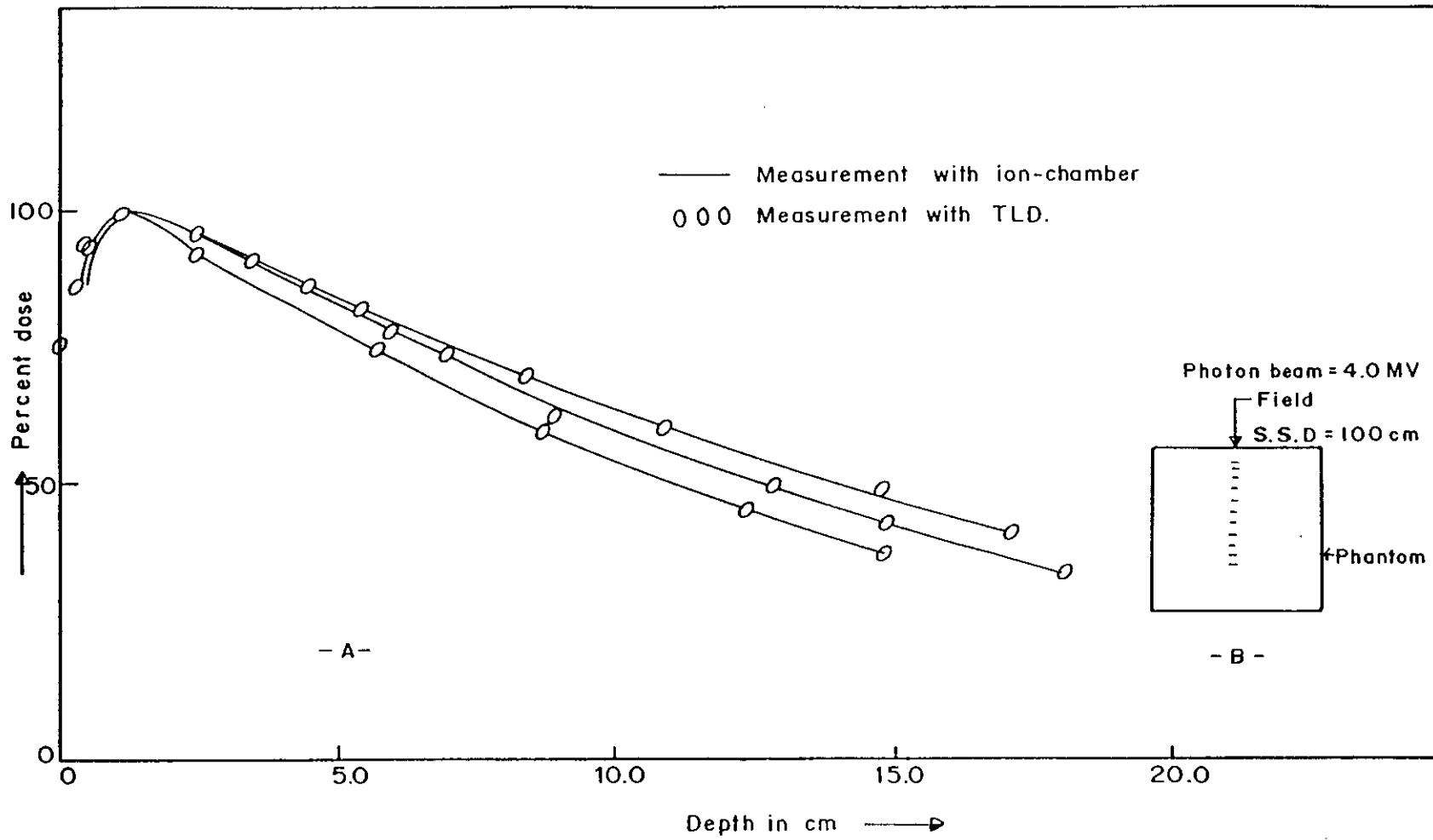


Fig. 7.5a Depth dose curves (A) in plexiglas phantom (B) for 4.0 MV photon beam. Field size 5 X 5, 10 X 10 and 15 X 15 cm² (upward); S.S.D. 100cm.

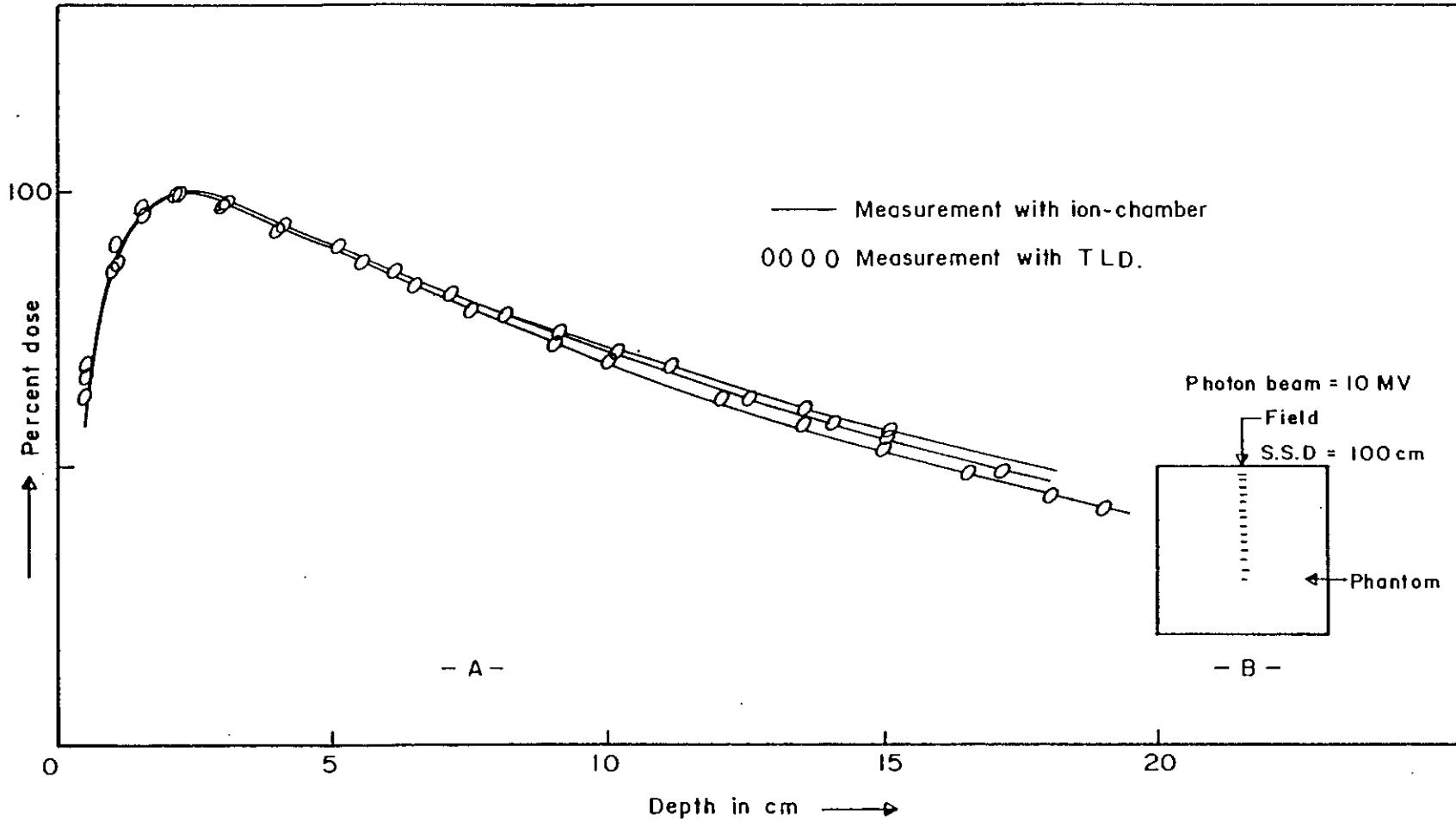


Fig. 7.5b Depth dose curves (A) in plexiglass phantom (B) for 10MV photon beam. Field size 5 X 5, 10X10 and 15 X 15 cm² (upward); S.S.D. 100 cm.

Table: 7.1

Photon Beams (MV)	Dosimeter used	Dose distribution	Fields(cm ²); S.S.D(cm)	others
4.0	TLD; Ion-chamber	(a) Depth dose curve	5x5; 10x10; 15x15;100	
10.0	TLD; Ion-chamber	(a) Depth dose curve	5x5; 10x10; 15x15;100	
4.0	TLD; Ion-chamber	(b) X-profile at 1.1 and 8.8 cm depth	5x5; 10x10; 15x15;100	
10.0	TLD; Ion-chamber	(b) X-profile at 1.1 and 8.8 cm depth	5x5; 10x10; 15x15;100	
4.0	TLD; Ion-chamber Markus chamber	(c) Penumbra region at 1.1 and 8.8 cm depth	5x5; 10x10; 15x15;100	
10.0	TLD; Ion-chamber Markus chamber	(c) Penumbra region at 1.1 and 8.8 cm depth	5x5; 10x10; 15x15;100	In Gummersbach
4.0	TLD; Ion-chamber Markus chamber	(d) Build-up region (from 0.5 to 5.0 cm depth)	5x5; 10x10; 15x15;100	
10.0	TLD; Ion-chamber Markus chamber	(d) Build-up region (from 0.5 to 5.0 cm depth)	5x5; 10x10; 15x15;100	
4.0	TLD; Ion-chamber Markus chamber	(e) Asymmetry or Block field at 1.1 cm depth	5x5; 10x10; 15x15;100	
6.0	TLD	Depth dose curve	10x10; 100	In Grossharder Univ. Klinik
⁶⁰ Co(1.25)	TLD	Depth dose curve	10x10; 80	In Essen Univ. Klinik

(b) Profile dose-distributions using TLDs and ion-chamber dosimeter.

The X-profile distributions were taken at the two depths of the phantom, one at the maximum dose depth (d_{max}) and the other was at the 8.8 cm (equivalent of 10cm water) depth in the plexiglas phantom, for the same fields used for depth dose distribution. The profile-dose distribution was carried out at points, every 1.0cm along the cross-distance of the photon beams using both TLDs and ion-chamber dosimeter.

The distribution curves were normalized with the dose of d_{max} . The curves are shown in figure 7.6, which are also well matched with ion-chamber measurement.

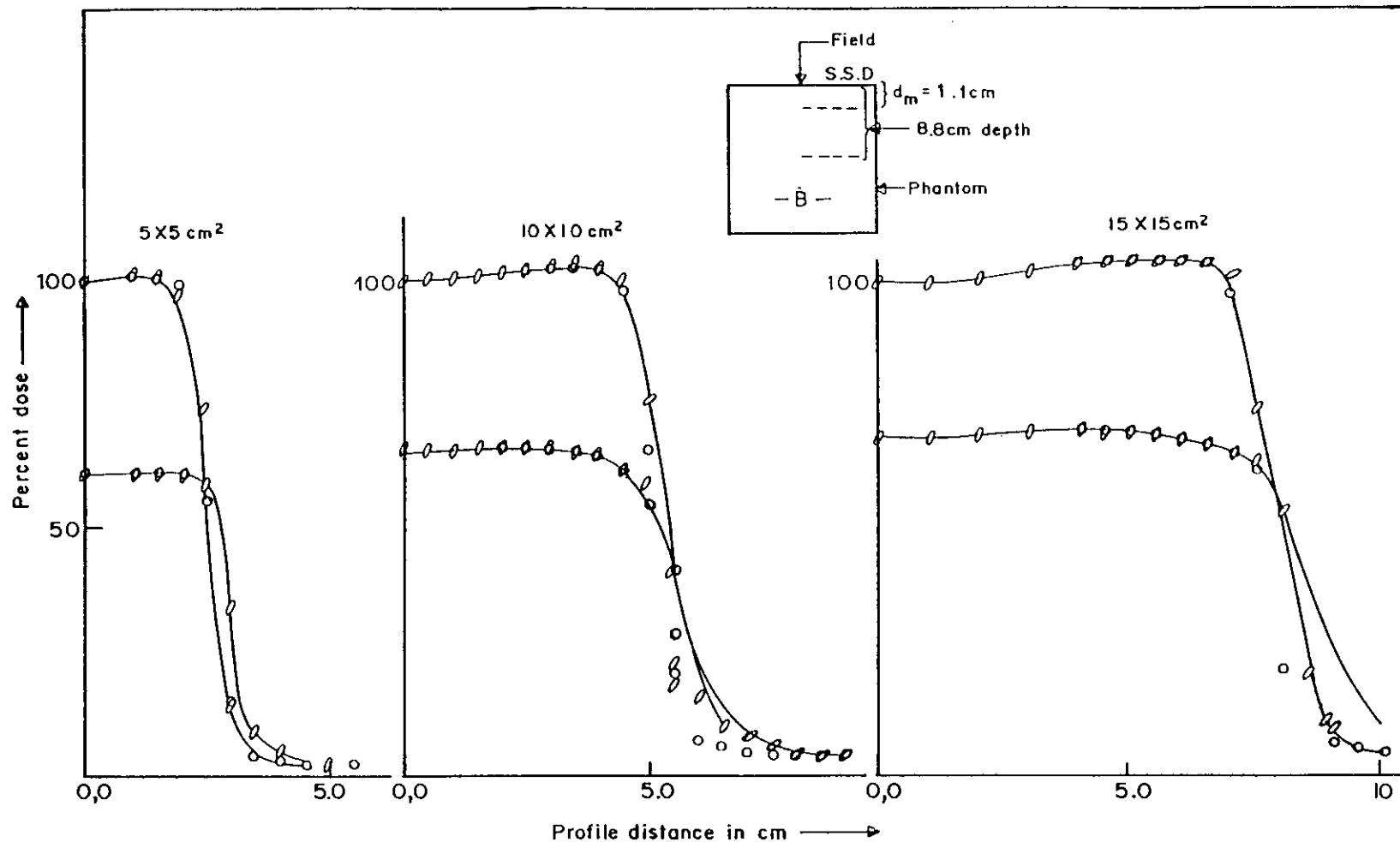


Fig. 7.6a Dose profiles in depth at 1.1 cm and 8.8 cm (down ward) in plexiglas phantom (B) for 4 MV photon beam for different field sizes; S.S.D. 100 cm. Measurement with ion-chamber (—) TLD (ooo) and Markus chamber (ooo).

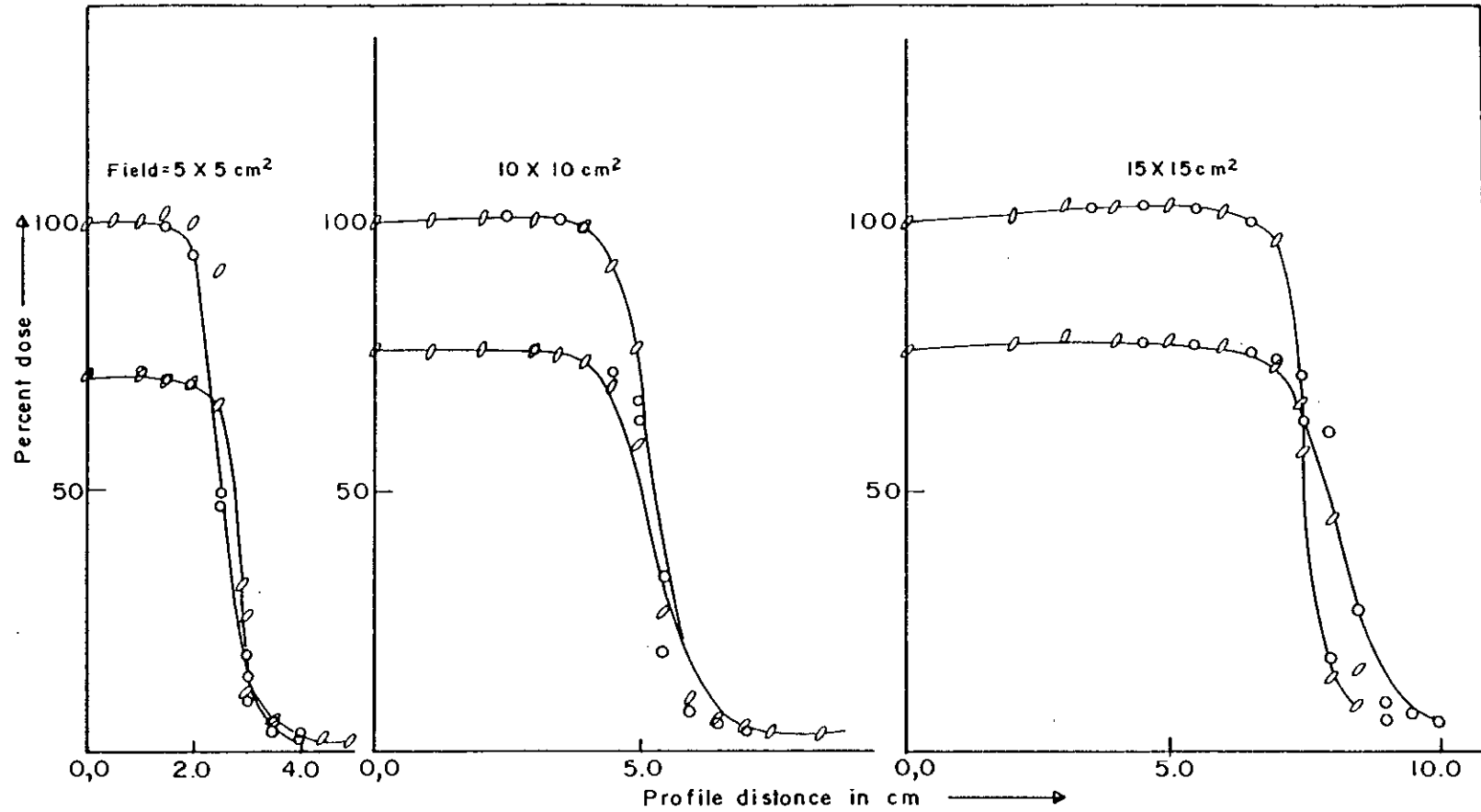


Fig. 7.6b Dose profiles in depth at 2.1 cm and 8.8 cm (down ward) in plexiglas phantom for 10.0 MeV photon beam for different field sizes; S.S.D. 100cm. Measurement with ion-chamber (—) TLD. (o o o) and Markus chamber (o o o o).

(c) Penumbra dose-distributions using TLDs ion-chamber and Markus chamber dosimeter.

The measurements were carried out on the Penumbra regions of photon fields of 5×5 , 10×10 and 15×15 of 100cm for both the photon beams using TLDs, ion-chamber and Markus chamber. The same electrometers were used for both the chamber measurements and were calibrated accordingly. The dose was measured at points every 0.5cm along the cross-distance of the photon beam.

The distributions were normalized at the maximum central depth-dose. The curves are shown in figure 7.7.

(d) Build-up region with TLDs, ion-chamber and *Markus* chamber dosimeter.

The absorbed dose-distribution close to the surface is of special interest in radiotherapy because of the skin sparing effect. So an investigation was carried out to observe the characteristic feature of the dose-distribution in the build-up region which occurs between the surface and the depth where the dose reaches its peak. For this, the dose-distribution using TLD, ion-chamber and *Markus* chamber for the field sizes of 5×5 , 10×10 and $15 \times 15 \text{cm}^2$ for the both photon beams of 4.0 and 10MV were used.

The dose distributions were normalized at the 5.0-cm depth dose value for better comparison. The distribution curves are shown in the figure 7.8.

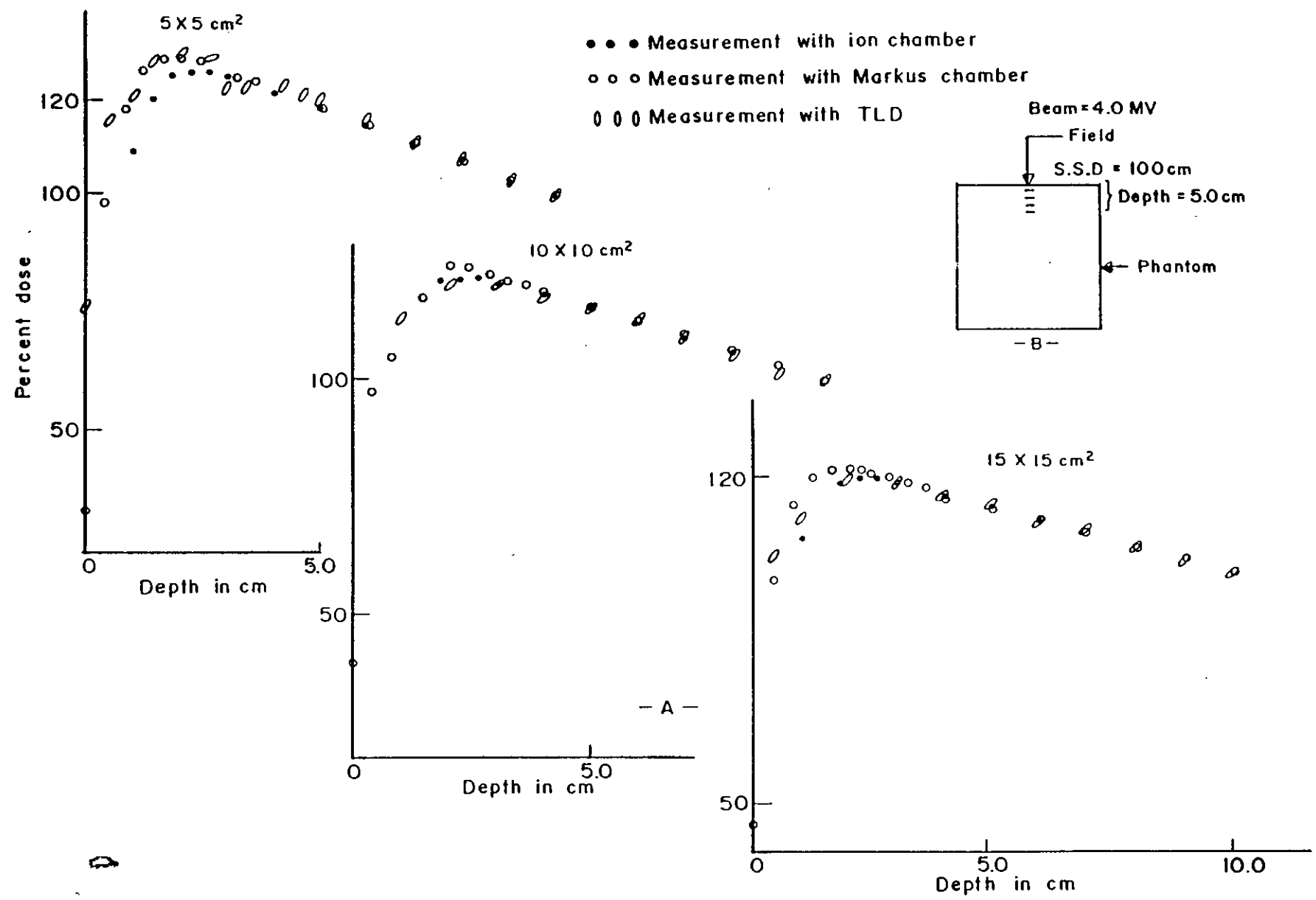


Fig.7.7a Depth dose curves (in Build up region) in plexiglas phantom for 4.0 MV photon beam for different field sizes; S.S.D. 100 cm.

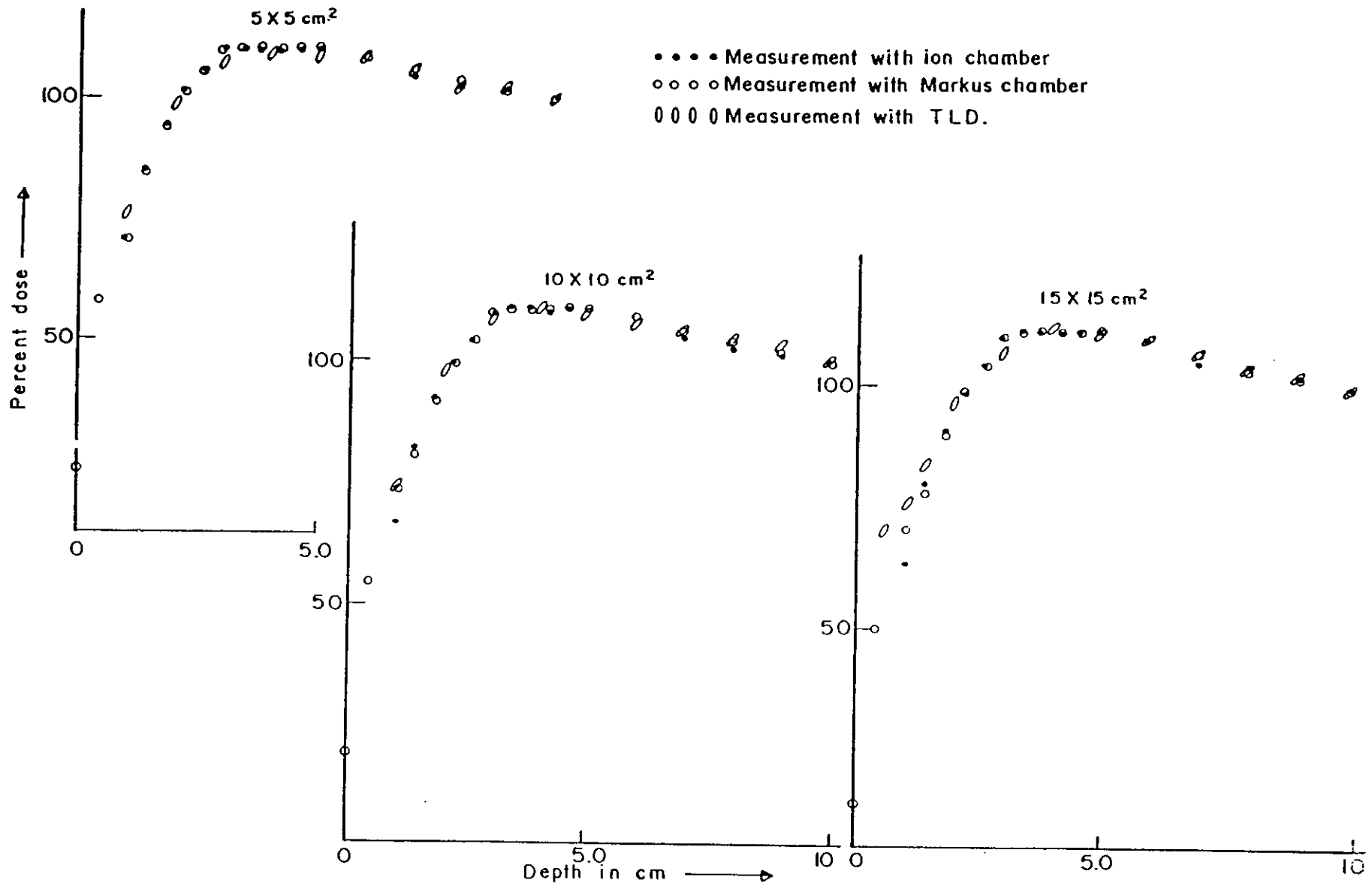


Fig. 7.7b Depth dose curves (in Build-up region) in plexiglas phantom for 10MV photon beam for different field sizes; S.S.D. 100cm.

(e) **Dose distribution of asymmetric collimated beam measured with TLD, ion-chamber and Markus chamber dosimeter.**

To investigate the features of the asymmetric beam, the TLD, ion-chamber as well as *Markus* chamber dosimeters were taken to measure the dose-distribution of 5×5 , 10×10 , and $15 \times 15 \text{cm}^2$ for the two photon beams of 4.0 & 10MV energy. The collimator of the accelerator was kept at 270° degree and the beams were directed at 90° degree perpendicularly on the phantom. For both the photon beams, the cross-profile dose-distribution was taken at the depth of d_{max} .

The dose-distribution curves were normalized at the central d_{max} for the symmetric field. The distribution curves carried out are shown in the figure 7.9.

In the dose distribution curve, at the half-width of the central maximum dose, the field size was found to be accurate for measurement with TLD. For the chambers, the field width was found to be lower. This happens, as the field edge does not cover the chamber volume completely as a result of which lesser doses were obtained than the actual dose.

The figure shows that all the distribution curves measured with TLDs were well matched with those measured by ion-chamber and Markus chamber dosimeter.

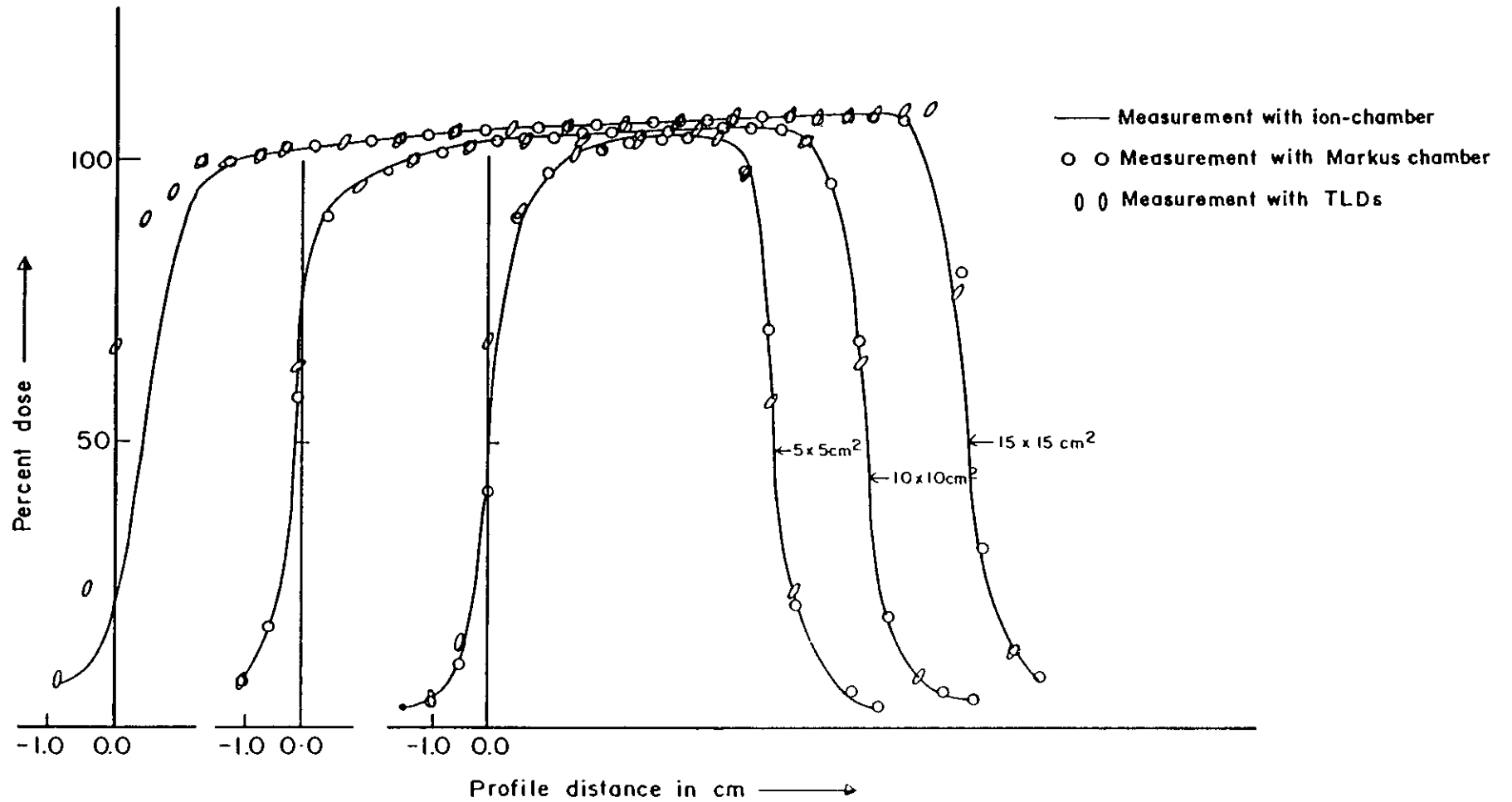


Fig.7.8 Dose profiles in depth at 1.1cm in plexiglass phantom for 4.0 MV photon beam for different asymmetric fields.

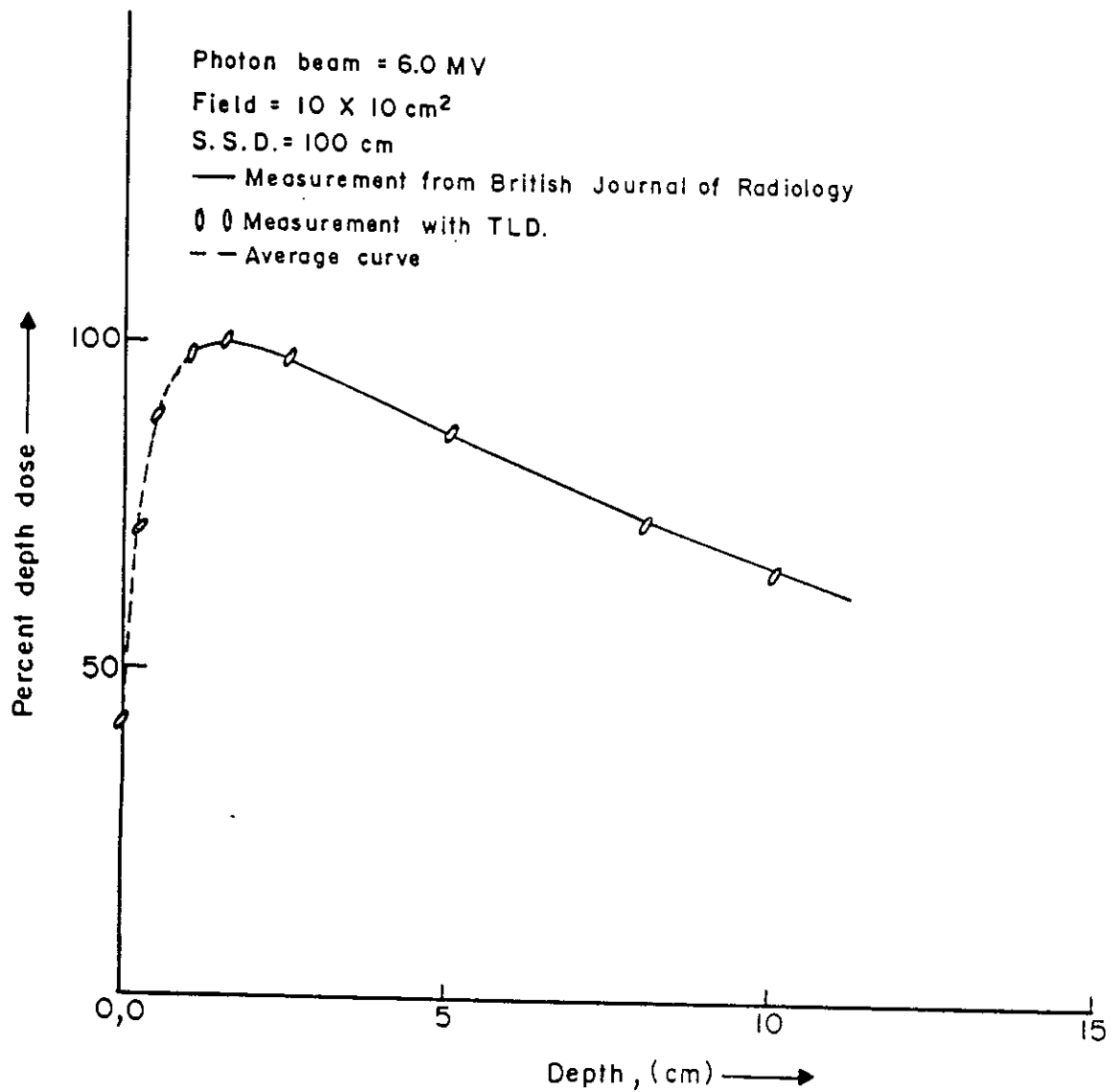


Fig. 7.9 Depth dose curve in polysterene phantom for 6.0 MV photon beam. Field size 10 X 10cm² ; S.S.D. 100cm.

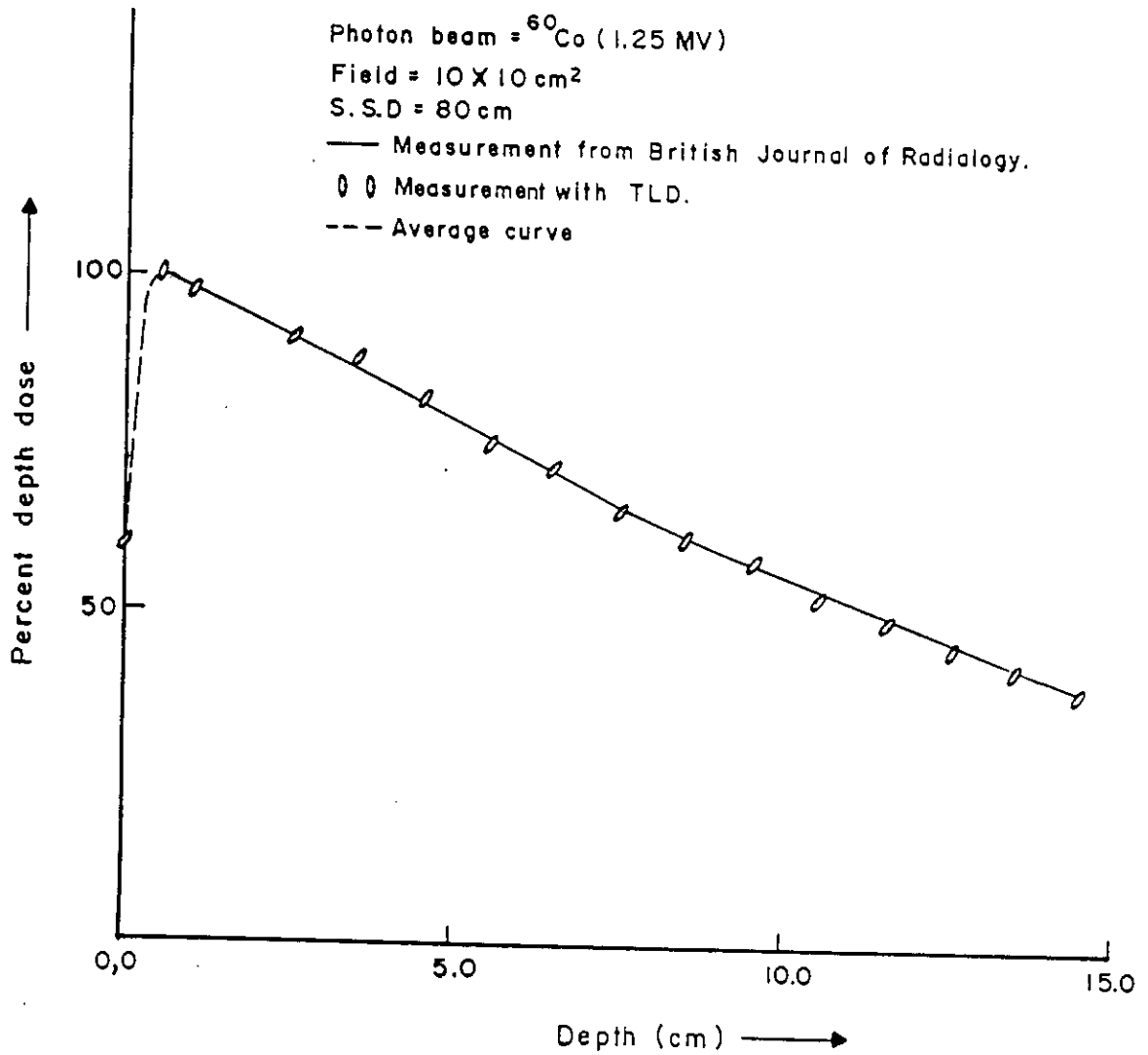


Fig. 7.10 Depth dose curve in polystyrene phantom for 1.25 MV (^{60}Co) photon beam. Field size $10 \times 10 \text{ cm}^2$; S.S.D. 100cm.

8.0 COMPARISON OF TL-DOSIMETRY WITH OTHER STANDARD DOSIMETRY IN SOME INHOMOGENEOUS SITUATIONS.

In inhomogeneous system, the measurements are described in the following four steps:

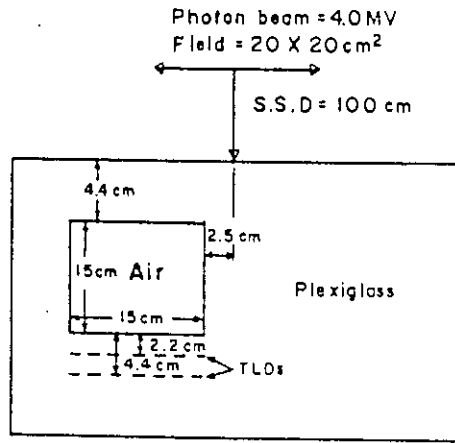
- 1.a.) *Dose distribution in phantom containing air inhomogeneity.*
- 1.b) *Dose measurement in Plexiglas-Cork-Plexiglas phantom to investigate the electronic equilibrium.*
- 2) *Dose distribution on a phantom for tangential field used in breast irradiation.*
- 3) *Depth dose and x-profile distribution in Lung-phantom of finite geometry.*
- 4) *Measurement of dose-distribution in the vicinity of Aluminum interface*

8.1.a. Dose distribution in phantom containing air inhomogeneity.

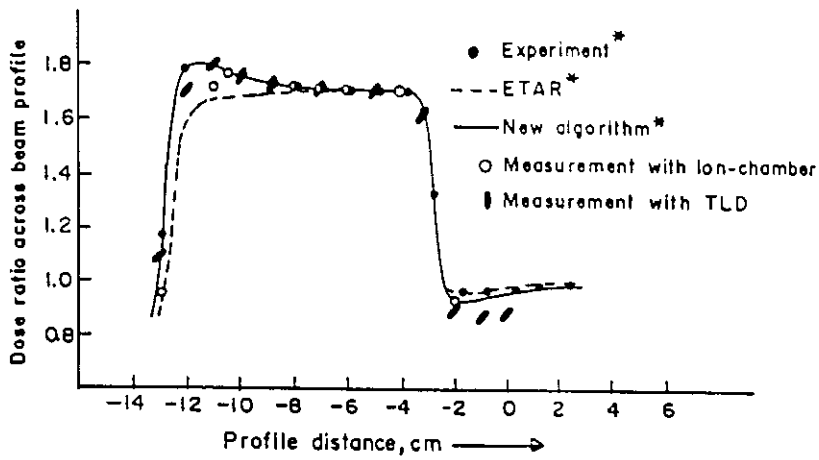
Methods and Materials

This experiment was carried out using 4.0MV-photon beam with 20x20cm² field and 100cm S.S.D on a phantom as shown in figure8.1a. A 15 × 15cm²-air inhomogeneity was taken inside the Plexiglas phantom at a depth of 4.4cm and at distance of 2.5cm from the central axis. Beam profiles were measured using TLD and also with ion chamber dosimeter along the central axis at a distance of 2.2cm & 4.4cm beyond the inhomogeneity.

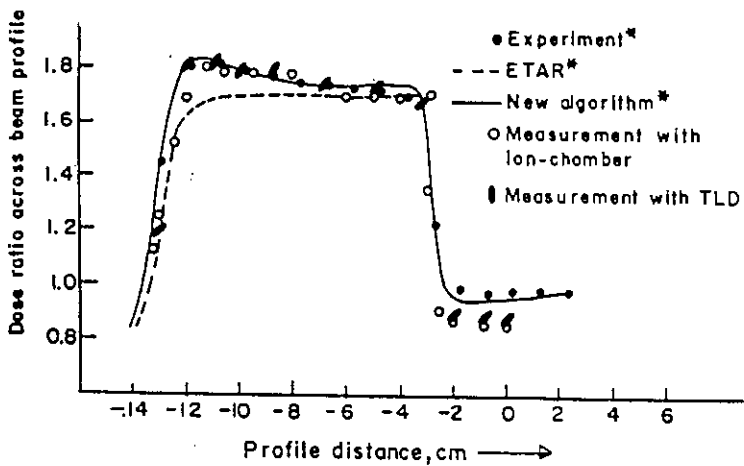
AT Redpath and D I Thwaites⁶⁰ using a therados RFA7 beam data-acquisition system in the dept. of Medical Physics & Medical Engineering, Edinburgh, UK (1991) carried out the same experiment. They used a water phantom and measured the same profile dose distribution using ion-chamber dosimeter.



(a) Experimental situation



(b) 2.2 cm beyond air inhomogeneity.



(c) 4.4 cm beyond air inhomogeneity.

Fig.8.1 Dose ratio (b,c) using air inhomogeneity [a]
(*experiment carried out by AT Red path and Thwaites.

In the present studies no measurement was made in sites close to the interface where electrons equilibrium does not exist. The ratio of the absorbed dose with an inhomogeneous to homogeneous phantom was taken. The results showed good agreement with the findings based on a new algorithm devised by AT Redpath and D I Thwaites. They carried out the experiment using the ion chamber dosimeter.

The dose ratio is the correction factor that would be applied to the dose measured in the unit density material. As change in the dose due to the presence of an inhomogeneity is small, the precision of the dosimetry must be ensured. Here it would be noted that the following experiment was carried out using one TLD at each point dose measurement. The same TLD for the same point dose measurement was used for both the situations (homogeneous and inhomogeneous) and the ratio gave a good result, which is shown in the figure 8.1(b,c). This may be due to the canceling of the fluctuating nature of the same TLD in its dose ratio calculation. Thus, in the dose ratio measurement, the single TLD arrangement for single irradiation would provide good result. On the contrary, with the ion chamber dosimetry it requires several irradiation to measure the same profile dose distribution measurement. Therefore, TLD would have better performance than other dosimeters in the type of studies mentioned above.

8.1.b Dose measurement in Plexiglas-Cork-Plexiglas phantom to investigate the electronic equilibrium.

Methods and Materials

For this, the Phantom was assembled with 2.6cm thick Plexiglas followed by 6.0cm cork and again 12cm thick slab of Plexiglas. The photon beam of 10MV was considered to be the higher one while the 4.0 MV beams was the lower one. In the same way two photon fields of $3\times 3\text{cm}^2$ and $20\times 20\text{cm}^2$ at S.S.D of 100cm were considered. Using these fields for both the energies individually, the depth dose distributions were measured using TLDs and ion-chamber dosimeter in the homogeneous and also in the inhomogeneous Phantom.

The measurements were all normalized to 100 for the maximum dose value. The distribution curves are shown in figure 8.2 to 8.5. It may be seen that the present result is in good agreement with results obtained by M.K. Woo, J. R. Cunningham and J. J. Jegioranski⁷³ in the dept. of Toronto University. In their experiment 18MV photon beam energy and a phantom of 5.0cm polystyrene followed by 8.0cm cork and again 7.0cm polystyrene were used. The depth dose distributions were measured and compared with calculated data from equivalent tissue air ratio (ETAR) method and also with the curve calculated from Monte Carlo.

Their results are shown in figure 8.6. It may be seen that the present result is in good agreement with those results.

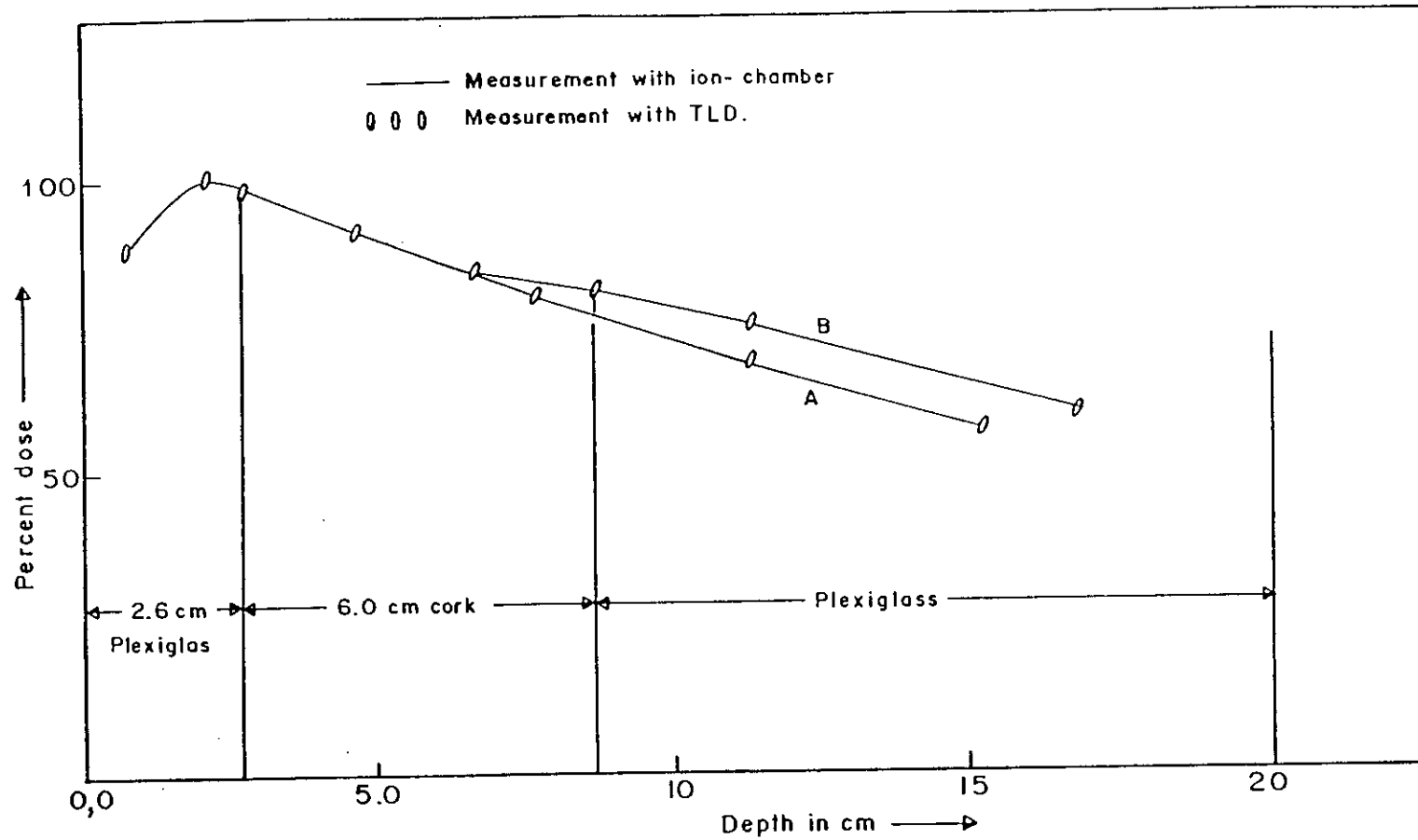


Fig. 8.2 Depth dose in plexiglas Cork-plexiglas (B) and in homogeneous plexiglas phantom (A) for 10MV photon beam. Field size 20 X 20 cm², S.S.D. 100cm.

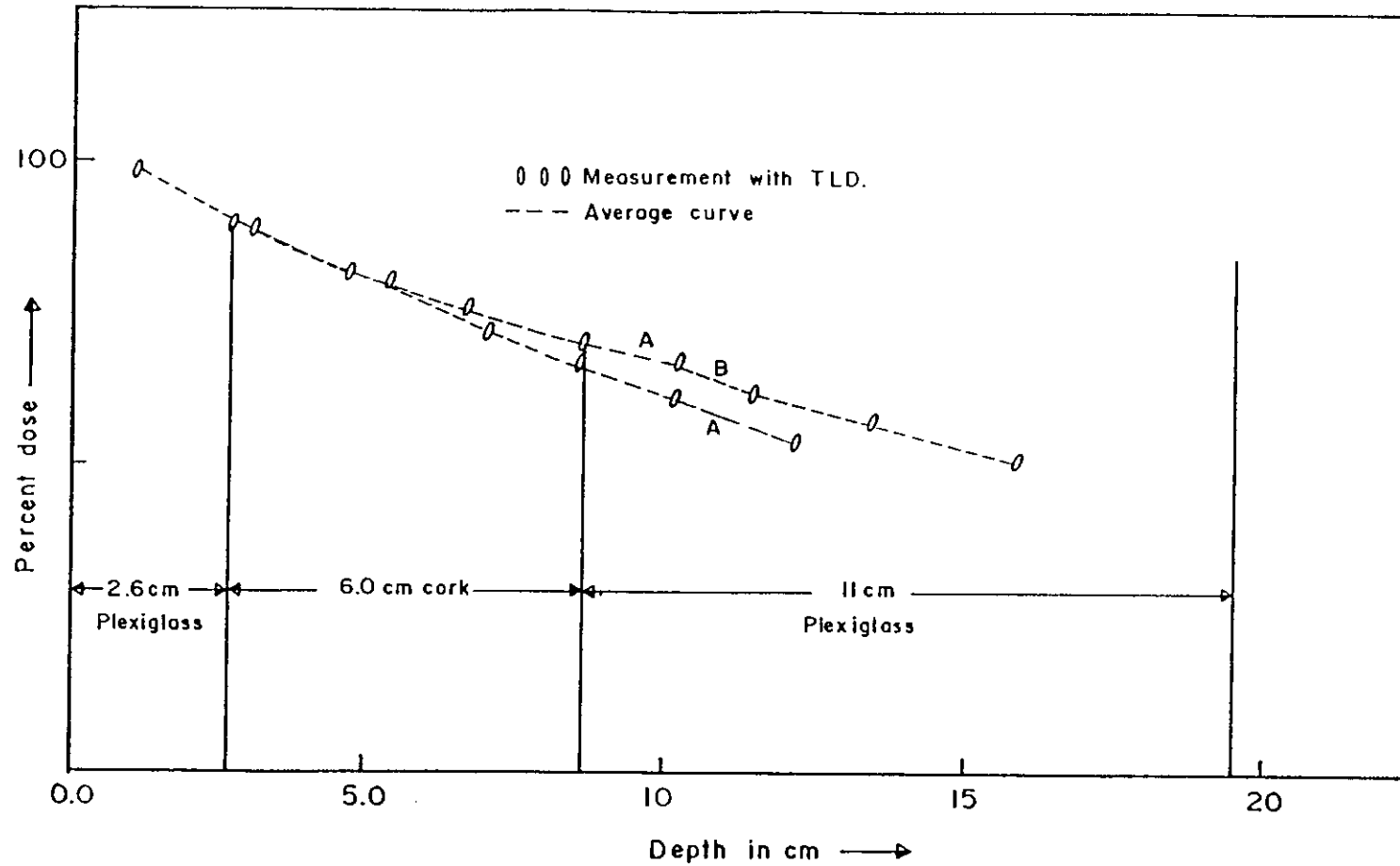


Fig. 8.3 Depth dose curve in plexiglas Cork-plexiglas (B) and in plexiglas phantom (A) for 4.0MV photon beam. Field size 20X20cm²; S.S.D. 100cm.

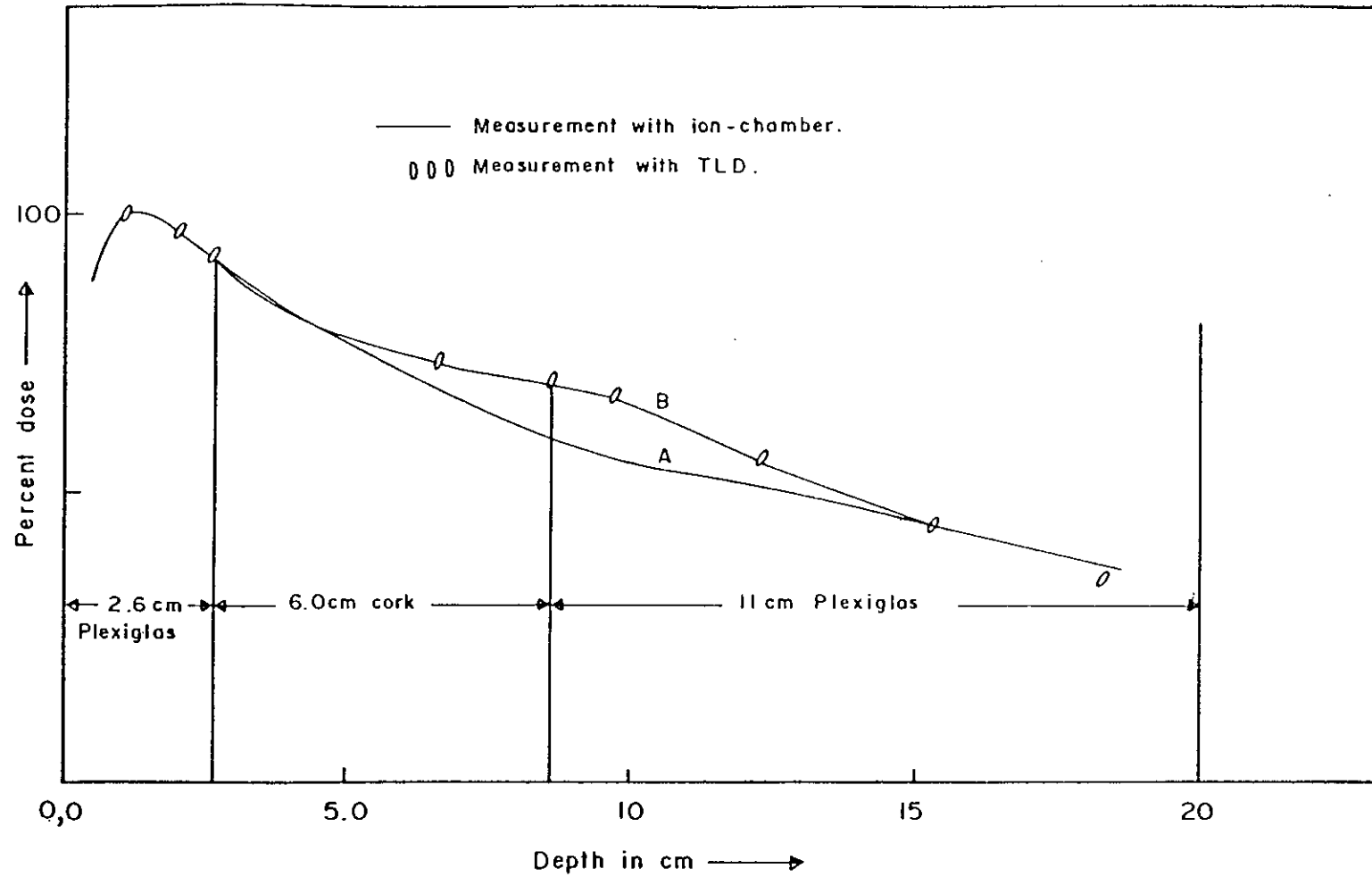


Fig. 8.4 Depth dose curve in plexiglas Cork-plexiglas (B) and in homogeneous plexiglas (A) phantom for 4.0 MV photon beam. Field size $3 \times 3 \text{ cm}^2$; S.S.D 100 cm.

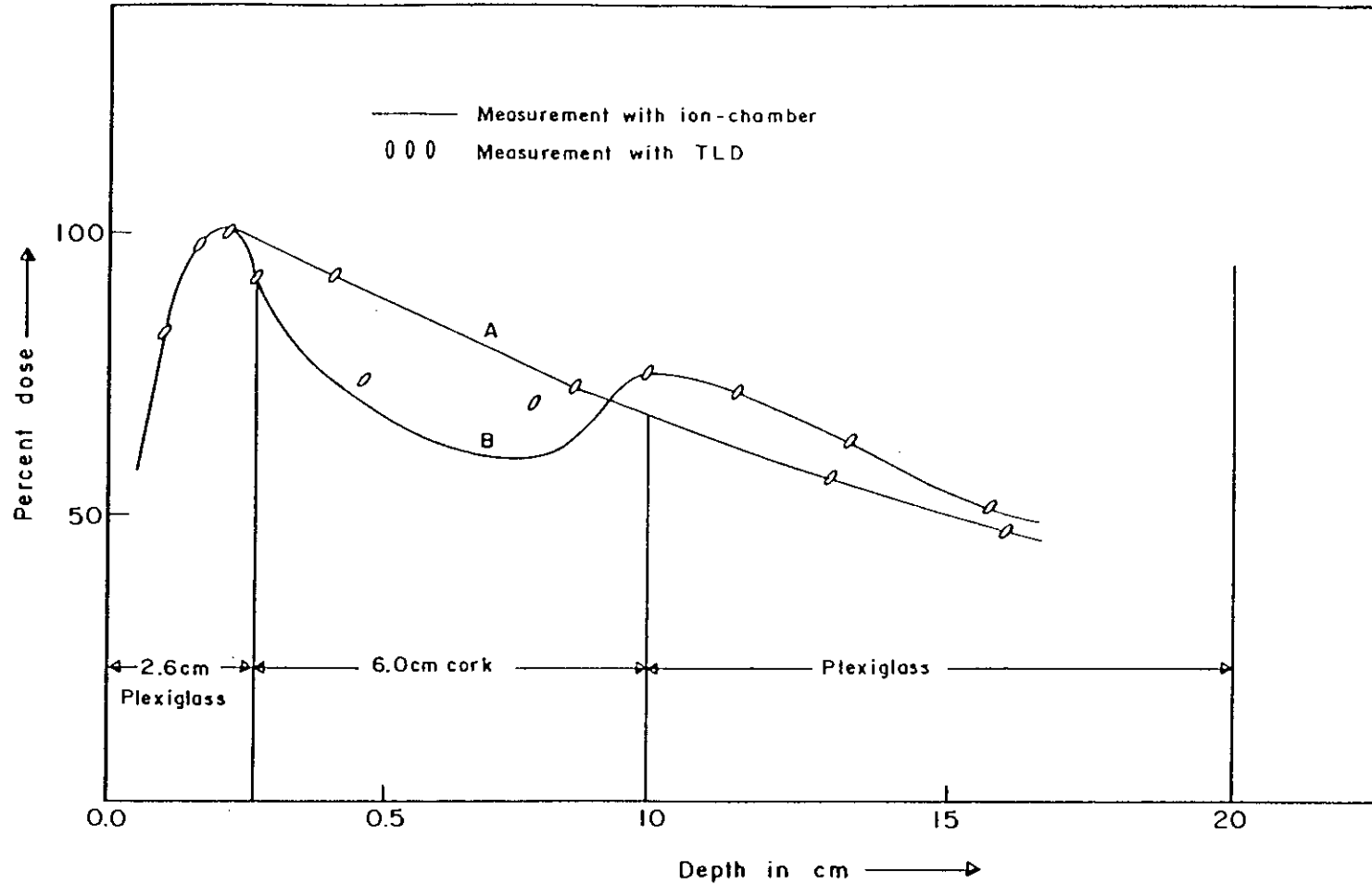


Fig. 8.5 Depth dose curve in plexiglass Cork-plexiglass (B) and in homogeneous plexiglass (A) phantom for 10MV photon beam. Field size $3 \times 3 \text{ cm}^2$, S.S.D. 100cm.

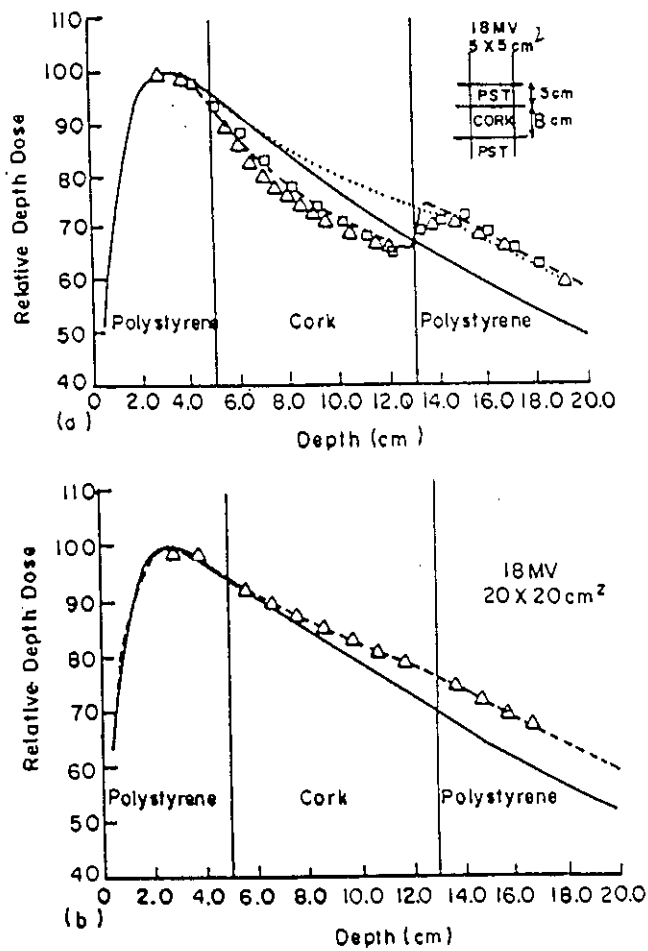


Fig. 86 Comparison of the calculated central axis depth dose to measured data. An 18MV beam was incident on either a homogeneous polystyrene phantom or a polystyrene-cork-polystyrene phantom. the triangles ($\Delta\Delta\Delta$) curve is measured data. The dotted (.....) curve is calculated using the equivalent tissue-air ratio method with the original tissue-air ratio data. The dashed (---) curve is calculated by the same method but with the new extended data. The squares ($\square\square\square$) curve is calculated from Monte Carlo.

8.2 Dose distribution on a phantom for the tangential field used in breast irradiation.

Methods and materials

The experimental situation as in figure 8.7A was taken to simulate a tangential field used in breast irradiation. A 15×15 -cm² beam from 4.0 MV was directed vertically into the slabs of plexiglas phantom with the central axis located 1.0 cm from the interface to ensure electron equilibrium.

Measurements were carried out on the mid-plane of a phantom of a 26.4cm thick plexiglas (30cm equivalent thickness of water phantom) using TLD and as well as ion chamber dosimeter. The measurements were taken with and without phantom to give full or partial scattering.

The same experiment were also carried out by AT Redpath and D I Thwaites in Western General Hospital, Edinburgh, UK. They compared their experimental result with those obtained from a similar theoretical comparison described by Wong and Hankelman (1983).

The present results were plotted on their experimental curve⁶⁰. A good agreement with their observation was obtained except the edge (Figure 8.7B).

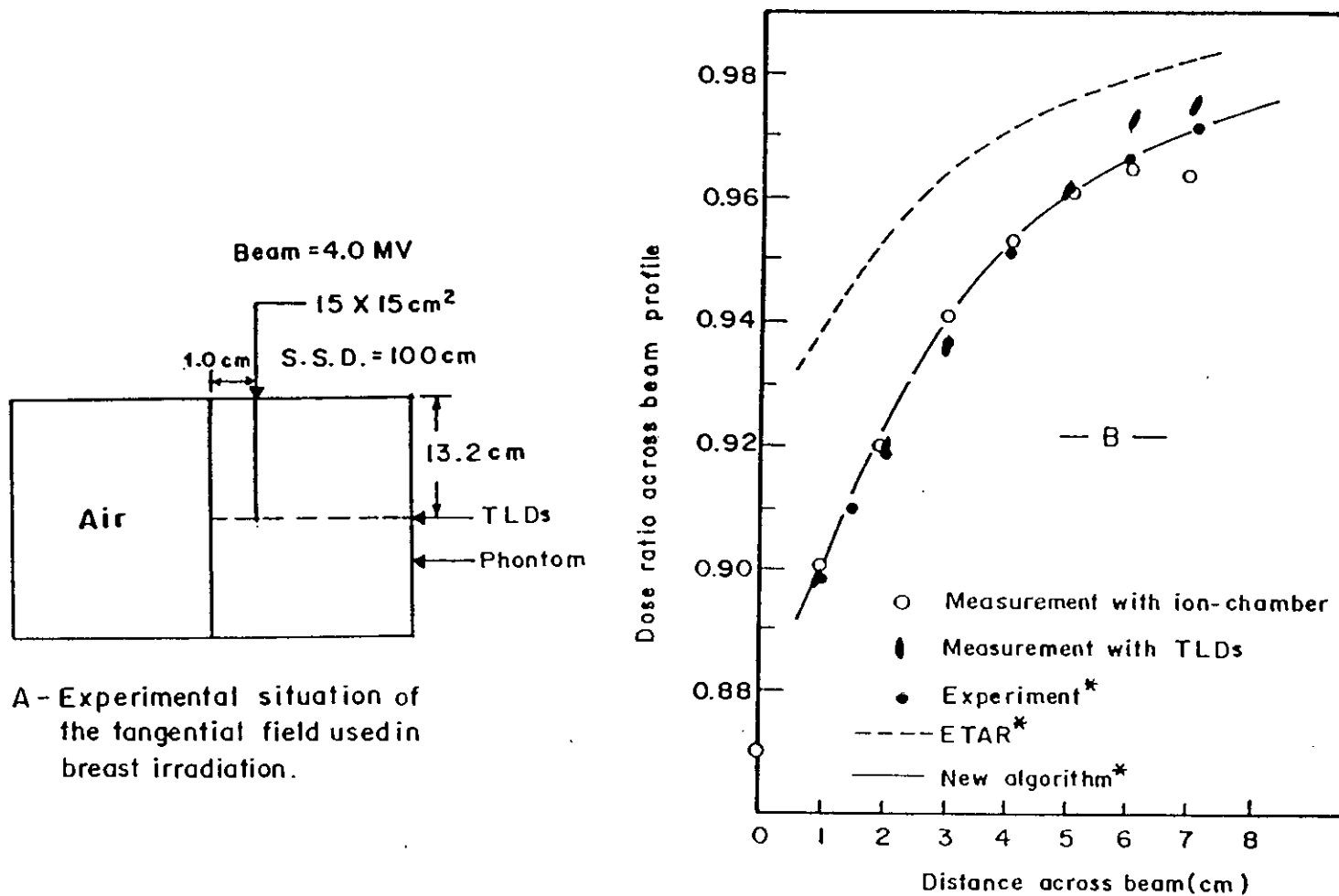


Fig. 8.7 Dose ratio across the beam (B) the experimental situation of A (*experiment carried out by AT Redpath and DI Thwaites).

8.3 Dose distribution in Lung-Phantom of finite geometry.

Methods and materials

A lung phantom ($29 \times 29 \times 29 \text{cm}^3$) with lung analogue ($=0.30 \text{g/cm}^3$) of a total $10 \times 10 \times 10 \text{cm}^3$ volume comprised of slices of different thickness surrounded by fixed polystyrene of same thickness as the slices was taken. Grooves for holding the TLD-rod were made on the two slices of which one was with lung analogue and the other was solid plate. The Phantom can be used as the half geometry representing one lung of the human body.

Taking the two different mediastinum cases used in treatment planning the measurements were carried out for the photon beam of 4.0 and 10MV.

- (i) the phantom with lung analogue at 5.0cm depth, a depth dose distribution along the line, 2.5 cm distance from the lung analogue and a cross-profile dose distribution at 10 cm depth for the field of $10 \times 10 \text{cm}^2$ and for 100cm S.S.D was measured.
- (ii) The phantom with the lung analogue at 3.0cm depth was taken. A cross-profile dose distribution at 10cm depth for the photon field of $20 \times 20 \text{cm}^2$ at S.S.D of 100cm taking the central beam at 3.0 cm from the lung analogue was measured. The same measurement was also carried out for the photon beam of $1.25(^{60}\text{Co})$ at the therapeutic physics department in Essen Univ. clinic.
- (iii) For the same condition of the beams for the same phantom described in (ii) a cross-profile dose distributions at 10-cm depth for the central beam through the central lung analogue were carried out.

All profile dose distributions were compared with those for homogeneous phantom measurements. The results obtained were shown in figure 8.8 to 8.13.

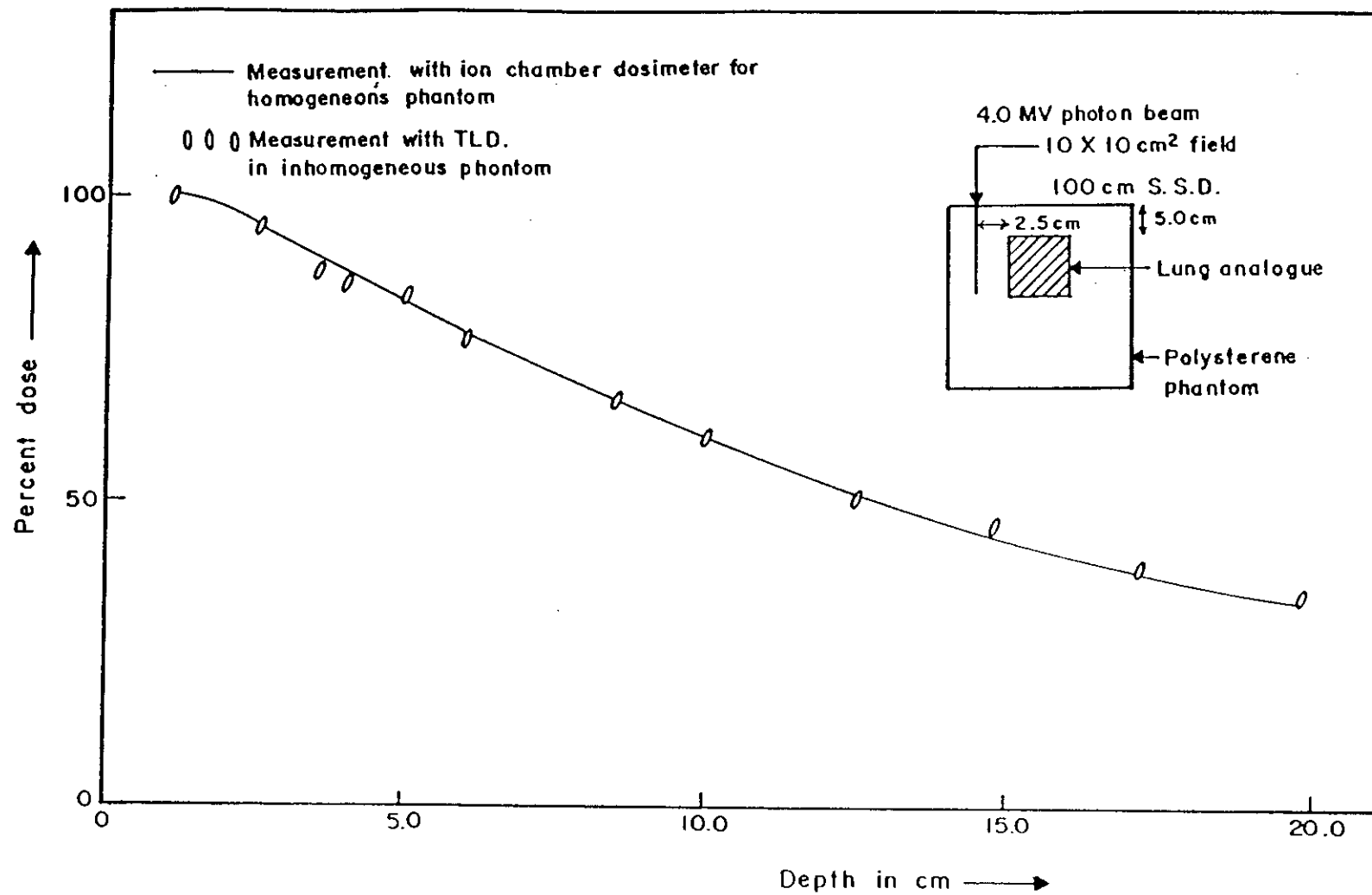


Fig.8.8 Depth dose curve at central axis in the mediastinum geometry 10 X 10 cm² field size, 100 cm S.S.D for 4.0 MV photon beam.

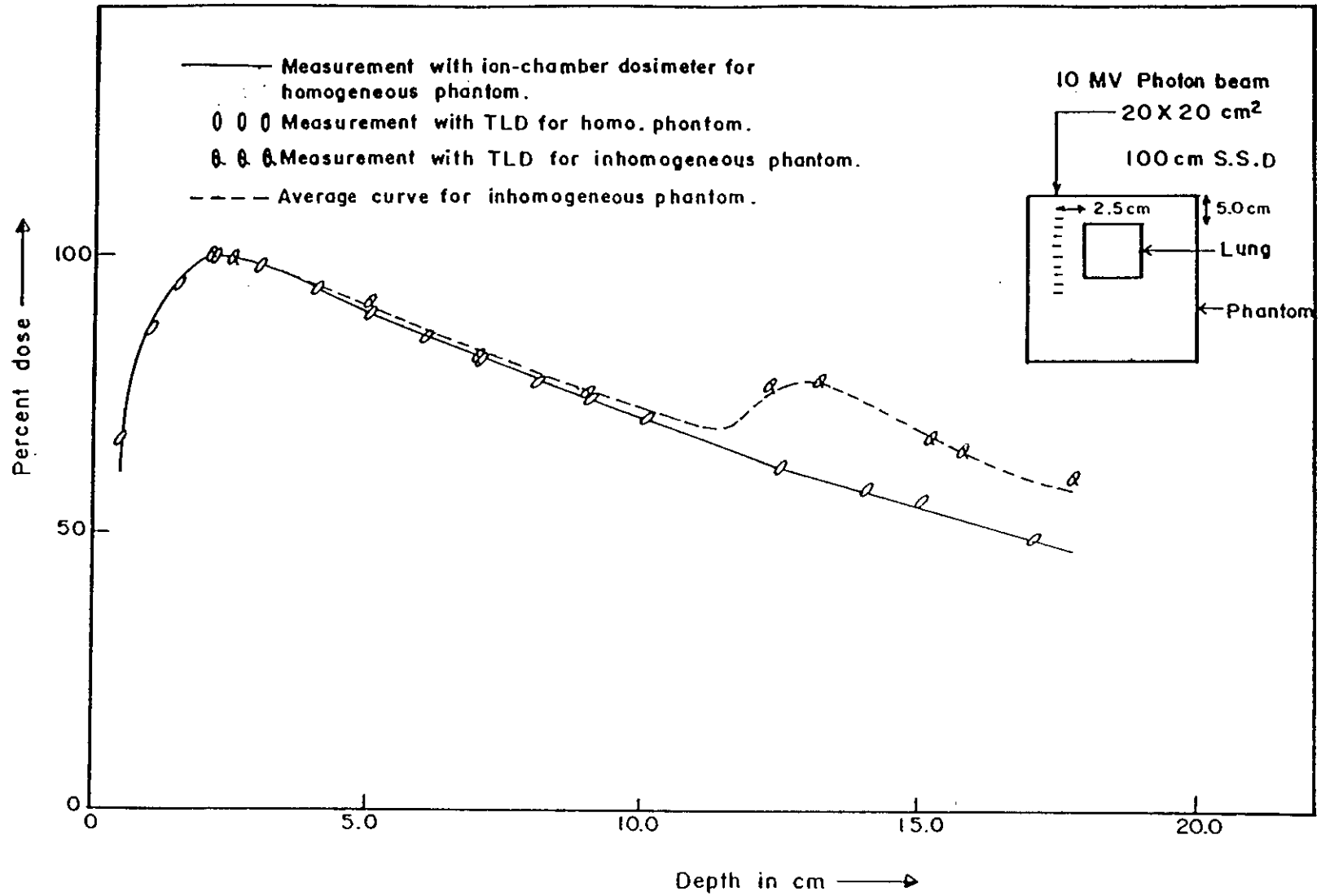


Fig. 8.9 Depth dose curve at central axis in the mediastinum geometry 10 X 10 cm² field size, 100cm S.S.D. for 10MV photon beam.

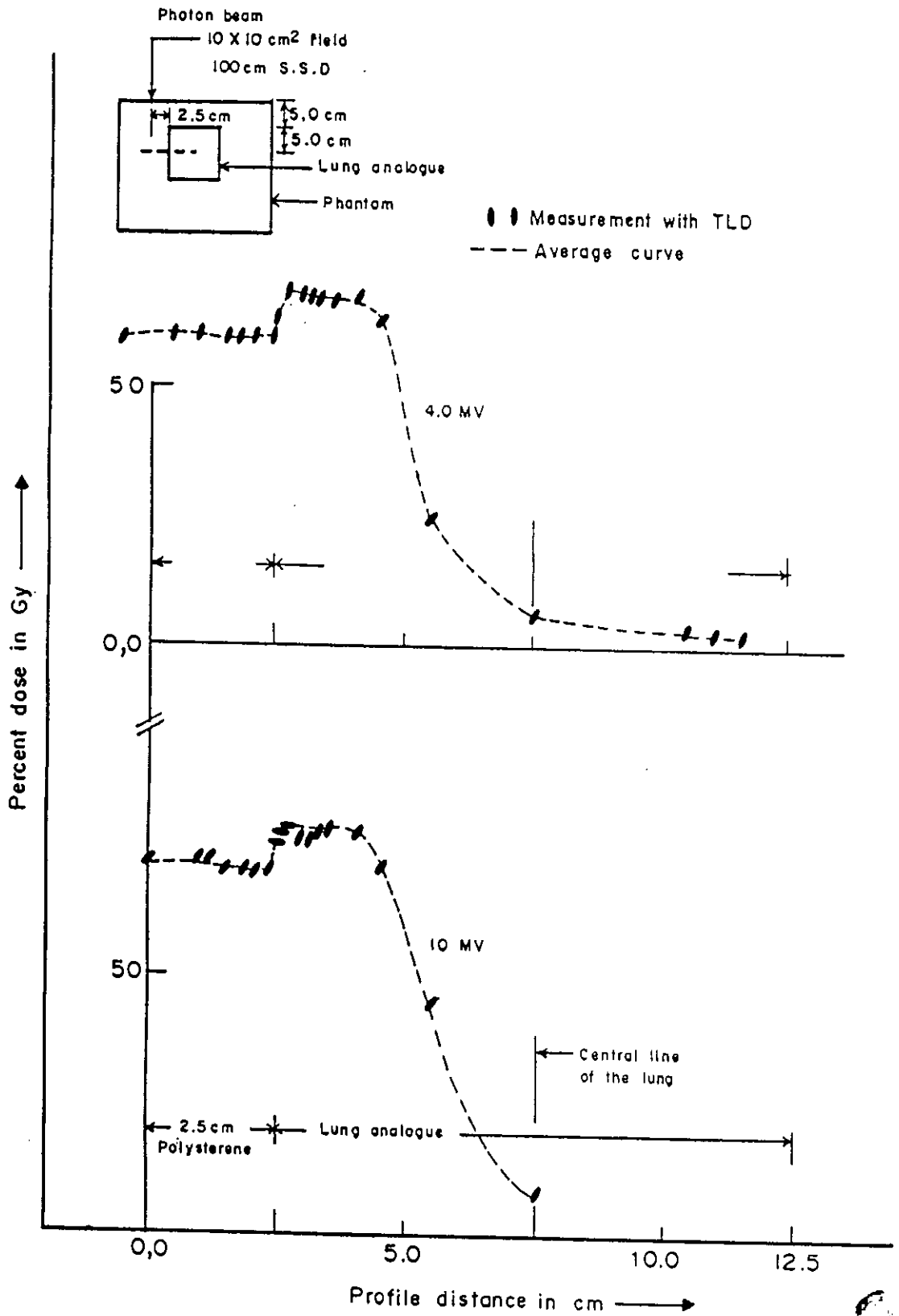


Fig. 8.10 Profile dose at 10cm depth used in the mediastinum treatment planning. 10X10 cm² field size, 100cm S.S.D. for (a) 4.0 MV and (b) 10MV photon beam.

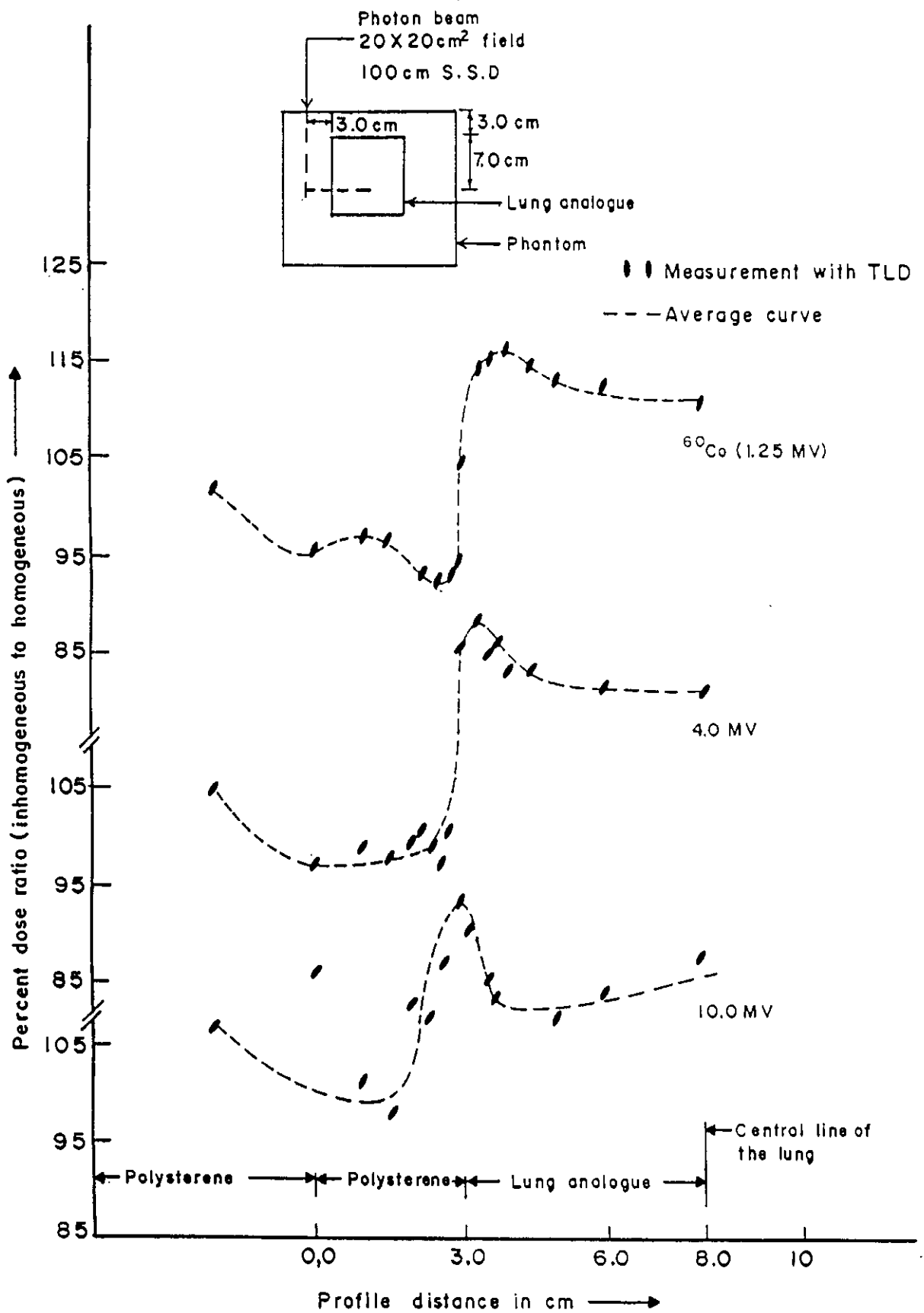


Fig.8.11 Profile dose ratios at 10cm depth in Lung phantom for 4.0 and 10MV; 20X 20cm² field size; S.S.D=100cm.

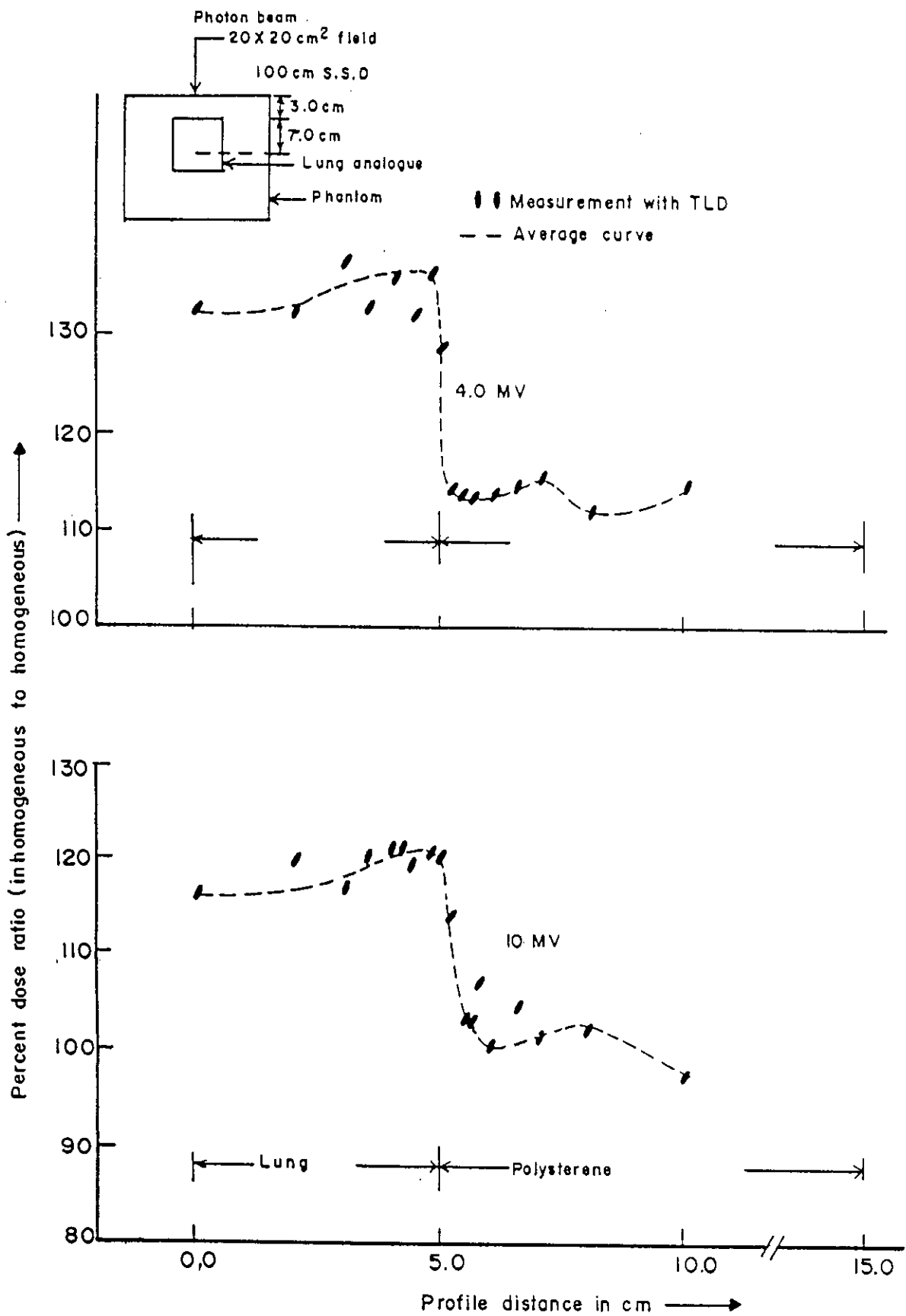


Fig.8.12 Profile dose at 10cm depth in Lung phantom for the central beam at 3.0 cm from the Lung analogue for the energy 1.25 (⁶⁰Co), 4.0 and 10MV 20X20cm² field size; S.S.D. 100cm

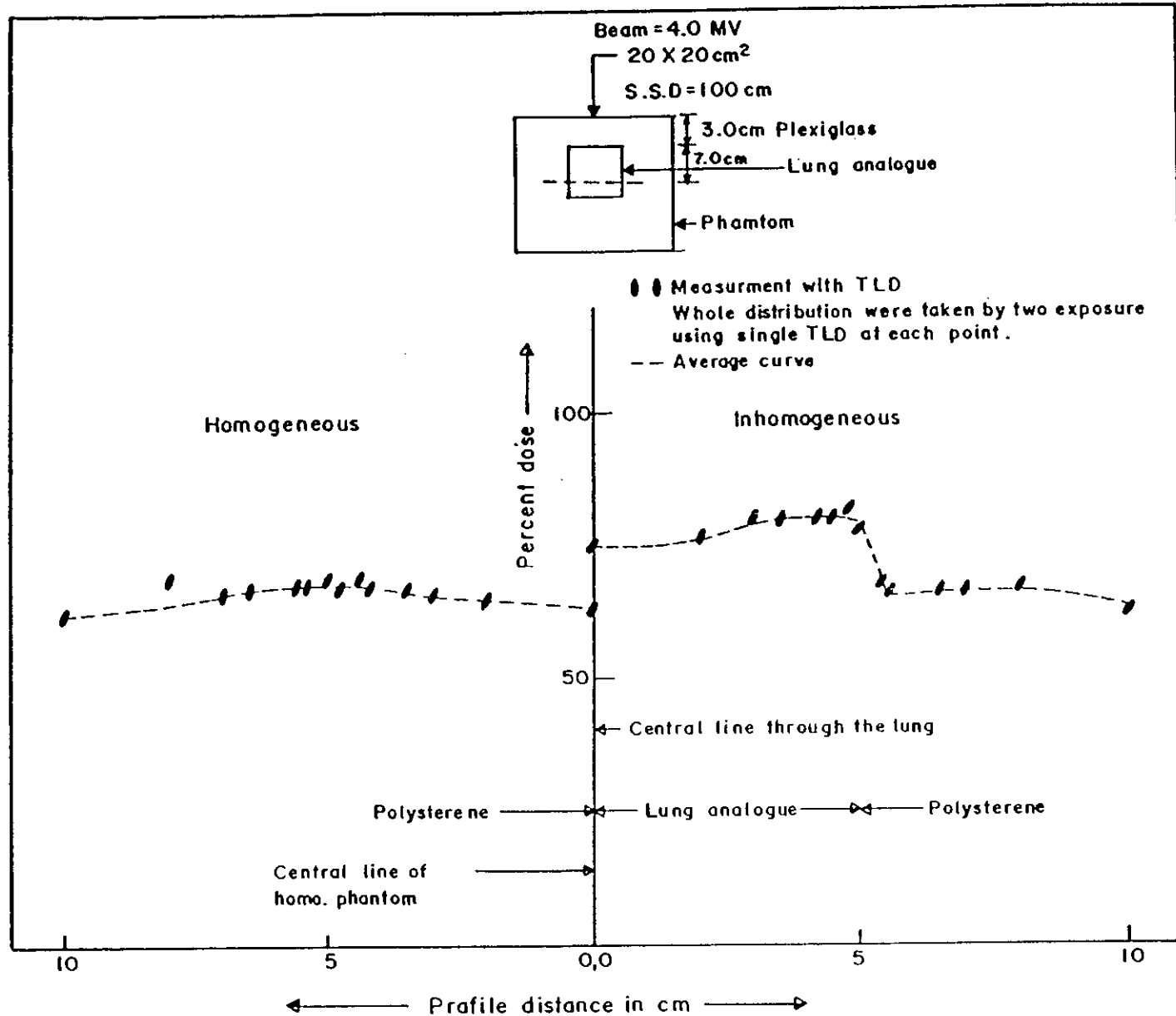


Fig. 8.13 Profile dose distribution at 10 cm depth in homogeneous and in inhomogeneous phantom for the photon beam of 4.0 MV; 20 X 20 cm² field size; S.S.D. 100cm.

8.4 Measurement of dose distribution in the vicinity of aluminum interface.

Introduction

Aluminum (Al) behaves similar to that of bone. The density of bone varies between about 1.2 & 1.8 whilst that of muscle is approximately 1.0gm/cc. The mass attenuation co-efficient of bone for mega-voltage beams is close to that of muscle since the Compton effect is the dominant photon interaction at these energies. Therefore, in megavoltage photon beam therapy, it is not common to take account of the effect of bone inhomogeneity⁹. However, some authors^{12,13,17} investigated a steep dose gradient especially in regions close to interface of Al surface as well as for the other metals required to be embedded into the body. The range of the overdose and underdose effect is in the order of 1.0cm in water⁶⁷. From radiological point of view the volumes concerned may not be negligible. Therefore, an investigation was carried out following the same methods as was done by Otto, A Sauer.

Methods & materials

Measurements were performed for 1.25, 4.0 & 10.0MV photon beams. Al-Plexiglas interface was taken for investigation. The thickness of the Al was 2.0cm. The dose-distributions in the vicinity of the interface were measured by using $1 \times 1 \times 6 \text{ mm}^3$ rod-type TL-dosimeter. For each point dose, 3TLDs were used. The isocenter distance of 100cm for the field size of $20 \times 20 \text{ cm}^2$ at the interface was performed.

The experiments were carried out by the two different arrangements of plexiglas phantom with the Al slab.

- (i) the dose distribution at the vicinity of 4.4cm thick plexiglas (the equivalent 5.0cm of water) in front of Al.
- (ii) the dose distribution at the vicinity of Al, taking it at the entrance surface of the phantom.

The arrangements and the results obtained are shown in figures 8.14 and 8.15.

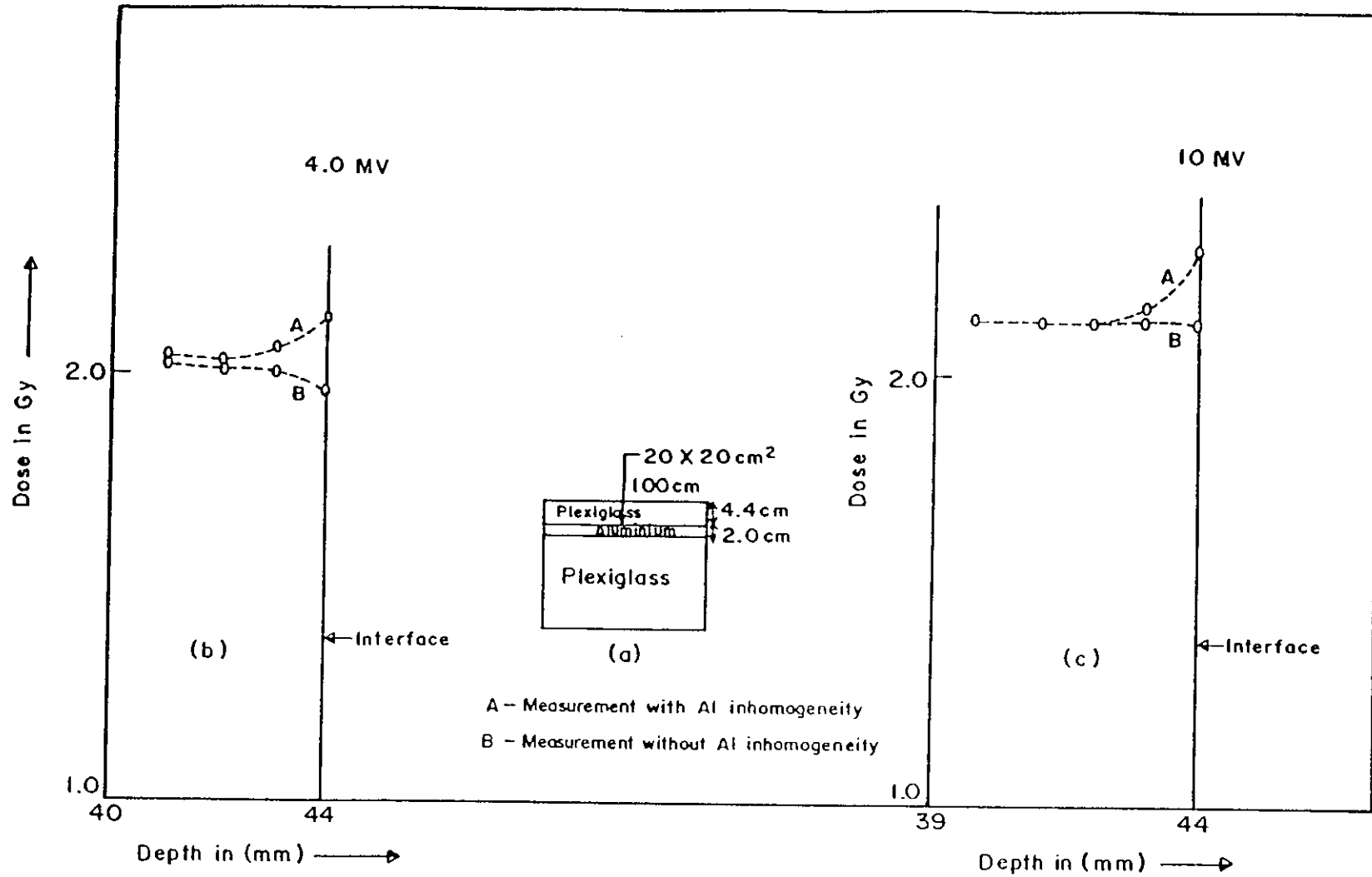


Fig.8.14 Depth dose curves (b,c) at the front interface of the plexiglas/aluminium (a) for the beam of 4.0 and 10MV energy; 20 X 20 cm² field size; 10 cm S.S.D.

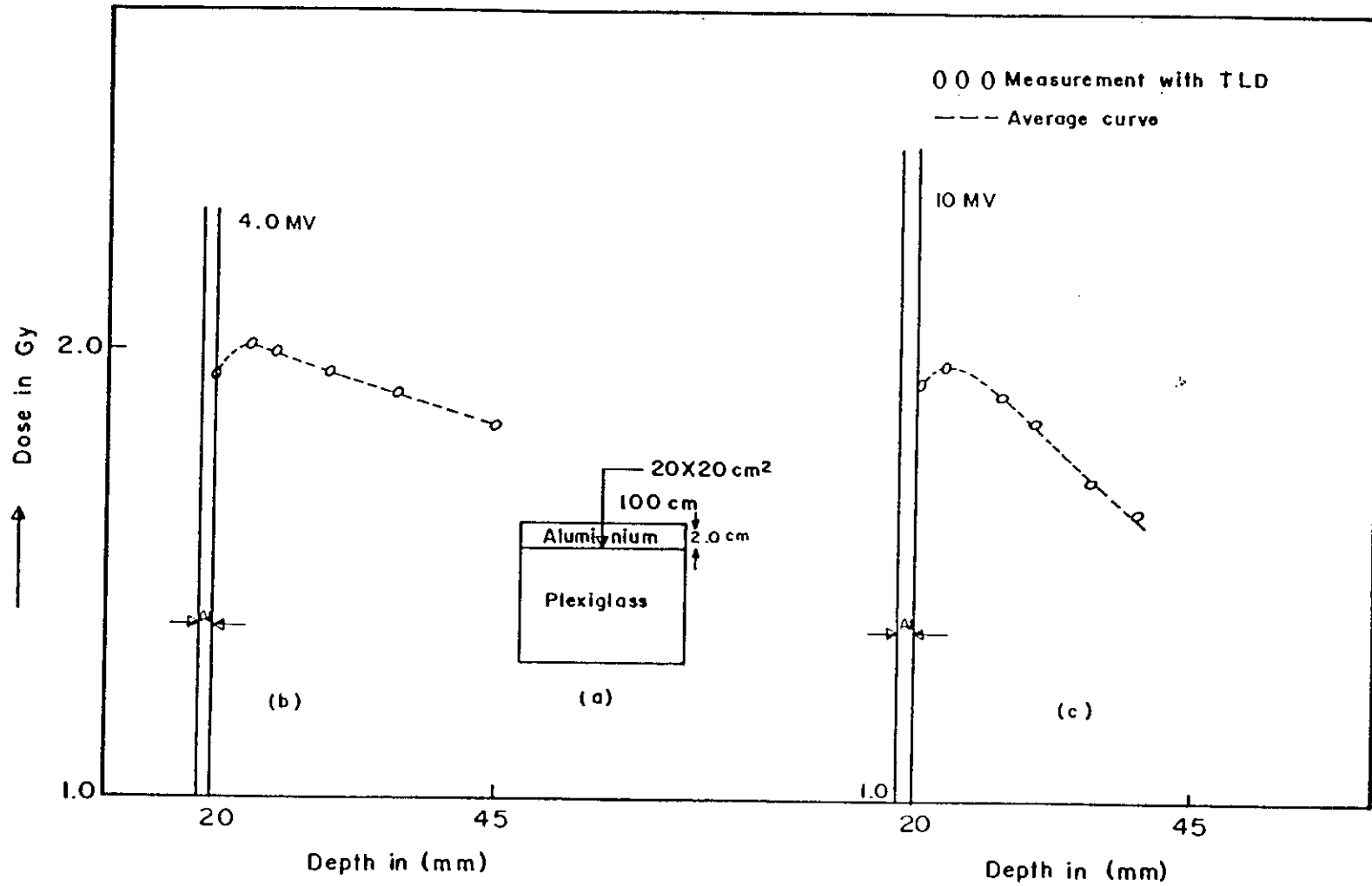


Fig.8.15 Depth dose curves (b,c) at the interface of plexiglas / Aluminium for the beam of 4.0 and 10MV energy ; Field = 20 X 20 cm²; S.S. D. 100cm (a).

9.0 CLINICAL APPLICATION OF TLDS AND ASSOCIATED METHODOLOGY

Introduction

The principal aim of TL-dosimeter is to check the target dose in order to verify the correct delivery of irradiation from high-energy photon beams. Sometimes it is impossible to introduce the detectors in the target volume. As a matter of fact, a check of the entrance (D_{entrance}) and exit (D_{exit}) doses can determine the indirect check of the target dose, which is just equal to the arithmetic mean of D_{entrance} and D_{exit} . This method which can be acceptable in some practical conditions may induce errors of several percents in others. A more accurate method is based on the symmetry (with respect to the midline point) of the thickness of the patient's body for instance. However, a prerequisite is that tissue inhomogeneity should be symmetrical and equally distributed with respect to the midline for reliable target dose determination.

Methods

The method is based on the concept of exit transmission, T_{exit} and midline transmission T_{mid} which are defined as the ratio of the dose at depths of ($Z-d_{\text{max}}$) and $Z/2$ respectively to the entrance dose (Figure 9.1). The depth Z is the water equivalent depth of the patient. In fact the target dose is estimated by following three steps:

firstly, the determination of the measured exit transmission (T_M) for a given patient:

$$T_M = \frac{D_{M_{\text{exit}}}}{D_{M_{\text{entrance}}}}$$

secondly, the derivation of the midline transmission (T_{mid}) for the given patient from the measured exit transmission with the help of two groups of curves (Figure 9.2)

finally, the estimation of the absorbed midline dose D_{mid} from the product of the measured entrance dose ($D_{M, entrance}$) and the midline transmission (T_{mid}) i.e.

$$D_{mid} = D_{M_{entrance}} \times T_{mid}$$

Derivation of midline transmission

The exit and midline transmission curves are established from the tissue phantom ratio (TPR) [also called as tissue maximum ratio (TMR)] taken either at the exit of the beam or from the midline depth. The middle of the patient being assumed to be at the iso-center, the source axis distance (SAD) from the source can be expressed as under:

$$T_{exit} = \frac{TPR(A', Z - d_{max})}{TPR(A', d_{max})} \times \left[\frac{SAD - Z / 2 + d_{max}}{SAD + Z / 2 - d_{max}} \right]^2 \times \frac{B_{A'}}{B_{A_0}} \cdot \frac{1}{B'_{A'}} \quad 9.1$$

$$T_{mid} = \frac{TPR(A, Z / 2)}{TPR(A, d_{max})} \times \left[\frac{SAD - Z / 2 + d_{max}}{SAD} \right]^2 \times \frac{B_A}{B_{A_0}} \quad 9.2$$

The TPR's are corrected by applying the inverse square law taking into account the differences in distances of the points compared. B_A , $B_{A'}$, and B_{A_0} are the back or peak-scatter factors for the field sizes A , A' and A_0 respectively at the iso-center ($Z/2$), at the exit dose point situated at ($Z-d_{max}$) and the entrance dose point situated at d_{max} (Figure 9.1).

$$A' = A \cdot \frac{SAD + \frac{Z}{2} - d_{max}}{SAD} \quad 9.3$$

$$A_0 = A \cdot \frac{SAD - \frac{Z}{2} + d_{max}}{SAD} \quad 9.4$$

$B'_{A'}$ is the correction factor for incomplete photon backscatter at d_{max} from the exit surface of the beam.

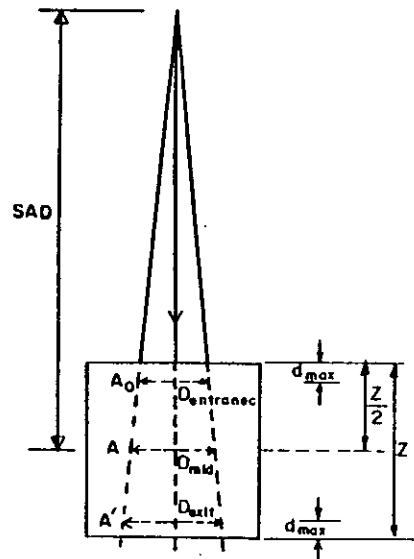


Fig.9.1 Schematic representation of the doses used in the definition of the different transmissions. The exit and midline transmissions, T_{exit} and T_{mid} respectively, are defined as the ratio of the exit dose D_{exit} and the dose D_{mid} at midline depth $Z/2$, to the entrance dose $D_{entrance}$

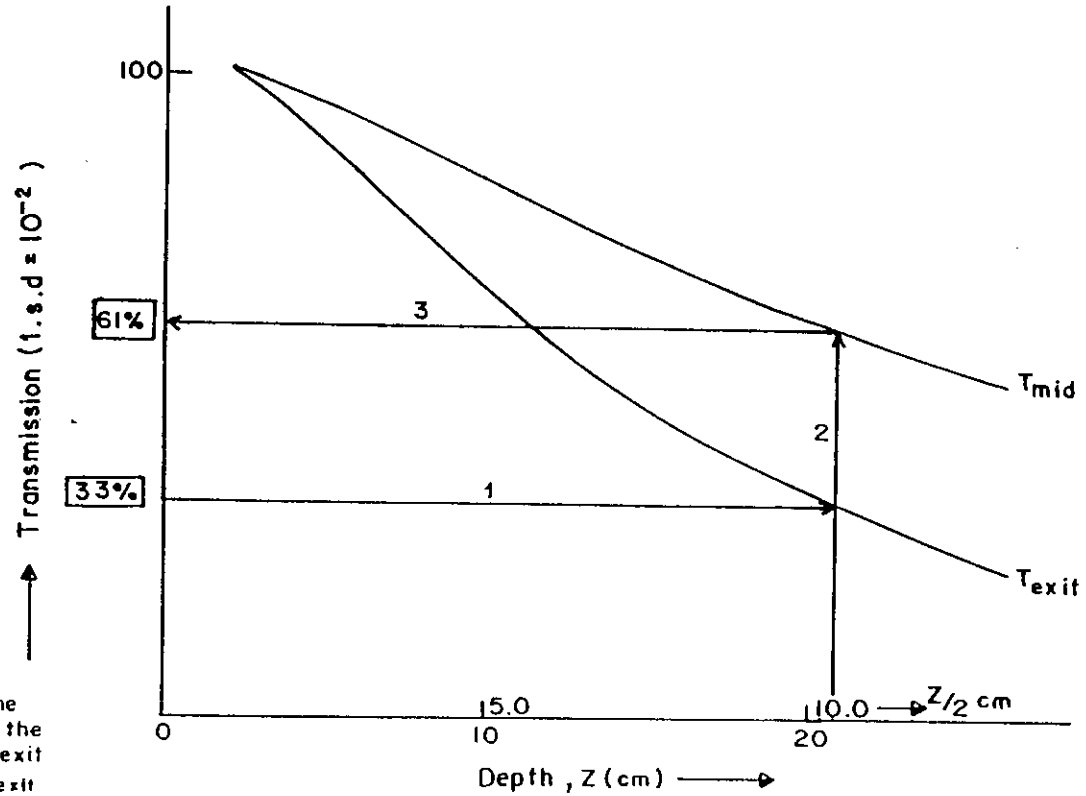


Fig.9.2 Transmission curves obtained for 4.0 MV photon beam. Field size $10 \times 10 \text{ cm}^2$.

Experiments using TLDs

A 20cm thick phantom was taken. The entrance, mid and exit doses were measured using TLDs for the 4.0MV-photon beams. At each depth 3TLDs were exposed for the field of $10 \times 10\text{cm}^2$ at isocentric distance (SAD) of 100cm. The measured doses were shown in Table 9.1.

Phantom width (cm)	Photon beam = 4.0 MV; Field = $10 \times 10 \text{ cm}^2$				From graph
	Entrance dose $D_{\text{max}}(\text{Gy})$	Measuring mid dose $D_{\text{mid}}(\text{Gy})$	Exit dose $D_{\text{exit}}(\text{Gy})$	Mean dose $\frac{D_{\text{max}} + D_{\text{exit}}}{2}$	$D_{\text{mid}} = D_{\text{entrance}} \times T_{\text{mid}}$
20	0.965	0.600	0.321	0.644	0.592
	0.977	0.587	0.317		
	0.971	0.593	0.317		

Table 9.1: Target dose checked by indirect method (the arithmetic mean of D_{entrance} and D_{exit}) and by using the new methodology.

Now, for the same field of the photon beam, the T_{exit} and T_{mid} were derived using a given tissue phantom ratio data. Figure 9.2 shows exit and midline transmissions curve as functions of water equivalent thickness (Z) and ($Z/2$) respectively. Once the exit transmission or the total water equivalent thickness of the patient is known, the midline transmission is determined as the read-out on the Y-axis of the T_{mid} curve for $10 \times 10\text{cm}^2$ field. For T_{exit} is 33%, T_{mid} is 61% (arrow 2 and 3), yielding a mid line dose of $0.971 \times 0.61 \text{ Gy} = 0.592 \text{ Gy}$. The result differs by 0.17% with the direct target dose measured by TLDs. The difference is 9.0% if the arithmetic mean of entrance and exit dose respectively is used.

The methodology contained in the ESTRO⁷² (European Society for Therapeutic Radiology and Oncology) has been followed in conducting the experiments using TLDs.

10.0 VERIFICATION OF CALCULATED DOSE DISTRIBUTION PERFORMED BY A NEW INSTALLED PC PROGRAMME FOR ASYMMETRIC PHOTON BEAMS USING TLD.

An independent collimator has been included in the 4.0MV linac (MV 6300, SIEMENS) that is capable of producing the asymmetric fields of photon beams. The main features of the asymmetric system are -

- matching of fields
- elimination of the beam divergence close to the organs at risk and
- achievement of tissue compensation.

The commercial treatment planning system is working with the photon beams of symmetric fields where they are unable to provide the dose-distributions for asymmetric fields. Zakaria, G.A, et al⁷⁸ have developed a new algorithm which can calculate the dose-distribution for all possible sizes of open and wedged symmetric and asymmetric field. As input, the algorithm needs the data of primary beam profiles for the maximum open ($40 \times 40\text{cm}^2$) and for wedged fields ($25 \times 25\text{cm}^2$). These are taken from the already existing measured basic data for symmetric open fields; along with, a few data of some standard asymmetric open and wedged fields. The measured profile dose-distribution data were taken with the ion-chamber at the d_{max} into the water phantom (Welhoefer water phantom). The same some measurements were also carried out with TL-dosimeter taking them into the Plexiglas phantom. The distributions were normalized to 100, to the dose at d_{max} for the symmetric phantom field. Additionally some direct measurement investigations were carried out using TLDs where the photon beams of asymmetric fields are needed for treatment. Three such typical treatment cases were considered which were

- asymmetric field in head and neck region (skull)
- asymmetric field in thorax region
- asymmetric field in abdomen region

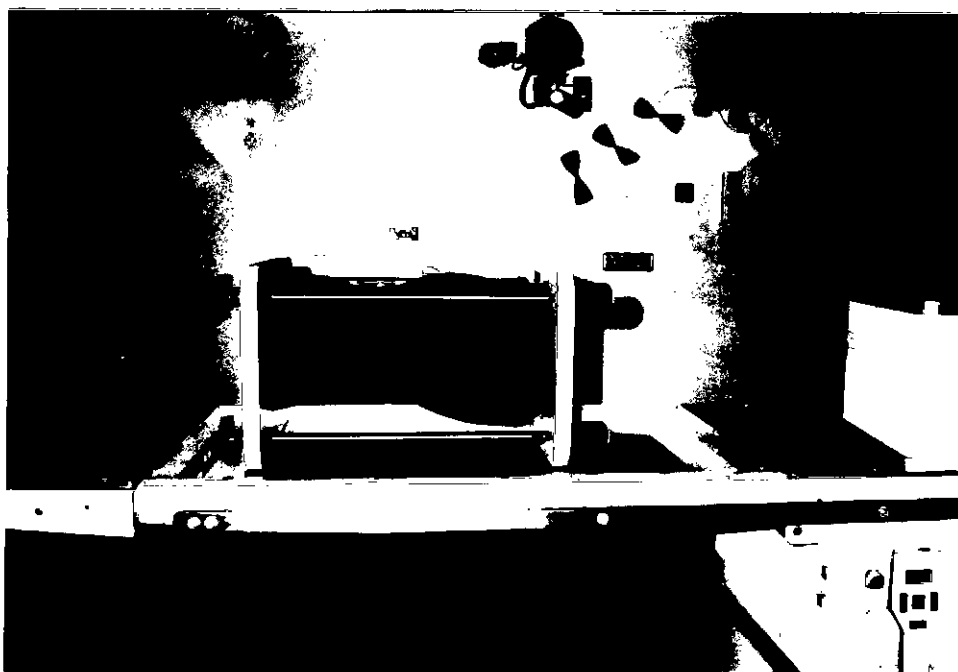


Fig. 10.1: Alderson phantom exposed to measure the dose in a particular region using TLDs

The Alderson (Figure 10.1) phantom was used as a patient and the required dose (Table 10.1) for symmetric and asymmetric fields were used from their installed programs with CT-picture. Accordingly the TLDs were inserted into the existing rod-size holes (distributed at distance of 2.5cm) over the cross-section slice of the patient phantom.

Accelerator: Mevatron : M6300

Energy :4.0MV

Strahlen type: Photon

Normalized at isocenter

Organ (Slice)	Field no.	Gentry angle	Field width		Field length mm	Coll. angle	ISD mm	Wedge filter	Weight	Doses (Gy)	Mon. unit (MU)
			Left mm	Right mm							
Brain (4)	1	270	0	80	80	90	927	0	1.00	1.00	132
	2	90	80	0	80	90	935	0	1.00	1.00	128
Thorax (17)	1	0	80	0	80	90	975	0	1.00	2.00	213
Abdomen (30)	1	300	50	0	50	90	821	0	1.00	0.67	178
	2	130	0	50	50	90	868	0	1.00	0.67	146
	3	60	25	25	50	90	817	0	1.00	0.67	158

Table 10.1: Plan for irradiation of different organs using asymmetric fields.

The distributed doses measured with TLDs were normalized to its maximum value of the pre-determined target point. The results are shown in figures 10.2 to 10.4. A good agreement of predicted and measured dose-distributions with $\pm 2.16\%$ S.D. is noted.

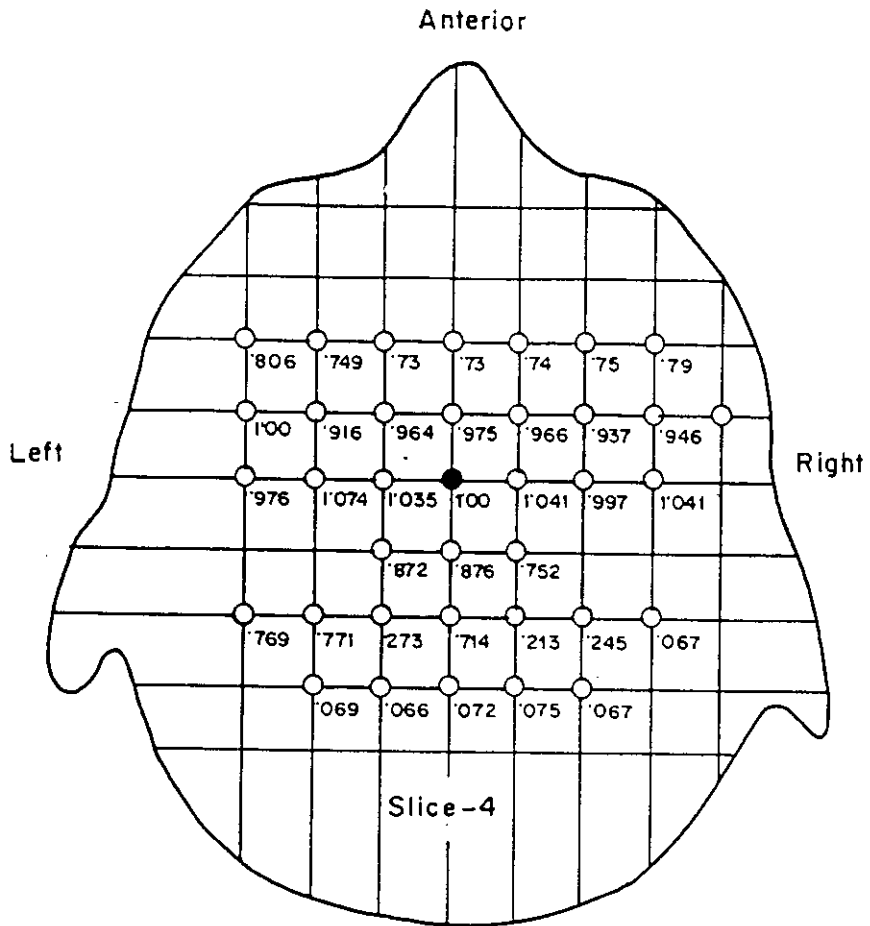


Fig. 10.2a. Dose measurement using TLDs for two lateral asymmetric fields of brain irradiation. Each circle represents the reading of a single rod.

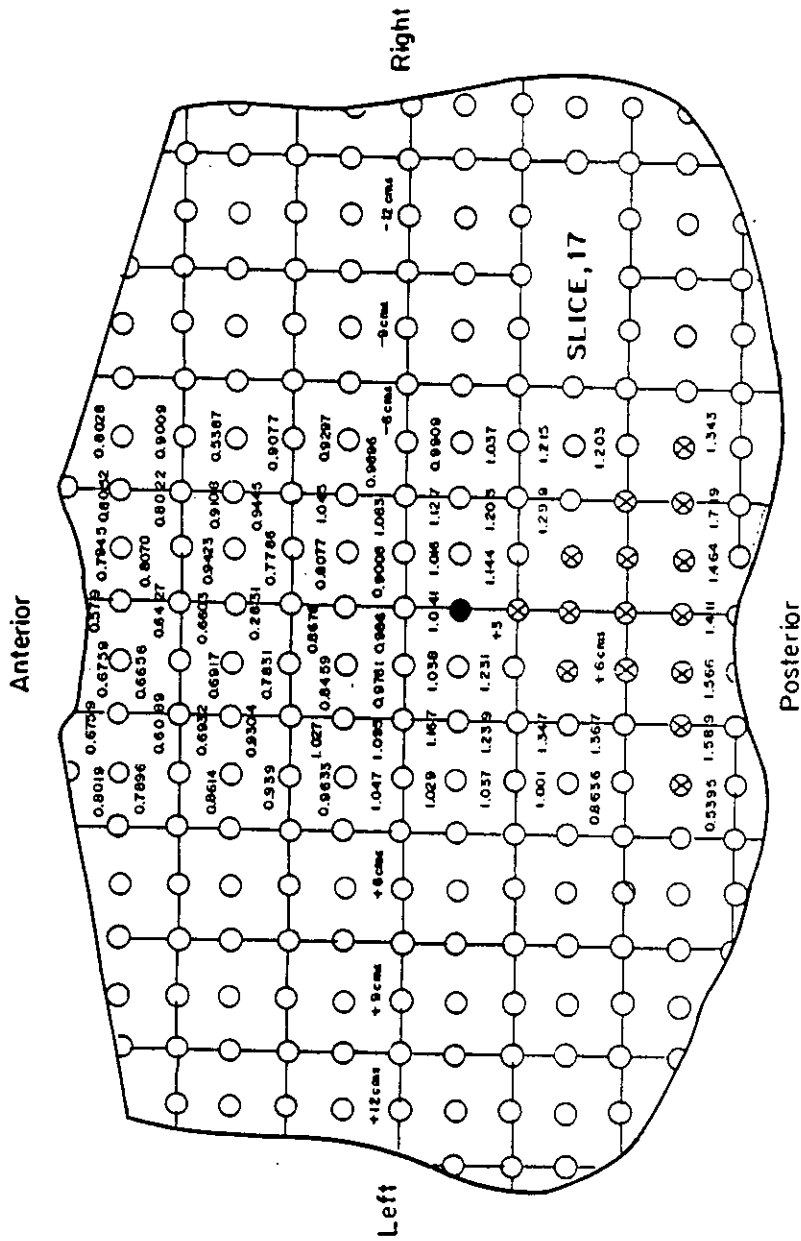


Fig. 10.3a Dose measurement using TLDs for the anterior field of thorax irradiation. Each circle represents the reading of a single rod.

Kreiskrankenhaus Gummersbach

Wilhelm Breckow Allee 20, 51643 Gummersbach
Abteilung Strahlentherapie + Med. Strahlenphysik
Chefarzt P.O. Dr. Prignitz, Ltd. Med. Physiker Dr. Zakeris

Patientenname: Aldersonphantom, slice - 30 *

CT-Nr. :
Diagnose :
Zielvolumen:

Normalized at Isocentre for Feld 1 118.12 % in Dose: maximum = 2.36 Gy

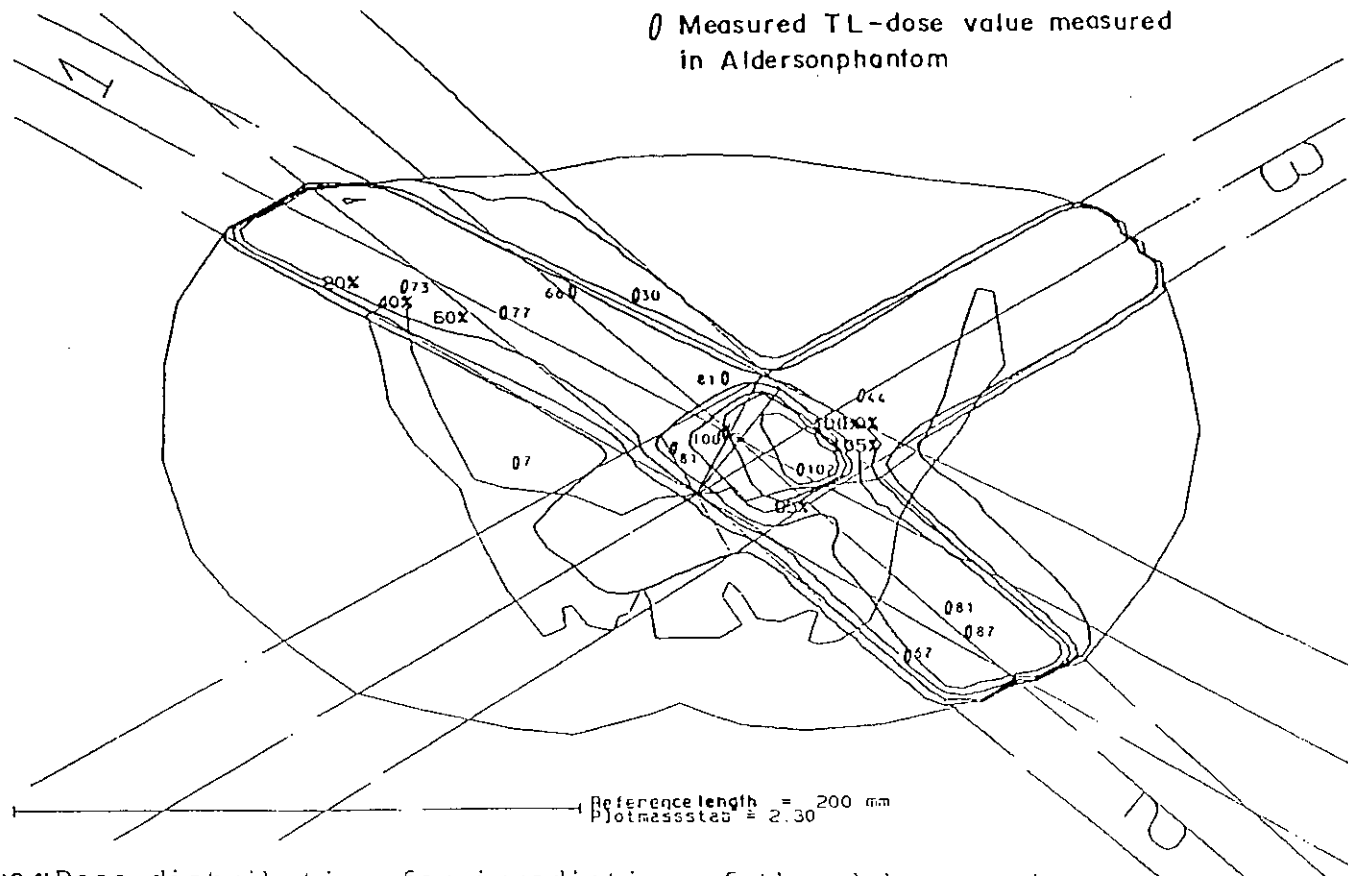


Fig.10.4b Dose distribution for irradiation of the abdomen using three-field technique

0 measured dose with TLD and → calculated isodose

Treatment using two asymmetric fields with matching condition

Another typical problem arising in clinical cases involving exposure to asymmetric fields with matching condition was studied. Here a low dose distribution effect was found at the interface of two fields as obtained by computer programming as well as measurement by film dosimetry (Figure 10.5). The same effect was also found by carrying out the same dose distribution using TLDs (Figure 10.5b). For this, the measurement of profile dose distribution was carried out at depth of 1.1 (d_{max}) into the plexiglas phantom. The two asymmetric fields of $6 \times 17 \text{cm}^2$ at 100 cm S.S.D were used. The central beam was directed along the same line for both the fields (fields with matching condition). To overcome the problem of lower dose effect at the interface region, the following measurement technique were adopted and studied using TLDs.

- (i) The dose distribution at the interface region of 3.0mm overlapping condition of central beam for two asymmetric fields.
- (ii) The dose distribution at the interface region of 3.0mm gap of the central beam for two asymmetric fields.

For this, a line arrangement of 3TLDs at 1.0mm distant apart were used at the gap of 1.0mm along the interface region. The arrangement of the TLDs across the field edge can be seen at the mid in figure 10.5. The measurement obtained with TLDs for the two different exposures of the same asymmetric fields of $6 \times 17 \text{cm}^2$ is shown in the figure 10.6. All measurements were normalized to 100 for the dose value at 3.0cm apart (the normal distance from d_{max}) for the symmetric field.

The results of these measurements have assured that a several exposures planning would have to be used for such clinical cases while exposing the patient with asymmetric fields with matching condition.

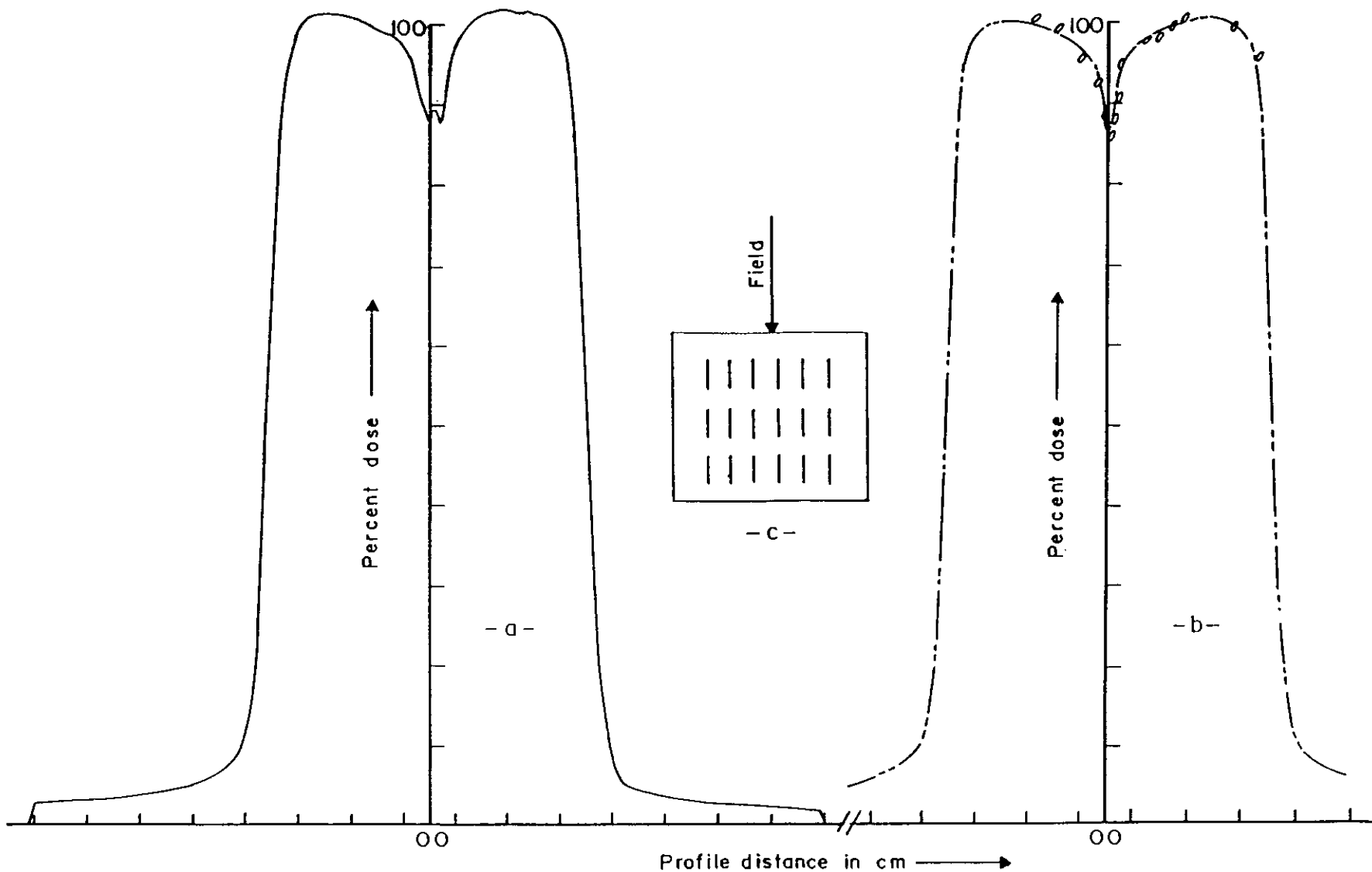


Fig.10.5 Profile dose distribution at 1.1cm phantom depth at the interface region of two asymmetric fields of $6 \times 17 \text{cm}^2$ at 100cm S.S.D (a) obtained by computer program (b) measurement by film dosimetry (---) and TLD (000). Photon beam is 4.0 MV. (c) Arrangement of TLDs (—) across the field edge.

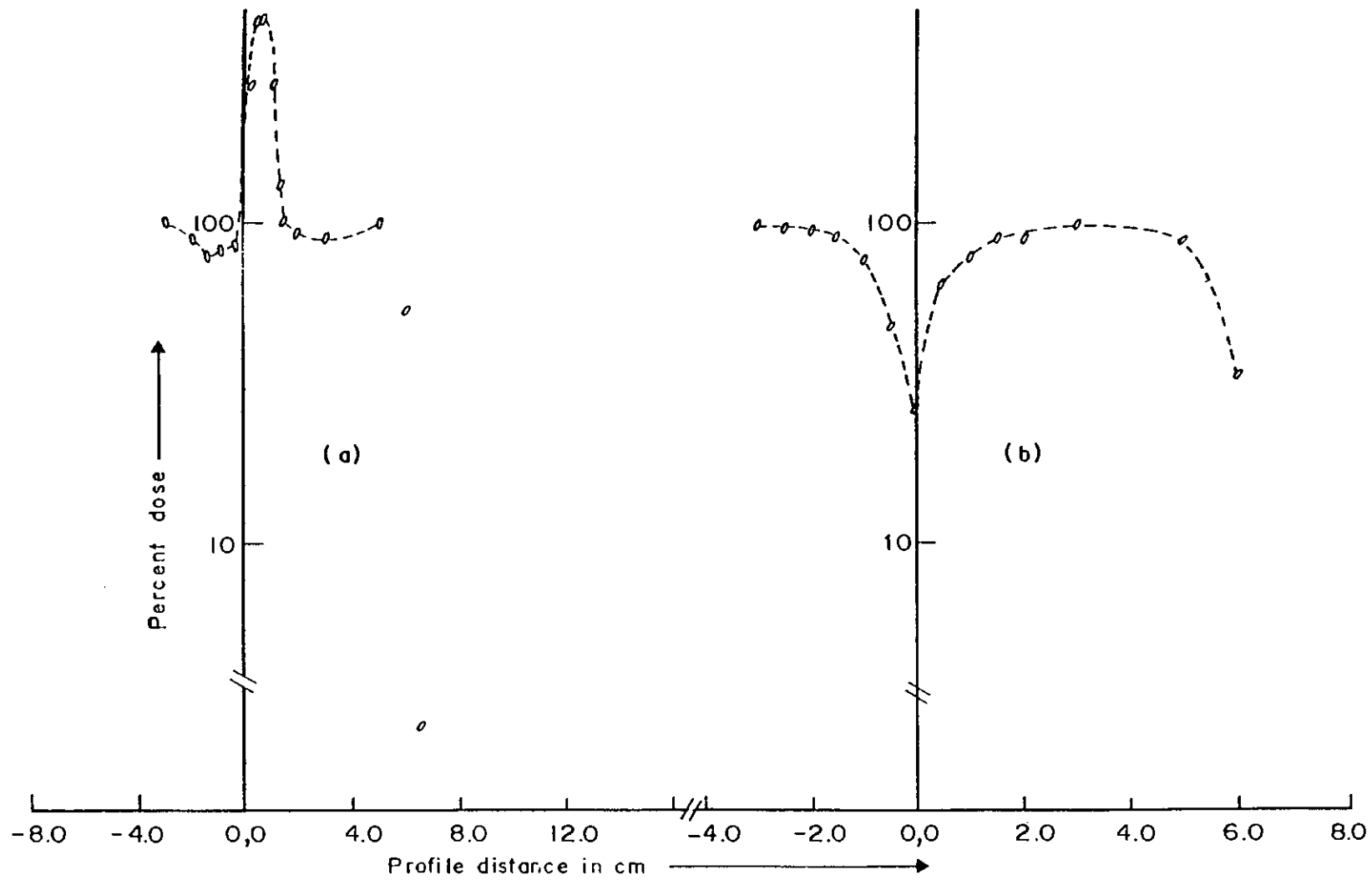


Fig.10.6 Profile dose distribution at 1.1 cm phantom depth at the interface region of two asymmetric fields of 6 X 17 cm at 100cm S.S.D. (a) 3.0mm over lapping (b) 3.0mm gapping condition.

11.0 MEASUREMENT OF DOSES USING TLD IN TOTAL BODY IRRADIATION

The total body irradiation (TBI) prior to bone marrow transplantation is very successful in the treatment of acute leukemia and other malignancies. Normally for TBI, a high dose of 10 to 12 Gy is used. The dose is delivered homogeneously over the whole body fractionated over two or three day's exposure. This implies 10% to 25% higher doses to the lung tissue, which exceeds the tolerance of organ at risk. The dose-effect relationship of lung toxicity is very steep, 20% increases for 5% higher dose⁵⁸. Thus, lung sparing is required. The physical conditions of the TBI treatment are completely different in radiotherapy than in normal treatment. The following two special benefits can be obtained if the patient is irradiated with the large field for a long source to patient distance.

- (i) the over dose effect at field matched region for multiple exposure can be avoided.
- (ii) the patient's tolerance (where the delivering dose rate is to be lowered due to long distance) is increased.

For arranging long distance, the patient has to be brought very close to the floor or wall as a result of which the total dose for the body of the patient increases because of scattered radiation. As such, it is impossible to calculate the applied dose directly from the existing planning system⁵⁸. For this, the applied dose is determined from the physical data and is verified directly during the exposure of the patient using ion-chamber dosimeter.

In Grossharder Univ. Clinic in Munich the planning and the verification of applied doses were done using TLDs. Previously, the whole body dose distribution was experimented using the Anthropomorphic phantom. Two depth dose distributions for the photon beam of 6.0MV-one across the thorax and the other through the abdomen of the phantom for the effective field length of 180cm at 6.0m source to surface of the patient distance were studied²³.

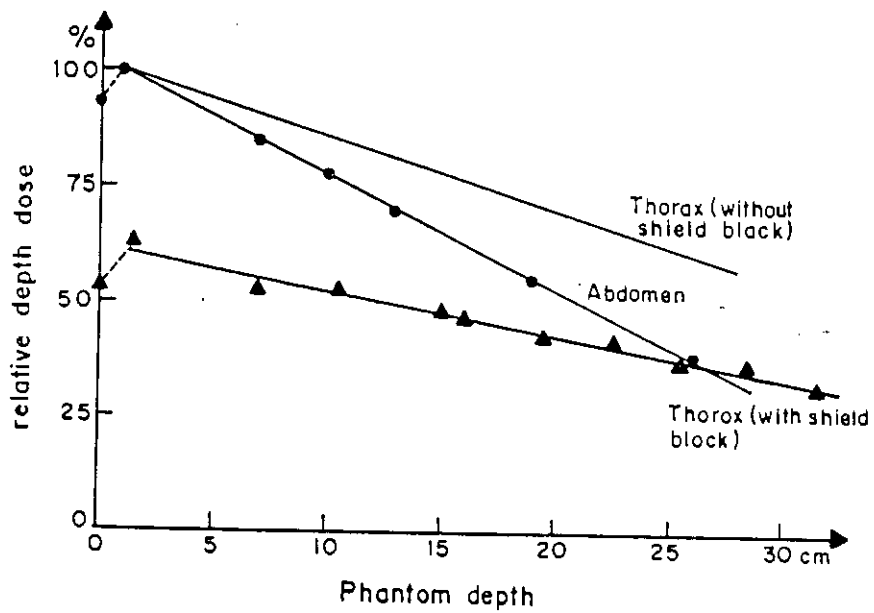


Fig.11.1 Relative doses in different depth of the Anthropomorphic Phantom through the thorax and abdomen using with and without using shielding. The experiment was carried out by Feist. H²³ using TL-LiF rod dosimeter for the photon beam of 6MV; 180cm effective field length for the body at 6.0 m S.S.D.

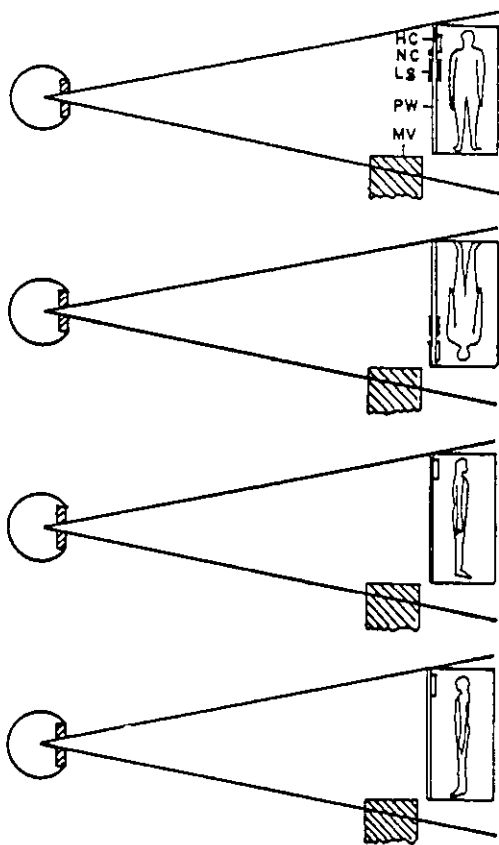
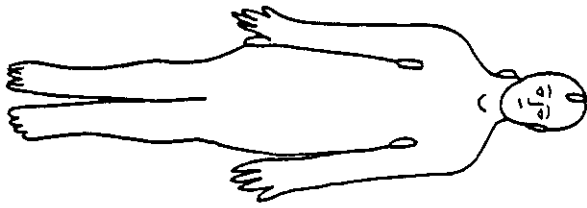
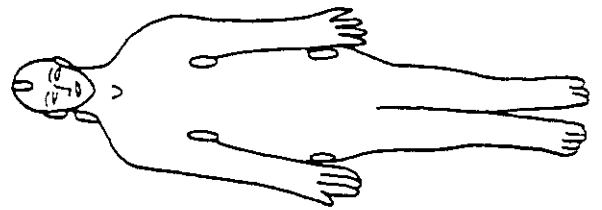


Fig. 2 The position of the patient in four individual exposure during TBI treatment.

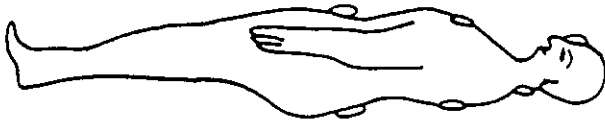
- HC = Head compensator
- NC = Neck shielding
- LS = Lung shielding
- PW = Plexiglas wall
- MV = Side of a wall.



(a) 1st exposure



(b) 2nd exposure



(c) 3rd exposure



(d) 4th exposure

Fig.11.3 The position of the patient in four individual exposure during TBI treatment. The sign, 0 (2 TLDs at each point) indicates the location of TLDs on the body during irradiation.

A straight line of depth dose distribution curve from the entrance to exit surface of the body was found for both the situations (Figure 11.1).

To find the linear depth-dose distribution at the starting of the body surface, a 1.2cm thick plexiglas wall placed by the side of the patient's bed, so that the wall acted as the dose build-up material and the maximum dose, the D_{entrance} became the surface dose to the patient. For head, plexiglas slabs of different thickness were attached to the Plexiglas wall as compensator. For shielding the lung and pharynx (for 40 to 50% dose reductions), lead mixed with iron (for stability and rigidity) slabs were used.

The patient was irradiated with four individual exposures by changing position of the patient as shown in figure 11.2, so that a homogeneous dose distribution through out the body is found. The same set of TLDs was used for the two exposures of the opposite beams. The arithmetic mean of the TLD-dose gives the applied dose. The total patient dose measured for verification by using TLDs is shown in Table 11.1. The measured dose agrees quite well with the planned dose.

Prof. Feist/Medical Physics

Whole body irradiation with 6.0 MV photon beams of Mevatron KD.Relevant parameter and calculated monitor scale division.

Patient Name	:	F
Date of Birth	:	12.12.1987
Height	:	123 cm
Weight	:	26 kg
Nature of the patient	:	Kind

Relevant estimation for dose determination.

Lateral diameter of the thorax	:	20.0 cm
Lateral diameter of the waist	:	20.0 cm
AP-across the thorax	:	16.0 cm
AP-across the waist	:	16.0 cm
AP-across the pelvice	:	14.0 cm
1. <u>Irradiation</u>		
Mean dose to the abdomen	:	4.00 Gy
Mean dose to the thorax	:	3.20 Gy
2. <u>Irradiation</u>		
Mean dose to the abdomen	:	4.00 Gy
Mean dose to the thorax	:	3.25 Gy
Lung shielding	:	0 (Field length on skin 11.5 cm)
No of irradiation	:	1 2 3
Date of irradiation	:	24.02.97 25.02.97 26.02.97

Monitor unit distribution :

Patient on back side without lung shielding	:	5165	4924 per side
Patient in lateral position without lung shielding	:	4010	1229 per side

Further information for 2 irradiation:

3600 Monitor unit per side at the back of the patient with 2.0 cm thick Plexiglas material on neck for shielding the larynx.

2 head plates each have 12 mm thick used. No pelvice cap used.

24.02.97 Dose calculation from TLD measurements.

Measurement at 1. The whole body irradiation of the patient with a body dose of 6.0 MV photon beam on 24.02.97. For TLD, the correction factor for considering the quality of the radiation of the photon beam: 1.036

Systematic change of the calibration measurement intensity in %: -1.41

Dose without TLD: 0.000 nC.

First supralinearity correction factor: 2.30% per 1.00 Gy calculated dose.

No of TLD	TLD-identification (No)	Response light (nC)	Cal. factor (Gy/ μ C)	Dose (Gy)	Measured organs
1	HP6 1	857.8	4.615	3.910	Over all head
2	HP6 2	745.0	5.284	3.890	
3	HP6 3	722.5	4.611	3.331	Over all larynx
4	HP6 4	640.6	5.149	3.300	
5	HP6 5	786.4	5.009	3.893	Over all neck
6	HP6 6	742.1	5.269	3.866	
7	HP6 7	588.7	5.201	3.078	Over all thorax
8	HP6 8	565.0	5.499	3.120	
9	HP6 9	889.3	4.588	4.021	Over all abdomen
10	HP6 10	875.3	4.705	4.056	
11	HP6 21	142.1	5.301	0.794	Backside of the Thorax entry v. le. ϕ 20.5 cm. 5165 MSkt.
12	HP6 22	144.8	5.117	0.781	
13	HP6 23	86.62	4.619	0.424	Backside of the Thorax exit
14	HP6 24	84.60	4.652	0.417	
15	HP6 29	235.0	4.757	1.171	Backside of the Thorax entry. v.dors. ϕ 15.5 cm. 4010MSkt.
16	HP6 30	210.9	5.305	1.172	
17	HP6 31	167.4	4.647	0.820	Backside of the Thorax exit Over all Thorax : 3.2030 Gy
18	HP6 32	169.9	4.622	0.827	
19	HP6 25	299.8	4.724	1.474	Backside of the Abdomen entry Rucken l.v.li. ϕ 20.5 cm.
20	HP6 26	298.4	4.745	1.474	
21	HP6 27	149.1	4.535	0.714	Backside of the Abdomen exit
22	HP6 28	126.8	5.306	0.710	
23	HP6 33	247.3	4.516	1.170	Backside of the Abdomen entry. v. dors. ϕ 15.5 cm
24	HP6 34	248.0	4.514	1.173	
25	HP6 35	131.3	4.570	0.634	Backside of the Abdomen exit, Over all Abdomen: 3.9970Gy
26	HP6 36	133.7	4.564	0.645	
27	HP6 37	891.3	4.641	4.072	Rectum prove
28	HP6 38	786.6	5.183	4.018	

Table 11.1: Measured organ doses using TLDs during whole body exposure.

Percentage of systematic change of TL-light value of the calibrated TLDs during TBI

No of TLD	TLD-identification (No)	Response light (nC)	Cal. factor (Gy/ μ C)	Deviation in %	STD deviation in %
1	HP6 11	186.4	5.295	-1.31	
2	HP6 12	207.4	4.742	-1.64	
3	HP6 13	185.2	5.313	-1.61	
4	HP6 14	213.5	4.627	-1.22	
5	HP6 15	198.9	4.929	-1.96	
6	HP6 16	212.2	4.631	-1.74	
7	HP6 17	188.0	5.256	-1.18	
8	HP6 18	216.3	5.546	-1.68	
9	HP6 19	202.5	4.817	-2.46	
10	HP6 20	187.1	5.259	-1.60	
11	HP6 39	197.3	5.023	-0.90	
12	HP6 40	186.1	5.338	-0.65	
13	HP6 41	188.3	5.288	-0.42	
14	HP6 42	191.2	5.197	-0.63	-1.36 ± 0.57

Percent change of TL-light value: -1.41 ± 0.39 without HP6 19, HP6 41 and HP642.

12.0 RESULTS AND DISCUSSIONS

For measuring the dose distribution of high-energy photon beams the TL-dosimeters should be used with a good degree of accuracy. In this respect details studies reported in this thesis show that:

The TL-light value always fluctuates. It is critically dependent on

- (i) the reproducibility of thermal treatment that depends on the placement of the heating tray in the oven and on the planchette of the reader and also the storage temperature of the TLD.
- (ii) the reproducibility of the emitting photon beams from the linac.

Efforts have been made to correct and minimize the influence of such variations by physical aspects during dosimetric evaluation and regeneration in the TLD application cycle.

It would be necessary to monitor the calibration factors time to time. For calibration using TLD shell model program, a pre-selective group of TLDs within 5% S.D. of reproduced sensitivity is required to get greater number of calibrated TLDs within 2% S.D. of 1.0 Gy dose measurement.

This work has established two techniques for achieving accurate dose measurement using TL-dosimeters.

- (i) the calibrated TLD must have measurement precision of maximum 2% S.D. of calibrated dose value.
- (ii) for better accuracy the 3TLDs-measurement technique will have to be used for each point.

Since TLD is a relative dosimeter, multiple number of TLDs with proper calibration can achieve precision. It has been found that the S.D. of the measured dose value can be brought within 1 to 1.5% by using 3TLD technique.

Placements play an important role in using the multiple TLDs especially at penumbra, steep gradient and in interface region. A series of 3TLD was placed tangentially at a gap of 1.0mm. But, when used in an Anderson phantom, average dose has been taken from three different exposures of same kind with one TLD in each exposure. This is done to avoid the problem with identification of individual TLDs. In this case more than 2% S.D. was found. It occurs either due to the variation of phantom placement or the variation of photon beam in successive exposures.

The precision of the dose measurement with TLDs is calculated from the reproducibility of dose reading of an individual crystal after correction with its sensitivity value. It was found that better reproducibility could be achieved with contact less nitrogen heating system.

It may be noted that the TL-dosimeters were all calibrated for the field of $10 \times 10 \text{cm}^2$ at 100cm S.S.D and for the depth of 5.0cm. The ion- chamber dosimeter is a standard dosimeter, which was primarily standardized by FeSO_4 dosimetry in PTW, Freiburg. The measurement using this dosimeter is independent of field or depth and material. As the dose distributions for different fields and depths measured by TL-dosimeters as shown in figures 7.5 - 7.8 are similar to that of ion chamber dosimeter, which indicates that the TL-dosimetry is also independent of field, depth, and material.

For measurement of dose distributions in the penumbra region for symmetric and asymmetric fields, the two methods (TLD and ion chamber) compared well. The decrease of dose towards the field edge in asymmetric field³³ using TLDs was seen clearly. A better performance was observed with TLDs than with ion and Markus chamber dosimetry. This is because of small dimension of TLD, which covers the field edge of a definite field of the photon beam. The ion and Markus chamber dosimeters on the contrary, have a large effective

measurement volume for which it is difficult to get the accurate result in steep gradient dose distribution by using these dosimeters. Besides, for each point dose measurement the dosimeter has to be set over and over again for taking the whole distribution. On the other hand by proper arrangement of the TLDs, the whole distributions can be measured by a single exposure only without disturbing the set up of the phantom arrangement. It protects the machine from over use and also protects the radiation workers from radiation hazards, as the radiation workers have to stay less in the radiation zone.

In the studies of dose distribution, following the method devised by AT Redpath and D I Thwaites in phantom containing air inhomogeneity, the dose ratios obtained by TLDs showed good agreement. They carried out the experiment using a Therados RFA7 beam data acquisition system. The dose ratios give the scattering factors due to air present in the inhomogeneous system. So, the results obtained by TLD indicate that the TLD has a good performance quality in scattering dose measurement situation.

The experiment carried out to investigate the electronic equilibrium, (the phantom containing 2.6cm thick plexiglas followed by 6.0cm cork and again 12cm thick slab of plexiglas) the dose distribution curves were unaffected up to first interface region of 2.6cm for both 3×3 and $20\times 20\text{cm}^2$ fields for the energies of 4.0 and 10.0MV. For $3\times 3\text{cm}^2$ field of 10MV energy, the dose is higher for the cork slab geometry than the homogeneous phantom in the region far beyond the cork slab because of the lower attenuation in cork. Inside the cork slab, however, the dose is lower because of electronic disequilibrium. When the field size is wide enough electronic equilibrium exists and the dose in cork is higher than in Plexiglas of the homogeneous phantom⁷³

It was noted that, in the measurement with TLD, the distribution curve in the cork ($\rho=0.22$ to 0.30 gm /cc) was little bit higher than that of ion-chamber dosimeter. It may be due to the more attenuation in the denser LiF ($\rho=2.64$ gm /cc) material.

The results presented in dose distribution on a phantom for the tangential field used in breast irradiation was superposed on the results of AT Redpath and DI Thwaites⁶⁰. A good agreement with their observation was obtained except of the edge (Figure 8.7B). It may occur due to change of positions of physical measurements when the inhomogeneity is inserted.

In the tangential situation, the amount of dose at the central edge of the phantom is less and increases along the X-axis. This is because, at the edge more loss of scattered dose occurs relative to the homogeneous condition. The loss becomes minimum as the distance increases along the X-axis due to finding of more homogeneous material. But the dose ratio is still less than 1 owing to the loss of scattered dose from the air inhomogeneity present in the situation.

The results obtained from the experiment of dose distribution in lung phantom of finite geometry (the cases used in mediastinum) were shown in figure 8.8 to 8.13. In the depth dose distribution for 4.0MV photon beam, no significant build-up dose was observed at the lung analogue underlining the solid phantom. And for 10MV photon beam the build-up at the first interface as given by the TLD readings was insignificant But beyond the lung analogue, there is a sudden increase in the dose starting from a depth of about 12cm which continues there after (Figure 8.9).

The other profile dose distributions carried out for $20 \times 20 \text{cm}^2$ field, a percentage of dose ratio for inhomogeneous (with lung analogue) to homogeneous phantom is shown in figures 8.10 to 8.13.

At the lung interface, a high dose ratio was observed. It might happen, because at lower density, the primary photons experience fewer interactions. Thus the fluency of primary photons is stronger than at the same depth in water equivalent homogeneous phantom²⁵.

Figures 8.14 and 8.15 show the results obtained from the measurement of dose distribution in the vicinity of aluminum interface. A significant overdose at the vicinity of the interface was investigated (in graph 8.14). Relative to the value in homogeneous plexiglas phantom, the dose enhancement in front of the Al are about 8.26% for 4.0MV and 8.8% for 10.0MV energy respectively. The same measurement for ^{60}Co was carried out using 5.0cm plexiglas and then 2.0cm Al in the phantom at the therapeutic dept. of Essen Uniklinik and dose was found to increase by 8.78%. The similar investigation which were done by Otto A Sauer found the dose increment of 14% at the Al interface for 5.0MV photon beams using the same fields as $20 \times 20 \text{cm}^2$. They used 0.25mm thick TLD chips at the interface. Again the same measurement was also carried out with the Markus chamber dosimeter. An 11% more dose for 4.0MV at the front interface of the phantom was obtained.

For the other situations, beyond the Al, a lower dose of 11.35% and 10.18% for 4.0 and 10.0MV energy respectively were found.

It was noted that the present experiment provides a less amount of overdose at the interface than those obtained by Otto A Sauer. It might happen due to the thickness of 1.0mm TLD as used here which is four times greater than the one used in their experiment. As the overdose region is of some μm around the inhomogeneity⁶⁷, 0.25cm thick detector would have definitely better resolving performance compared with the 1.0mm thick TLD.

A methodology contained in the European Society for Therapeutic Radiology and Oncology⁷² was followed in conducting the experiments using TLDs, which has been described in chapter 8.0. The calculated dose obtained differs by 0.2% with the direct target dose measured by TLDs. However, the difference is 9% if the arithmetic mean of the entrance and exit dose is used.

The verification of calculated dose distribution performed by a new installed PC program for asymmetric photon beams by using TLDs has been described in chapter 9. Here three typical treatment cases were measured and the results are shown in figures 10.2-10.4. A good agreement of predicted and measured dose-distribution with $\pm 2.16\%$ S.D. is noted.

Another typical problem arising in clinical case involving exposure to asymmetric fields with matching condition was studied. To overcome the problem, a different technique of exposure planning was adopted and studies using TLDs. The results are shown in the figure 10.6.

Finally, the TLDs were used for dose measurement in total body irradiation. The experiment was carried out at Großharder Univ Clinic in Munich, Germany. The 6.0Mv photon beams was used. The total patient dose was verified by using the TLDs (Table 11.1). The measured dose agrees quite well with the planned dose.

Because of its compatibility with ion chamber and Markus chamber dosimeter, patient doses have been measured by TLD, which indirectly reflects the quality control of the machine itself. It can be used as convenient device for comparison of therapy doses within different institutions at home and abroad and can ideally be replicated.

Appendix - A

The linear Accelerator

In the linear accelerator (linac), the electrons from a hot filament or cathode in an evacuated tube are accelerated with a fixed voltage range from about 4MV to 35MV. A tungsten target stops the electrons adroitly and as a result a bundles of photon beams (x-rays) each having a frequency of 3000MHz are produced which are passed through a thick collimator. A number of auxiliary systems are essential for operation, control and monitoring of the linac treatment unit. The systems, together with the major components are shown in Fig. A.1. The modulator cabinet and control console, shown on the left, are located outside the treatment room; the stand, gantry and treatment couch, shown on the right are inside.

The gantry is mounted on the stand containing electronics and other systems. It can be rotated about the horizontal gantry axis for use in treatment. The beam emerging from the collimator is always directed through and centered on the gantry axis.

The modulator cabinet contains a power supply for klystron (produce microwave) and the electron gun when triggered by a timing pulse from the control console. The timing pulse rate is set by the technologist and provides the linac output dose rate.

The vacuum system provides the extremely low pressures needed for operation of the electron gun, accelerator structure, and bending magnet system. Without a vacuum, the electron gun would rapidly 'burn out' like a light bulb filament exposed to air. In addition, the accelerated electrons would collide with air molecules, deflecting them and reducing their energy. An electronic ion pump maintains the vacuum. The pressure system pressurizes the wave-guide with Freon or sulfur hexafluoride gas. This is needed to prevent electrical break down from the high power microwave electric fields. A cooling system providing temperature controlled water, establishes the operating

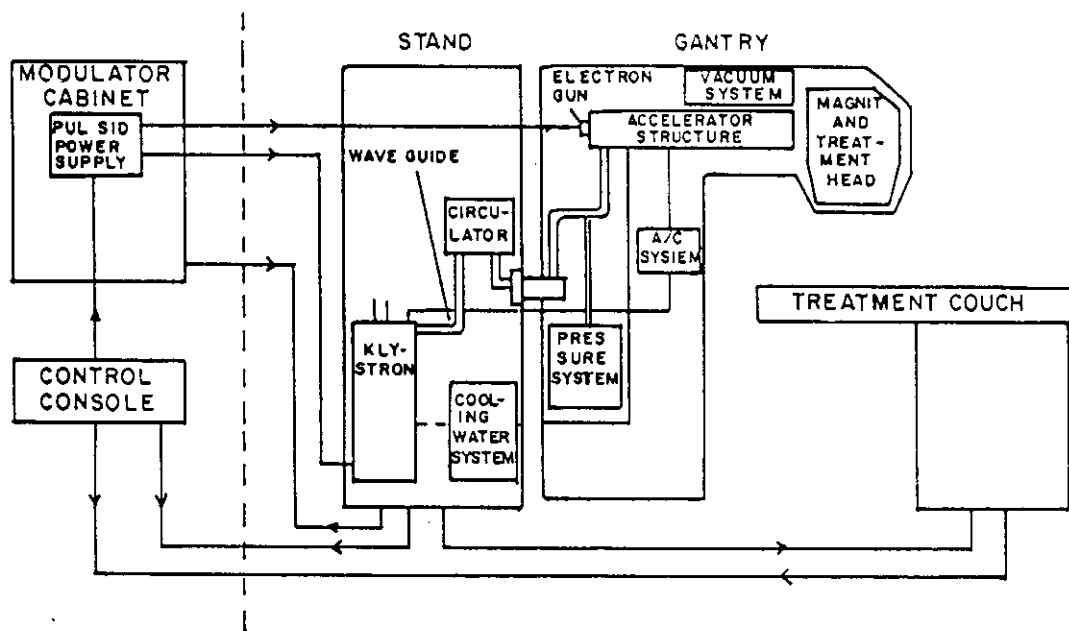


Fig.A.1 Block diagram of a high energy bent-beam medical linac. Major components, auxiliary systems and interconnections are identified. (Clinac 18, courtesy of Varian Associates.)

temperature of sensitive components and operates primarily to remove residual heat dissipated in other components. An automatic frequency control (AFC) system continuously senses the optimum operating frequency of the accelerator structure to maximize radiation output. It uses the information to 'tune' the klystron to the microwave frequency.

The monitor and the control system maintain control of linac operation and patient treatment. It monitors operation to assure proper linac performance and to ensure that the prescribed treatment is faithfully delivered in a safe manner. Deviations, depending on their nature and magnitude, will give rise to fault warning signals or termination of the treatment when appropriate. The center of this monitor and control function is at the control console provides status information on treatment modality accessories in use, prescribed dose, and dose delivered, interlock status, emergency off, as well as other data to linac operation and patient treatment. Frequently, the monitor function is directly linked to the control function and correct status information is used in a feedback manner to maintain optimal performance. A multitude of quantitative and procedural checks is incorporated in the console to assure correct, safe operation. The digital logic circuits used in modern computers are the basis for these checking procedures. They can be carryout in a few seconds and are assessed automatically prior to each treatment.

A counting system, lied to the dose monitor, terminates the treatment when the preset dose monitor prescription is delivered. An interval timer is set to terminate treatment in the event of dose monitor failure. The technologist monitors the treatment both visually and aurally.

A closed circuit TV system provides visual contact and a two-way audio system facilitates instant communication with the patient.

Appendix - B

Definitions and explanations of the terms.

Beam

The region of space traversed by radiation from the source. Its edges are determined by the collimator, its cross-section perpendicular to the beam axis is the field and its direction is that of photon or particle travel.

Build-up

An increase in absorbed dose with depth below a surface irradiated by a beam of high-energy radiation.

Build-up region and electron equilibrium

A volume in a patient where the electrons by photon interactions is not in equilibrium. This may be near the patient surface or an interface between two

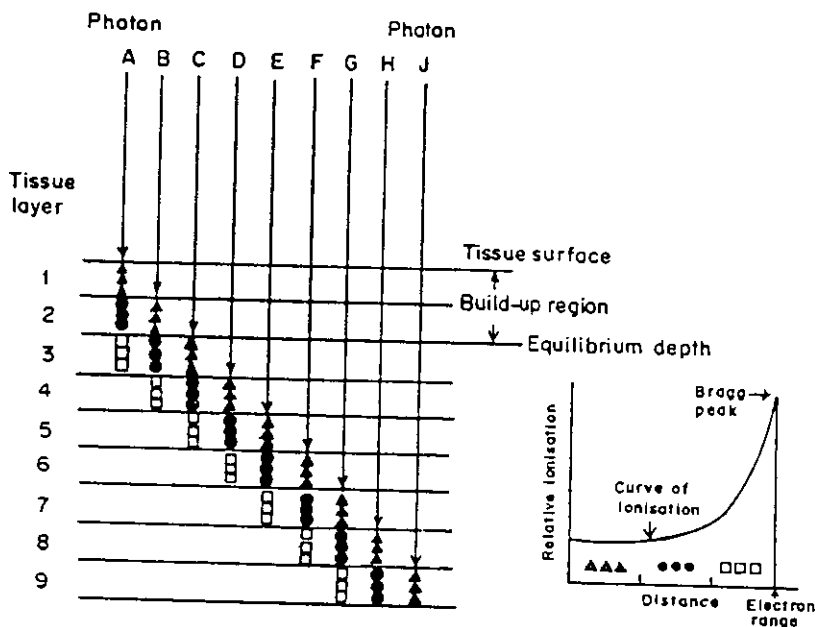


Fig.D.1 Schematic diagram illustrating the build-up effect for megavoltage beams of photons.

materials with widely varying electron densities. The megavoltage radiation, which may be either χ or γ - radiation is directed on to the surface of tissue and

the incident photons will undergo atomic interactions at various depths in the tissue, producing Compton electrons. Assume that these electrons travel in a forward direction along a straight line. Ionization is produced by the electron along its track, and will increase towards the end of the electron range. The absorbed dose is proportional to the ionization produced in each layer and in figure D.1 an electron track range extends for three tissue layers. The ionization produced along its length is symbolized by three squares. The last three symbols represent the ionization peak, which occurs at the end of the electron track. It is assumed that the same number of electron tracks are set in motion in all nine tissue layers, and it is seen that for the third and subsequent tissue layers, equilibrium has been achieved. The total energy deposited in each layer is now exactly equal to the energy removed by electrons generated in that layer.

Collimator

A diaphragm or system of diaphragms made of an absorbing material and designed to define the dimensions and position of a beam of radiation.

Depth in the phantom

This is a key parameter. The depth of the point of interest is always measured from the surface of the phantom along the beam axis. For all the data, the surface of the phantom is normal to the beam axis.

Depth of maximum dose (d_m)

For a given beam quality, the depth at which maximum dose occurs. It will vary to some extent with field size and source surface distance.

Diaphragm

The part of the collimator that controls the beam size.

Field

A plane section of the beam perpendicular to the beam axis.

Filter

An attenuating material inserted into the beam in order to modify its spectral composition, to suppress particular components of a mixed beam or to modify the spatial distribution of energy fluency rate or absorbed dose rate.

Invivo

An investigation carried out in the living organism or human body.

Medical Physics

Medical physics is a branch of applied physics. It deals with the application of laws and methods of physics to solve problems in medicine. It mainly exercised in research work, education and medical care.

Output factor

The absorbed dose rate at the point on the beam axis at the depth d_m for a given field size normalized to unity for a specified standard field size (usually 10cm×10cm).

Peak scatter factor (PSF)

PSF is defined as the value of the scatter factor at the depth of maximum dose. The scatter factor at a point in water phantom is the total absorbed dose at that point divided by the absorbed dose arising from primary photons at the same depth on the beam axis.

$$\text{PSF} = D(\text{FS}, d_m) / D(0, d_m)$$

Where FS is the field size.

Penumbra

The penumbra generally defined as the lateral distance between the 80% and 20% of the maximum dose points one side of a beam profile.

Percentage depth dose (PDD)

The PDD at a point in a water phantom (Fig.D.2) exposed to a radiation beam is the quotient (expressed as a percentage) of the absorbed dose at that point, divided by the absorbed dose at a point on the beam axis at the depth d_m .

$$\text{PDD} = 100 \times D_x / D_y$$

Phantom

A tank of water or blocks of tissue equivalent material is used as phantom material.

Simulator

Machine which emulates the geometry of a treatment machine but which uses diagnostic energy x-rays to take images of the patient in the treatment position. The simulator plays a major role in "conventional" treatment planning.

Source-Surface Distance (SSD)

The distance measured along the beam axis from the front surface of the source to the surface of the irradiated object, percentage depth dose is a function of SSD and therefore the definition of this parameter is important.

Supralinearity

For an ideal TL-dosimeter, the total light yield would be directly proportional to the absorbed dose, and the response of the TL-dose would be perfectly linear. TLD displays nonlinear increase in response dose per unit exposure, a behavior is known as supralinearity.

Scatter factor

Scatter factor is defined as the ratio of the total exposure (or absorbed dose) at a point in a phantom to that part of the exposure (or absorbed dose) which is produced by primary photons.

Tissue air ratio (TAR)

The TAR at a point in a water phantom (Fig.D.2) is the quotient of the total absorbed dose at that point, divided by the absorbed dose at a point on the beam axis at the same distance from the source but with the surface moved so that this point is at the depth d_m and this absorbed dose originates from primary photons only.

$$\text{TAR} = D_x / D_{x'} = \text{TMR} (FS, d) \times \text{PSF}$$

Tissue equivalent material

A material whose absorption and scattering properties for a given radiation quality simulate those of a given biological material, such as soft tissue, muscle, bone or fat.

Note: 1. Tissue equivalent material can be either solid or liquid.

Note: 2. Water is the most commonly used tissue equivalent material for χ and γ -ray.

Tissue compensator

Tissue compensator using bolus bags to obtain a flat surface between the applicator and irradiated tissue.

Tissue phantom ratio (TPR)

The TPR at a point in a water phantom irradiated by a photon beam is the total absorbed dose at that point divided by the total absorbed dose at a point on the beam axis at the same distance from the source but with the surface of the phantom moved so that this point is at a specified reference depth.

Tissue maximum ratio (TMR)

A special case of tissue phantom ratio in which the reference depth (Fig.D.2) is specified as the depth d_m .

$$\text{TMR} = D_x / D_{x''} = \text{PDD} (FS, d) \times [(SSD + d) / (SSD + d_m)]^2 \text{ (simplified)}$$

$$\text{TMR} (0, d) = \exp. -\mu (d - d_m)$$

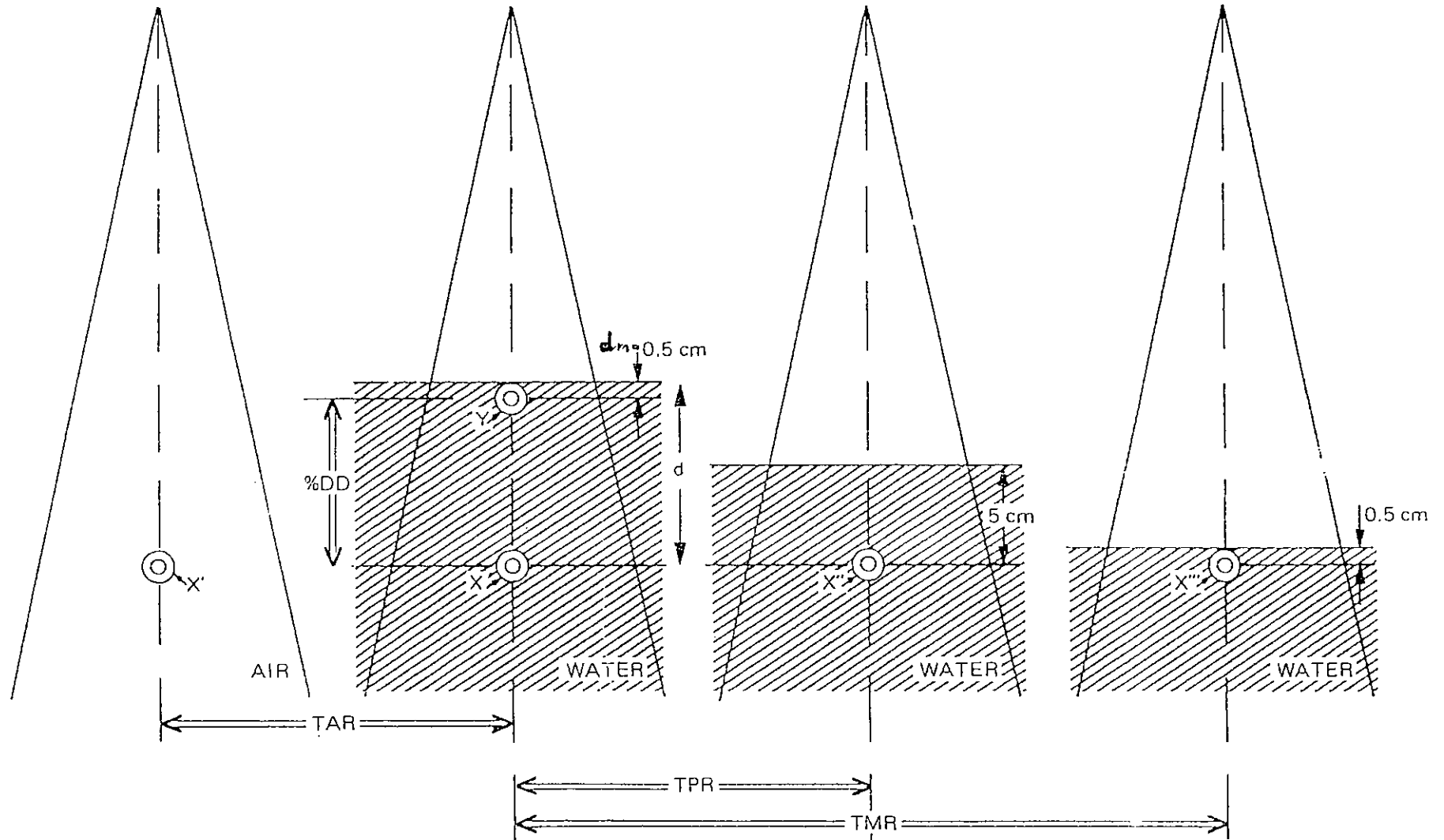


FIG.D.2. Functions used in determining absorbed dose at any point in a phantom

The indicated depths of the reference points, i.e. 0.5 and 5 cm, apply specifically to cobalt-60 γ -rays and these values (especially the depth of Y and X'''') will be different for other radiations.

Appendix - C

Verifikationsmessungen mit Thermolumineszenz-Dosimetern für ausgewählte asymmetrische Felder

F. Nasreen^(1,2), G.A. Zakaria⁽¹⁾, G. U. Ahmad⁽²⁾

⁽¹⁾Abt. für Med. Strahlenphysik, Kreiskrankenhaus Gummersbach, 51643 Gummersbach

⁽²⁾Dept. of Physics, Bangladesh University of Engineering & Technology, Dhaka - 1000

EINLEITUNG

Das im Kreiskrankenhaus Gummersbach entwickelte und bereits vorgestellte PC-Programm "ASYMM" erlaubt die Berechnung der Dosisverteilungen symmetrischer und asymmetrischer offener Felder und Keilfilterfelder. Durch Vergleichsmessungen im Wasserphantom wurde die Genauigkeit der Dosisverteilungen für verschiedene Feldgrößen und Einstellungen für 4MV-Photonen überprüft. Die Abweichungen lagen im Bereich von $\pm 2\%$ [1]. In dieser Arbeit haben wir Verifikationsmessungen für verschiedene ausgewählte asymmetrische Felder im Plexiglas - und im Aldersonphantom mit Thermolumineszenz-Dosimetern (TLD) durchgeführt und mit den Berechnungen verglichen. Wir haben folgende asymmetrische Einstellungen für die Verifikation des Programms ausgewählt:

- Messung des Anschlusses zweier Felder im Plexiglasphantom
- Messungen in unterschiedlichen Aldersonphantom-Schichten unter Berücksichtigung klinischer Aspekte: Schädelebene unter Minimierung der Augenbelastung, Thoraxebene zur Schonung der Lunge und Abdomenebene zur Schonung des Rückenmarkes.

METHODE UND EXPERIMENT

Für die Messungen in den Phantomen haben wir TLD-Rods mit einem \varnothing 1-mm und einer Länge von 6 mm aus Lithiumfluorid (Charge R0090 6-7-8-9) der Fa. Harshaw/Bicron benutzt. Die Auswertung erfolgte mit dem Reader Harshaw QS, Modell 3500 in Verbindung mit einem Commodore PC50-II.

Zur Vorbereitung der TLD's zur Bestrahlung und Auswertung diente ein Ofen des Typs TLDO der Fa. PTW Freiburg. Dieser Ofen stellt 2 Temperaturprofile zur Verfügung:

- Profil 1: zum Ausheizen und damit vollständiges Löschen der Haftstellen (Pre irradiation annealing) vor jeder Bestrahlung, Zyklus: 1 h bei 400°C und anschließend 3 h bei 100°C
- Profil 2: zum Vorbereitung der Auswertung (Pre readout annealing) vor jeder Bestrahlung, Zyklus: 20 min bei 100°C und Abkühlung auf Raumtemperatur vor jeder Auswertung.

Als Strahlenquelle diente ein Linearbeschleuniger Mevatron M6300 der Fa. Siemens mit einer Photonenenergie von 4MV. Der Beschleuniger besitzt 2 unabhängige Blenden in der Inplane-Ebene, die bis zu maximal 10 cm über den Zentralstrahl hinaus in negativer Richtung gefahren werden können (Overtravel).

Vor der ersten Anwendung der TLD's zur Bestimmung der Dosis mußten diese sich 30 Wärmebehandlungen unterziehen, um eine brauchbare Stabilität des Ansprechvermögens zu erreichen. Von 100 TLD's konnten auf diese Weise 83 TLD's ausgewählt werden, die in 8 Gruppen mit jeweils unterschiedlichem Ansprechvermögen eingeteilt wurden, wobei innerhalb einer Gruppe das Ansprechvermögen bis zu maximal $\pm 2.5\%$ variierte.

Vor der ersten Bestrahlung wurde eine Kalibrierung durchgeführt. Sie dient zur Bestimmung des allgemeinen Energie-Dosis-Umrechnungsfaktor RCF und des TLD-individuellen Korrekturfaktors ECC und besteht aus 3 aufeinanderfolgender Schritten. Entgegen der im Manual [2] angegebenen Empfehlung wurden keine TLD's als Calibration dosimeters

ausgesondert, sondern alle TLD's als.

Field dosimeters für unsere Experimente benutzt. Da sich die Stabilität der TLD's nach einer gewissen Anzahl Messungen veränderte, musste die Kalibration in regelmäßigen Abständen neu erfolgen. Dabei wurden die TLD's auch neuen Gruppen zugeordnet.

Die Kalibrierung der TLD's wurde in 5 cm wasseräquivalenter Tiefe im Plexiglas mit 4MV-Photonen durchgeführt. Die Wasserenergiedosis in 5 cm Wassertiefe ist durch Messungen mit Ionisationskammern genau bekannt. Bei den Messungen mit TLD's haben wir folgende Bedingungen eingehalten:

- Die Kalibration erfolgte im Plexiglasphantom. Der Kalibrierfaktor eines einzelnen TLD's durfte nicht um mehr als $\pm 2.5\%$ vom Mittelwert der Kalibrierfaktoren aller TLD's einer Gruppe abweichen.

- Die Aufnahme der Dosisprofile im Plexiglasphantom wurde in 1 cm-Schritten durchgeführt, wobei im Bereich von Halbschatten und Aufbauregion die Schrittweite kleiner als 0.5 cm war. Jeder Punkt eines Profils wurde simultan mit jeweils 3 TLD's ausgemessen.

- Da die gleichzeitige Messung mit 3 TLD in jedem Punkt im Aldersonphantom nicht möglich war, wurden jeweils 3 aufeinanderfolgende Messungen am gleichen Ort im Phantom durchgeführt.

Zur Verifikation des Feldanschlusses wurden 2 asymmetrische Felder der Größe $17 \times 6 \text{ cm}^2$ nebeneinander mehrfach mit Überlappungen zwischen - 3 und 3 mm bestrahlt. Im Anschlußbereich betrug der Abstand der TLD 1.5 mm voneinander.

Als weiteres wurde die Dosisverteilung in den Schichten 4 (Schädel), 17 (Thorax) und 30 (Abdomen) des Alderson-Phantoms mittels TLD bestimmt. Die angewendeten Feldkonfigurationen sind auf Grund der medizinischen Aspekte besonders für asymmetrische Felder geeignet (s. Einleitung).

ERGEBNISSE UND DISKUSSION

Bei Vorangegangenen Messungen im Homogenen und inhomogenen Modellphantom konnte eine Übereinstimmung zwischen TLD's und Ionisationskammer von 2% festgestellt werden, dieses veranlaßte uns, die Verifikation der Berechnungen mit dem Programm "ASYMM" mit unseren TLD's durch zu führen.

Die Feldanschluß-Messungen im homogenen Plexiglasphantom ergaben, daß für eine homogene Querverteilung im anschlußbereich eine Überlappung von 3 mm vorhanden sein muß und das bei der Feldgrößeneinstellung die Blenden auf Grund des Blendenspiels aufgeföhren werden müssen.

Die Abweichungen der Meßwerte am Aldersonphantom wichen von den berechneten Werten um bis zu $\pm 5\%$ in und hinter Inhomogenitäten (Lungen- und Knochengewebe) ab. Ursache hierfür ist die fehlende Berücksichtigung der Streustrahlung für andere Dichtebereiche als Wasser bei der Berechnung. Im homogenen Bereich stimmten die berechneten und gemessenen Werte innerhalb $\pm 2\%$ überein.

TLD-Messungen haben sich bei der Verifikation des Planungsprogrammes bewährt, auf Grund der Instabilität der TLD's mußten wir aber einen erhöhten Aufwand bei der Kalibrierung und den Messungen betreiben.

LITERATUR

- [1] Zakaria, G. A., Schütte, W. und Radant, J.: Berechnung der Dosisverteilung für asymmetrische Felder bei einem 4MV-Linearbeschleuniger. Z. f. Med. Physik4 (1994) 28-32
- [2] Usqr' Manual, Model 3500 Manual TLD Reader, July 27, 1993

REFERENCES

1. Arrone, M. J. and Attix, F. H. : Damage effects in CaF: Mn and LiF thermoluminescence dosimeters. *Health Phys.* 10(1964) 1431-36.
2. Attix, F. H.: Proc. 4th Int. Conf. on luminescence dosimetry, Krakowed T. Niewiadomski (Krakow: Institute of Nucl. Phys.), *J. Appl. Phys.* 46, (1975), 31,81.
3. Attix, T, Metcalfe, P. and Wong, T: Thermoluminescence dosimetry of therapeutic x-rays with LiF ribbons and rods. *Phys. Med. Biol.* 38, (1993), 833-45.
4. Arthur, L. Boyer and Edward C. Mok.: Calculation of photon dose distributions in an inhomogeneous medium using convolutions. *Med. Phys.*, 13(4), (1986), 503-09.
5. Aukett, R. J.: A comparison of semiconductor and TL-dosimeters for invivo- dosimetry. *Br. J. Radial.*, 64, (1991), 947-52.
6. Attix, F. H.: Isotopic effect in lithium fluoride thermoluminescent dosimeters. *Phys. Med. Biol.*, Vol. 14 No.1, (1969), 147-148.
7. Bengt, K. A. M.: Thermoluminescence of LiF: A statistical analysis of the influence of pre-annealing on the precision of measurement. *Phys. Med. Biol. Volm.* 14.01, (1969), 119-30.
8. Bradbury, M. H. and Lilley, E. *Phys. D: Appl. Phys.* 10, (1977), 1261.
9. Burger, G: Treatment planning for external beam therapy with neutrons: Urban & Schwarzerberg. Mülinchan- wien- Baltimore, (1981), 93-97.
10. Cammeron, J. R Dewerd, J., Wagner, C., Wilson, K., Doppke, and Zimmerman, D.: Non-linearity of thermoluminescence as a function of dose of LiF (TLD-100) (*Int. At. Energy, Vienna* 1967).
11. Carlsson, A. Carl.: Thermoluminescence of LiF: Dependence of thermal history. *Phys. Med. Biol.*, Vol. 01, (1969), 107-18.
12. Ciesielski, B., Reinstein, L. E, Wielopolski, L. and Meek, A.: Dose enhancement in build-up region by lead, Aluminum, and Lucite absorbers for 15 MV_p photon beam. *Med. Phys.*, 16(4), (1989), 609-13.
13. Das, Indra, J. and Khan, Faiz. M.: Scatter dose perturbation at high atomic number interfaces in meghavoltage photon beams, *Med. Phys.*, 16(3), (1987), 367-75.

14. Dawson, D. J., Harper, J. M., and Akinradewo, A. C.: Analysis of physical parameters associated with the measurement of high-energy X-ray penumbra. *Med. Phys.*, 11(a), (1984), 491-97.
15. Dobbs, J., Barrett, A. and Ash, D.: Practical radiotherapy planning, 2nd Ed., British Library Cataloging in publication data.
16. David Steidley, K and Rosen, Coleman W.: Dosimetric aspects of a 3.3MV linear accelerator. *Med. Phys.*, 17(3), (1990), 474- 80.
17. Das, Indira, J. and Kase, Kenneth. R.: Validity of transition-zone dosimetry at high atomic number interfaces in megavoltage photon beams. *Med. Phys.*, 17(1), (1990), 10 -16.
18. El- Khatib, Ellen., Antolak, John and Seringer, John.: Evaluation of film and thermoluminescent dosimetry of high-energy electron beams in heterogeneous phantoms, *Med. Phys.* 19(2), (1992), 317-23.
19. Essers, M. et al: The accuracy of CT-based inhomogeneities corrections and mivivo-dosimetry for the treatment of lung cancer. *Radiotherapy and Oncology*, 37, (1995), 199-204.
20. Feist, H., Blank, P.: Qualitätssicherung in der Strahlen therapie mit TL-dosimeteren aus LiF. Erste Ergebnisse Von Dosisvergleichsmessungen. *Med. Physik*, (1992), 76-77.
21. Feist, H. : Entwicklung der thermolumineszenzdosimetrie mit LiF zu einer Präzisionsmethode für Absolute Energiedosisbestimmungen in der Strahlentherapie mit photonener and Electronstrahlen Hoher Energie. Als Habilitationsschrift zur. Erlangung des grades eines habilitierten Doktors der Medizin an der Ludwig- Maximilians- Universität, (1992).
22. Folkard, M., Roper, M. J. and Michael, B. D.: Sensitivity enhancement effects in the thermoluminescence of LiF TLD-100 at a radiation bellow 10 Gy. *Med. Phys. Biol.*, 32, (1987), 769-73.
23. Feist, H und Nanjokal, B.: Bestrahlung planung und Dosimetrie mit Thermolumineszenzdosimeteren bei Ganzkörper bestrahlungen in 6M Abstand des Patienten vom Beschleuniger. Radiologische Klinik der Universität München, Klinikum Großhadern.
24. Feist, H.: Einfluß des Regenerier und Auswertverfahrenens auf das Supralineare verhalten von LiF-Thermolumineszenzdosimeteren. *Strahlentherapie und Onkologie*, 164, (1988), 223- 227, (Nr.4).

25. Gläser, L.: Influence of the lung tissue on the dose- distribution of high-energy photon beams. *Strahlentherapie and Onkologie*, 162, Nr.4, (1984), 266-70.
26. Gerbi, Bruce J. and Khan M. Faiz. : Measurement of dose in the build up region using fixed-separation plane-parallel ionization chambers. *Med. Phys.*, 17(1), (1990), 17-26.
27. Johns, H. E. and Cunningham, J. R. : *The Physics of Radiology*, 4th Ed., Thomas, Springfield, (1983).
28. Jens Juul Cristensen and Ahmed Akmal Safwat.: Dose to the lung, calculated and measured in an Alderson phantom under TBI conditions. Department of radiotherapy, National Cancer Institute, Cairo University, Egypt.
29. Kenneth, R and et al.: Dosimetric evaluation of the pencil- beam algorithm for electrons employing a two-dimensional heterogeneity correction, *Int. Publication Oncology. Biol. Phys.*, Vol.10, (1984), 561-69.
30. Kirby, T, H., Hanson, W. F., Johnston, D.A.: Uncertainty analysis of absorbed dose calculations from the thermoluminescence dosimeters. *Med. Phys.*, 19(6), (1992), 1427-43.
31. Knöös Tommy, Ahnesjö-Anders, Nelsson Per and Weber, L.: Limitation of a pencil beam approach to photon dose calculation in tissue, *Phys. Med. Biol.*, 40, (1995), 1411-29.
32. Korn, T., Metcalfe,P., and Wong, T.: Thermoluminescence dosimetry of therapeutic X-rays with LiF ribbons and rods. *Phys. Med. Biol.*, 38, (1993), 833-45.
33. Kron, Tomas., Elliot, Andrew, Metcalfe, Peter: The penumbra of a 6MV x-ray beam as measured by thermoluminescence dosimetry and evaluated using an inverse square root function. *Med. Phys.*, 20(5), (1993), 1429-38.
34. Kuszpet, M. E., Feist, H., Collin, W. and Reich, H.: Determination of C_λ and C_E conversion factors and stopping power ratios using calibrated ferrous sulphate dosimeters. *Phys. Med. Biol.*, Volm. 27, No.12, (1982), 1419- 33.
35. Kannan, A., Naik, S. B., Soman, A. T., Shigwan, J. B. and Sumant, Viivita : Signal correction technique for dose measurements with TL dosimeters. *Journal of Med. Phys.*, 21, 3, (1996), 85.

36. Kron Tomas and Ostwald Patricia. : Skin exit dose in megavoltage x-ray beam determined by means of a plane parallel ionization chamber (Attix Chamber). *Med. Phys.*, 22 (5), (1995), 577-78.
37. Korn, Tomas and others : Clinical thermoluminescence dosimetry : How do expectations and results compare ? *Radiotherapy and Oncology*, 26, (1993), 159-61.
38. Korn, Tomas et al.: X-ray surface dose measurements using TLD extrapolation, *Med. Phys.*, 20(3), (1993).
39. Khan, Faiz. M., Bruce, J. Gerbi, and Firmin C, Dei.: Dosimetry of asymmetric χ -ray collimators., *Med. Phys.*, 13(6), (1986), 936-41.
40. Karzmark, C. J., Morton, Robert J.: A primer on theory and operation of linear accelerators in radiation therapy MHS Publication (FDA), (1988), 1,5,27, 28
41. Laughlin, Johns., Mohan, R and Kutcher, G, J.: Choice of optimal megavoltage for accelerators for photon beams treatment, *Int. J. Radiation Oncology Biol. Phys.*, Vol.12, 1551-57
42. Lübbert, K., Rahim, H.: Verifikationsmessungen mit TLD-100 Stäbchen für ausgewählte Strahlenfelder. *Strahlenther, Onkol.*, 165, 08, (1989), 604-510.
43. Mckinlay, A.F. : Thermoluminescence dosimetry, *Medical Physics Hand Books 5*, Adam Hilger Ltd. Britistol, (1981).
44. Mayles, W. P. M., Heisig, S., and Mayles, H. M. O.: Treatment verification and invivo dosimetry, *Radiotherapy Phys. in practice*, Edited by william, J. R. and Thwaites, D. I.: Oxford Medical Publication, (1993), 227-50.
45. Members of the joint working party: Bewley, D. K, et al: Central axis depth dose data for use in radiotherapy: *British Journal of Radiology*. British Institute of Radiology, London, (1983).
46. Mayhugh H. R., Cristy, R. W. and Johnson, N. M.: Proc 2nd Int. conf. on luminescence dosimetry, Gattinburg Ed. JA Auxier et. al., (Tennessee: USAEC and Oak Ridge National Laboratory), Conf-680920, (1968), 294.
47. Metcalfe Peter; Kron, Tomas; Elliott, Andrew and Wong, Tony. : Dosimetry of 6MV X-ray beam penumbra, *Med. Phys.*, Vol. 20, No. 5, (1993), 1439-45.

48. Mijnheer, B. J., Rice, R. K. and chin, L. M. : Lung dose measurements performed at the joint center for radiation therapy, Boston, USA.
49. Meigooni, Ali. S. and Mishra, Vivek, Panth, Hark Williamson, Jeffrey.: Instrumentation and dosimeter size artifacts in quantitative thermoluminescence dosimetry of low-dose fields, *Med. Phys.*, 22(5), (1995), 555-61.
50. Mould, R.F.: Radiotherapy Treatment Planning, Adam Hilger Ltd.
51. Millin, A. E. and Smith C. W.: A beam profile generation algorithm for wedged half-beam blocked asymmetric fields. *Phys. Med. Biol.*, 39, (1994), 63-73.
52. Mark G.Marshall. : Three-field isocentric breast irradiation using asymmetric jaws and a tilt board. *Radiotherapy and Oncology*, 28, (1993), 228-232.
53. Nilsson, B., Montelius, A. Andreo, P.: A study of interface effects of ^{60}Co beams using a thin wall parallel plate ionization chamber. *Med. Phys.*, 19(6), (1992), 1413-21
54. Nath Ravinder and et al.: AAPM code of practice for radiotherapy accelerators: Report of AAPM Radiation Therapy Task Group No. 45, *Med. Phys.*, 21(7), (1994), 1093-1121.
55. Ognnleye, O. T., Attix, F. H and Paliwal, B. R.: Companoson of burlin cavity theory with LiF TLD measurements for ^{60}Co gamma rays. *Phys. Med. Biol.*, Vol. 25.2, (1980), 203-13.
56. Pradhan, A. S., Gopalakrishnan, A. K. and Lyer, P. S.: Dose measurement at high atomic number interfaces in megavoltage photon beams using TLDs. *Med. Plys.*, 19(2), (1992), 355-56.
57. Pointon, R.C.S.: The radiotherapy of malignant disease, 2nd Ed. British Library Catalogue in Publication Data, (1991).
58. Quast, U.: The dose to lung in TBI: *Strahlenther. Onkol.*, 167, (1991), 135-151(Nr.3).
59. Peter R. Almond.: Quality Assurance of Linear Accelerators. Harvard Medical School. Joint Centre Radiation Therapy Boston, Massachusetts, 02115.

60. Redpath, A.T. and Thwaites, D. I.: A 3-dimensional scatter correction algorithm for photon beams, *Phys. Med. Biol.*, Vol. 3606, (1991), 779-98.
61. Robinson, R. C. and Kirby, T. H.: Energy response of LiF TLD-100 to high-energy photon beams. *Med. Phys.*, 15, (1988), 438.
62. Robinson, C.: Energy response of LiF TLD-100 to high energy photons. Master of science thesis, Univ. of Texas at Houston Graduate School of Biomedical Science, (1989).
63. Redpath, A. T. et al.: Dose calculation within the patient. *Radiotherapy Physics in practice*. Edited by J. R. Williams and D. I. Thwaites, Oxford Medical Publication, (1993).
64. Spanne, Per and Carlsson, A.Carl.: Efficiency variation of thermoluminescence LiF caused by radiation and thermal treatment, *Radiation Phys. Dept. Linkoping Univ. S-581*, 85, Linkoping, Sweden.
65. Sidos/ Euados/ Somadas Recommendations for measurement.
66. Svensson, H. Hanson, G. P. and Zsolanszky, K.: The IAEA/WHO. TL-dosimetry service for radiotherapy centers, (1969-87). *Acta Oncologica*, 29, (1990).
67. Sauer, Otto. A.: Calculation of dose distributions in the vicinity of high- Z interfaces for photon beams. *Med. Phys.*, 22(10), (1995), 1685-90.
68. Suendra N. Rustgi.: Evaluation of the dosimetric characteristics of a diamond detector for photon measurements. *Med. Phys.*, 22(5), (1995), 567-70.
69. Suntharalingam, N. and Cammeron, J. R. Thermoluminescent response of lithium fluoride to radiations with different LET.
70. Tsuda, M., Ohizumi, Y., Mori, T.: LiF and CaF : Dy thermoluminescent dosimeters, *Strahlentherapie*, 156.10, (1980), 708-713.
71. Thomas, S. J. and Thomas, R. L.: A beam generation algorithm for linear accelerators with independent collimators. *Phys. Med. Biol.*, (1990), Vol. 35, No. 3, 325-332.
72. Van Dam, J. and Marinello, G.: Methods for invivo dosimetry in external radiotherapy. ESTRO and Garant Publishers,(1994),1st Ed Booklet No. 1.

73. Woo, M. K., Cunningham, J. R. Jezoranski, J. J.: Extending the concept of primary and separation to the condition of electronic disequilibrium. *Med. Phys.*, 17(4), (1990), 588-95.
74. Wong, T. P.Y., Metcalfe, P. E. and Chan, C. L.: The effects of low-density media in x-ray dose distribution, *Media Mundi. A review of modern diagnosis*, 39, 134-138.
75. Wolfgang Petzold, rer. nat. and Hannokrieger, rer. nat., *Strahlenphysik, Dosimetrie und Strahlenschutz. Band 1, Grundlagen*, B. G. Teubner Stuttgart, (1998).
76. Werner, B. L. Das, I, J. Khan, F. M. and Salk W. N.: Dose perturbations at interfaces in photon beams. Secondary electron transport, *Med. Phys.*, 17, (1990), 212-226.
77. Zakaria, G. A., Schütte, W. and Radant, J.: Berechnung der Dosisverteilung für Asymmetrische Felder bei einem 4MV-Linearbeschleuniger, *Z. f. Med. Phys.*, 4, (1994), 28-32.
78. Zakaria, G. A., Schütte, W. and Radant, J.: Ein erweitertes Berechnungsverfahren für Asymmetrische Felder unter Verwendung von Keilfiltern bei einem Linearbeschleuniger. *Z. F. Med. Phys.*, 4, (1994), 143- 48.
79. Zimmerman, D. W., Rhyner., C. R., and Cammeron, J. R.: Thermal annealing effects on the TL of LiF. *HiTh Phys.*, 12, (1966), 525-31.
80. Technical Reports Series No. 374; Calibration of dosimeters used in radiotherapy; A manual sponsored by the IAEA and WHO. International Atomic Energy Agency, Vienna, (1994), 98-9.
81. Technical Reports Series No. 277; Absorbed dose determination in photon and electron beams; An International Code of practice; International Atomic Energy Agency, Vienna, (1987).

